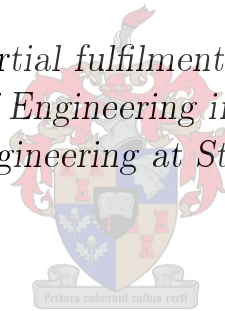


Low-cost, portable biosensors for *Escherichia coli* detection in water

by

Michael Benjamin Maas

*Thesis presented in partial fulfilment of the requirements for
the degree of Master of Engineering in Electronic Engineering
in the Faculty of Engineering at Stellenbosch University*



Department of Electrical and Electronic Engineering,
University of Stellenbosch,
Private Bag X1, Matieland 7602, South Africa.

Supervisor: Prof. W.J. Perold and co-supervisor: Prof. L.M.T. Dicks

December 2015

Declaration

By submitting this thesis electronically, I declare that the entirety of the work contained therein is my own, original work, that I am the sole author thereof (save to the extent explicitly otherwise stated), that reproduction and publication thereof by Stellenbosch University will not infringe any third party rights and that I have not previously in its entirety or in part submitted it for obtaining any qualification.

December 2015

Copyright © 2015 Stellenbosch University
All rights reserved.

Summary

Low-cost, portable biosensors for the detection of *Escherichia coli* (*E. coli*) in water were investigated. The operating principle of various biosensors is discussed at the hand of a biosensor model. These methods, including electrical and optical methods, are evaluated for use in low-cost sensors. An electrically and optically based biosensor are compared.

An electrochemical impedance biosensor that detects bacteria using non-linear AC harmonics is evaluated. Various electrode geometries and materials patterned on glass chips were tested. Ionic solutions were tested and a sensitivity of 0.01 mg/L for NaCl, KCl and MgCl₂ was achieved. *E. coli* B44 was tested, and bacterial concentration curves for the sensor was derived. The limit of detection (LOD) of the sensor was 1.1×10^{10} CFU/ml, and the response time less than 4 minutes.

A fiber-optic biosensor, operating using evanescent wave modulation, was tested. A low-cost testing method, using simple optoelectronics, was derived and hand-made fibers were manufactured. The fibers were immobilised with primary anti-*E. coli* antibodies by covalent attachment with a (3-Glycidyl oxypropyl) trimethoxysilane (GPS) crosslinking agent. The immobilisation efficiency was determined using Wide Field Fluorescence microscopy. Bacterial concentrations (*E. coli* DH5 α) were tested, and bacteria was successfully detected. The LOD of the sensor was 3×10^7 CFU/ml, and the response time less than 120 minutes.

The two sensors are compared and evaluated for use in low-cost, portable biosensing systems for water testing. Recommendations for future development of a low-cost, portable biosensing prototype is discussed, including a system model and possible specifications. Possible applications for future biosensor development is discussed in detail.

Opsomming

Lae-koste, draagbare biosensors vir die opsporing van *Escherichia coli* (*E. coli*) in water word ondersoek. Die opsporingsmetode van onderskeie biosensors word bespreek, met die hulp van 'n biosensor model. Hierdie metodes, insluitend elektroniese en optiese metodes, word evalueer vir gebruik in lae-koste sensors. 'n Elektroniese en optiese gebaseerde biosensor word vergelyk.

'n Elektrochemiese impedansie biosensor wat bakterieë opspoor met behulp van nie-lineêre WS harmoniese pieke word evalueer. Verskeie elektrode geometrieë en materiale, wat op glass skyfies geëts is, is getoets. Ioniese oplossings is getoets en 'n sensitiwiteit van 0.01 mg/L vir NaCl, KCl en MgCl₂ is bepaal. *E. coli* B44 is ook getoets, en bakteriële konsentrasiekurwes is afgelei. Die limiet van opsporing van die sensor was 1.1×10^{10} KVE/ml, en die reaksietyd minder as 4 minute.

'n Optiese vesel biosensor, wat van verganklike golfmodulasie gebruik maak, is getoets. 'n Lae-koste toetsmetode, wat gebruik maak van eenvoudige optoëlektroniese komponente, is ontwerp en handgemaakte vesels is vervaardig. Die vesels is geïmmobiliseer met primêre teenliggaampies deur kovalente bindings met 'n (3-Glycidyoxypropyl) trimethoxysilaan (GPS) kruisbindingsagent. Die immobiliseringseffektiwiteit is bepaal deur Wye Veld Fluoresensie mikroskopie. Bakteriële konsentrasies (*E. coli* DH5 α) is getoets, en bakterieë is opgespoor. Die limiet van opsporing van die sensor was 3×10^7 KVE/ml, en die reaksietyd minder as 120 minute.

Die twee sensors is vergelyk en evalueer vir gebruik in lae-koste, draagbare biosensorstelsels vir watertoetse. Voorstelle vir die toekomstige ontwikkeling van 'n eenvoudige, draagbare biosensor-prototipe word bespreek, insluitend 'n stelselmodel en moontlike spesifikasies. Moontlike toepassings vir toekomstige biosensor ontwikkeling word in detail bespreek.

Acknowledgements

I would like to thank the following people for their contribution to the successful completion of my thesis:

Arnoux Rossouw for his advice and help regarding the start of my thesis.

Wynand van Eeden for allowing me to bother him with all the small details, and for all the good chats.

Lize Engelbrecht for showing me bacteria for the first time, and for her uncanny ability to find bacteria on fiber surfaces.

Larry Morkel for all the administration.

Jenny Martin for sorting out all my orders.

Thank you to Professor Łos and those involved in the non-linear harmonic project for allowing me to work on your sensors.

I would also like to thank my co-supervisor Prof. L.M.T. Dicks for allowing me to work at the Department of Microbiology and for guidance on the microbiological parts of my thesis.

I would specially like to thank the Technical University of Munich's Lehrstuhl für Medizinelektronik for hosting me for 6 months during my studies, especially my supervisor Dr. Martin Brischwein. Danke schön Martin!

I would specially like to thank Deon Neveling for his knowledge, support, motivation and guidance while working at the Department of Microbiology. Awe Deon!

I would also like to thank my family for their support during the completion of my thesis.

Lastly I would like to acknowledge my supervisor Prof. Willem Perold. Thank you for your knowledge, calmness, sense of humour, professionalism, encouragement and support over the past few years. Dankie Prof!

Contents

Declaration	i
Summary	ii
Opsomming	iii
Acknowledgements	iv
Contents	v
List of Figures	viii
List of Tables	xiii
Nomenclature	xiv
List of Abbreviations	xvi
1 Introduction	1
1.1 Background	1
1.2 Motivation	3
1.3 Literature synopsis	5
1.4 Objectives of the investigation	8
1.5 Contributions made	9
1.6 Summary	10
2 Literature Review	11
2.1 Biosensors	11
2.1.1 Introduction	11
2.1.2 Biosensor model	12
2.1.3 Biorecognition elements	12
2.1.4 Immobilisation methods	16
2.1.5 Transducers	17
2.1.6 Conclusion	25
2.2 Escherichia coli detection in water	25

2.2.1	Introduction	25
2.2.2	Microbiological water standards	25
2.2.3	Escherichia coli	27
2.2.4	Established methods for Escherichia coli detection	28
2.2.5	Biosensors for Escherichia coli detection	31
2.2.6	Conclusion	36
3	Theory	37
3.1	Electrochemical impedance biosensor	37
3.1.1	Introduction	37
3.1.2	Impedance spectroscopy	37
3.1.3	Equivalent circuits	38
3.1.4	Harmonic spectra	39
3.1.5	Electrode material, geometry and interfacial effects	41
3.1.6	Conclusion	42
3.2	Fiber optic biosensor	42
3.2.1	Introduction	42
3.2.2	Biosensor model	42
3.2.3	Ray tracing model	43
3.2.4	Antibody immobilisation	45
3.2.5	Conclusion	46
4	Electrochemical Impedance Biosensor	48
4.1	Introduction	48
4.2	Test protocols	48
4.2.1	Electrodes	48
4.2.2	Impedance spectra	48
4.2.3	Harmonic spectra	49
4.2.4	Electrode re-usability	50
4.2.5	Bacterial suspensions	51
4.2.6	Non-viable bacteria	51
4.3	Impedance spectra	52
4.4	E. coli detection	52
4.4.1	Ionic solutions	53
4.4.2	E. coli suspensions	55
4.4.3	Viable vs non-viable E. coli	58
4.4.4	Electrode geometry effects	59
4.5	Conclusion	59
5	Fiber-Optic Biosensor	61
5.1	Introduction	61
5.2	Test protocols	61
5.2.1	Optical fibers	61
5.2.2	Surface hydroxylation	62

<i>CONTENTS</i>	vii
5.2.3 Antibody immobilisation	62
5.2.4 Bacterial suspensions	63
5.2.5 Measurement setup	64
5.3 Antibody immobilisation on glass slides	65
5.4 Antibody immobilisation on fibers	68
5.5 E. coli binding on fiber surfaces	75
5.6 E. coli detection	78
5.7 Conclusion	81
6 Recommendations for Future Development	83
6.1 Evaluation of sensors	83
6.2 Recommended specifications and applications	84
6.3 System model	86
6.4 Future development	87
7 Conclusion	89
Appendices	92
A Microfluidics	93
A.1 Introduction	93
A.2 Literature review	93
A.2.1 Electrowetting-on-dielectric (EWOD) microfluidics	94
A.2.2 EWOD theory	95
A.2.3 Recent developments in low-voltage EWOD	95
A.2.4 Dielectric thin-films	96
A.2.5 Printed circuit board microfluidics	97
A.3 Suggested design	98
A.4 Conclusion	101
B Technical Drawings	102
C Calculations	107
D Additional Figures	110
D.1 Electrochemical impedance biosensor	110
D.2 Fiber-optic biosensor	118
E Datasheets	122
List of References	147

List of Figures

1.1	A biosensor model indicating the detection process	5
2.1	A biosensor model indicating the detection process	12
2.2	The induced fit model of a typical enzymatic reaction	14
2.3	Antibody illustration indicating (a) the various regions and (b) the three-dimensional protein structure	15
2.4	Antibody structure indicating the functional groups for covalent attachment	17
2.5	Chart indicating transducer types, methods and signals detected in biosensors	18
2.6	Interdigitated microelectrode biosensor diagram. Bacteria binds onto the antibodies, creating links between the electrodes. The bacteria can be quantified by measuring the impedance over the electrode array.	20
2.7	Electrical double layer schematic indicating the adhesion of ions to the surface of electrodes resulting in a capacitance	21
2.8	Field effect transistor schematic. As the gate potential is changed by bacteria binding, the IV characteristics of the transistor is modified.	21
2.9	U-bent fiber-optic biosensor indicating the evanescent wave modulation during bacterial detection in the fiber. The fiber is bent to increase the amount of light travelling in the evanescent field. . . .	22
2.10	A lateral flow assay (LFA)	23
2.11	Surface plasmon resonance sensing mechanism	24
2.12	Enzyme-linked immunosorbent assay (ELISA) schematic	24
2.13	An electron micrograph of E. coli bacteria (10 000 × magnification)	28
2.14	An E. coli bacterium diagram	29
2.15	E. coli colonies grown on an agar nutrient plate	29
2.16	Polymerase chain reaction (PCR) cycle representation	30
2.17	Potaflex water testing kit	31
2.18	(a) AFM scan of microelectrode array and (b) SEM image of E. coli bacteria creating links between electrodes	33
2.19	Battery-operated mobile device developed by You et al.	34

2.20	A lateral flow assay (LFA) of bioactive paper for the detection of <i>E. coli</i>	35
3.1	Equivalent circuit diagram of a bipolar electrochemical cell setup	38
3.2	Equivalent circuit diagram of an IME array electrochemical cell setup	39
3.3	Current-voltage (IV) characteristic curve indicating the linear range	40
3.4	Harmonic spectrum of an electrochemical cell ($V_{p-p} = 3$ V, $f = 1$ kHz)	40
3.5	Simplified fiber optic biosensor schematic	42
3.6	Ray tracing model of light travelling in an optical fiber	43
3.7	V -number vs excitation wavelength. As the excitation wavelength increases, the V -number decreases, resulting in more power present in the evanescent field.	45
3.8	Evanescent wave vs angle of incidence. As the angle of incidence increases above the critical angle, the penetration depth of the evanescent wave increases.	46
3.9	Antibody immobilised optical fiber model indicating the evanescent field. As the light travels through the fiber, the evanescent field interacts with the material/bacteria on the surface of the fiber.	46
3.10	Covalent bonding of borosilicate glass fiber with GPS crosslinker	47
3.11	Crosslinking IgG antibody to borosilicate glass fiber and GPS crosslinker	47
4.1	IntelliTUM chip with patterned electrodes as provided by TUM (Pt or Ti, 7.5 mm×15 mm)	49
4.2	Measurement setup for measuring harmonic spectra. The electrode chip was placed in a holder, and connected to a UR 22 audio interface. Spectra were measured using a computer.	50
4.3	Impedance spectrum at varying bacterial concentrations (Pt electrodes) showing the a.) complex impedance diagram and b.) the bode plot. As the bacterial concentration increased, the impedance decreased.	52
4.4	Harmonic spectrum of distilled water ($V_{p-p} = 2.987$ V, $f = 1$ kHz, Gain = 0.6), indicating only the fundamental frequency.	53
4.5	Harmonic spectrum of NaCl ($V_{p-p} = 2.987$ V, $f = 1$ kHz, Gain = 0.6, 0.01 mg/L). Increases in the harmonics are clearly seen.	54
4.6	Harmonic spectrum of NaCl ($V_{p-p} = 2.987$ V, $f = 1$ kHz, Gain = 0.6, 10 mg/L). As the concentration of ionic solutions increased, the harmonic peaks increased.	54
4.7	Concentration curve of NaCl on Pt electrodes ($V_{p-p} = 2.987$ V, $f = 1$ kHz, Gain = 0.6)	55
4.8	Concentration curve of NaCl on Ti electrodes ($V_{p-p} = 2.987$ V, $f = 1$ kHz, Gain = 0.6)	56

4.9	Harmonic spectrum of <i>E. coli</i> on Pt electrodes (1.1×10^{10} CFU/ml). The presence of bacteria is clearly seen due to the presence of harmonics.	56
4.10	Harmonic spectrum of <i>E. coli</i> on Pt electrodes (1.1×10^{12} CFU/ml). As the bacterial concentration increased, the harmonic amplitudes increased as well as more harmonics emerging in the spectrum.	57
4.11	Concentration curve for Pt electrodes (3rd harmonic)	57
4.12	Concentration curve for Ti electrodes (3rd harmonic)	58
5.1	Fiber-optic biosensor measurement setup	64
5.2	Fluorescence image of glass slide (Glass + GPS + PAb + SAb). The slide was immobilised with the crosslinker, primary antibody and secondary fluorescence antibody. The fluorescence indicates that successful immobilisation took place.	65
5.3	Fluorescence image of glass slide (Glass + SAb). The slide was only exposed to the secondary antibody, resulting in very low fluorescence levels.	66
5.4	Fluorescence image of glass slide (Glass + GPS + Sab). The slide was exposed to the secondary antibody and the crosslinker. This resulted in very low fluorescence levels.	66
5.5	Fluorescence image of glass slide (Glass + GPS + PAb + SAb). The primary antibody was covalently immobilised onto the glass slide. The high level of fluorescence indicates that successful antibody immobilisation took place.	67
5.6	Micrograph of an optical fiber	68
5.7	Fluorescence micrograph of a fiber (Glass + SAb). The fiber was only exposed to secondary antibodies, resulting in low levels of fluorescence.	69
5.8	Z-stack fluorescence micrograph of a fiber (Glass + SAb)	69
5.9	Fluorescence micrograph of a fiber (Glass + GPS + SAb). The fiber was exposed to the secondary antibody, after crosslinker adhesion. This resulted in low levels of fluorescence.	70
5.10	Z-stack fluorescence micrograph of a fiber (Glass + GPS + SAb)	71
5.11	Transmitted light image of a fiber (Glass + GPS, $4\times$ magnification). The image indicates some non-uniformity in the surface after crosslinker attachment.	71
5.12	Fluorescence micrograph of a fiber (Glass + GPS + PAb + SAb). The high level of fluorescence indicates that successful primary antibody immobilisation occurred.	72
5.13	Z-stack fluorescence micrograph of a fiber (Glass + GPS + PAb + SAb)	73
5.14	Relative fluorescence values (glass slides). The level of fluorescence drastically increases after primary antibody immobilisation.	73

5.15	Relative fluorescence values (optical fibers). The level of fluorescence drastically increases after primary antibody immobilisation, similar to that on glass slides.	74
5.16	Glass surface with immobilised PAb and stained to indicate bacteria movement and adhesion	75
5.17	Optical fiber immobilised with PAb and exposed to bacterial suspension (1 hour). A few bacteria can be seen on the surface of the fiber.	76
5.18	Optical fiber immobilised with PAb and exposed to bacterial suspension (4 hours). As the exposure time increases, the amount of bacteria adhered on the fiber increased.	77
5.19	Optical fiber immobilised with PAb and exposed to bacterial suspension (5 hours). After a few more hours many bacteria can be seen adhered to the surface of the fiber.	77
5.20	PBS control test	78
5.21	<i>E. coli</i> test (3×10^7 CFU/ml, test 1). After two hours a clear increase in the signal can be seen. This may be due to the change in refractive index occurring due to bacterial adhesion onto the fiber surface.	79
5.22	PBS control test	79
5.23	<i>E. coli</i> test (3×10^7 CFU/ml, test 2). After two hours a clear increase in the signal can be seen. This may be due to the change in refractive index occurring due to bacterial adhesion onto the fiber surface.	80
5.24	<i>E. coli</i> test on optical fiber (5.77×10^8 CFU/ml). After two hours a clear increase in the signal can be seen. The linear regression fit gradient is slightly higher for the higher concentration of bacteria.	81
6.1	System model	86
A.1	Surface charging and contact angle change during EWOD	94
A.2	Droplet splitting from a reservoir on an EWOD microfluidic platform	95
A.3	Cross-section of PCB substrate microfluidics device	97
A.4	Cross section of EWOD microfluidic platform	98
A.5	Top view of bare electrode array on EWOD platform	98
A.6	Actuation vs breakdown voltage for Al_2O_3 thin-film. As the thickness of the layer increases, the dielectric breakdown voltage increases. The crossing point between the dielectric breakdown and the required actuation voltage is the theoretical limit for successful droplet movement.	100
A.7	Microfluidic control circuit	101
C.1	Evanescent wave vs excitation wavelength	107
C.2	V-number vs core radius	108

C.3	LED circuit diagram	108
C.4	Photodiode circuit diagram	109
D.1	Interdigitated microelectrode (IME) chip provided by TUM (Pt, 10 mm×10 mm)	110
D.2	Symmetrical electrode chip provided by TUM (Pt, 24 mm×36 mm)	111
D.3	Chip holder (polycarbonate, 25 mm×25 mm×15 mm)	111
D.4	Impedance spectrum at varying bacterial concentrations (Ti electrodes)	112
D.5	Impedance spectrum at varying bacterial concentrations (Symmetrical electrodes)	112
D.6	Concentration curve of NaCl on Ti electrodes ($V_{p-p} = 2.987$ V, $f = 1$ kHz, Gain = 0.6)	113
D.7	Concentration curve of KCl on Ti electrodes ($V_{p-p} = 2.987$ V, $f = 1$ kHz, Gain = 0.6)	113
D.8	Concentration curve of MgCl ₂ on Ti electrodes ($V_{p-p} = 2.987$ V, $f = 1$ kHz, Gain = 0.6)	114
D.9	Concentration curve of NaCl on Pt electrodes ($V_{p-p} = 2.987$ V, $f = 1$ kHz, Gain = 0.6)	114
D.10	Concentration curve of KCl on Pt electrodes ($V_{p-p} = 2.987$ V, $f = 1$ kHz, Gain = 0.6)	115
D.11	Concentration curve of MgCl ₂ on Pt electrodes ($V_{p-p} = 2.987$ V, $f = 1$ kHz, Gain = 0.6)	115
D.12	Harmonic spectrum of E. coli on Ti electrodes (1.1×10^{10} CFU/ml)	116
D.13	Harmonic spectrum of E. coli on Ti electrodes (1.1×10^{12} CFU/ml)	116
D.14	Concentration curve for Pt electrodes (5th harmonic)	117
D.15	Concentration curve for Ti electrodes (5th harmonic)	117
D.16	Fluorescence micrograph of Glass-PAb-SAb slide (20× magnification)	118
D.17	Fluorescence micrographs of Glass-PAb-SAb slides (4× magnification)	119
D.18	Transmitted light image of a fiber (Glass, 10× magnification)	120
D.19	Transmitted light image of a fiber (Glass + GPS, 10× magnification)	120
D.20	Transmitted light image of optical fiber with crosslinker and PAb (4× magnification)	121

List of Tables

2.1	A comparison between polyclonal and monoclonal antibodies	16
2.2	The World Health Organisation (WHO) E.coli concentration and risk guideline	26
6.1	Design specifications for a biosensor prototype	85

Nomenclature

Constants

π	=	3.141 592 654
e	=	2.718 281 828
i	=	$\sqrt{-1}$
ϵ_D		Dielectric constant
ϵ_O		Permittivity of free space
A_n		Analog input
Ab		Antibody
Me		Methane group

Variables

n_1		Refractive index of fiber core
n_2		Refractive index of fiber cladding
NA		Numerical aperture
V		V-number

Variables with units

α		Angle of incidence	[rad]
γ_{lv}		Liquid-vapour interfacial energy	[N/m]
λ		Wavelength	[nm]
θ_0		No-voltage contact angle	[rad]
θ_c		Critical angle	[rad]
θ_V		Applied voltage contact angle	[rad]
ω		Angular frequency	[rad/s]
d		Dielectric layer thickness	[nm]
d_p		Evanescant wave penetration depth	[nm]
f		Frequency	[Hz]
f_{fund}		Fundamental frequency	[Hz]
f_x		Harmonic frequency	[Hz]
h		Spacer height	[m]
t		time	[s]

C_{dl}	Double layer capacitance	[F]
C_{sol}	Solution capacitance	[F]
E_{DB}	Dielectric Strength	[V/m]
$I(t)$	Current vector	[A]
$P_{EW\%}$	Power in the evanescent wave	[W/W]
R	Electrode width	[m]
R_{cell}	Cell resistance	[Ω]
R_O	Fiber core radius	[m]
R_{sol}	Solution resistance	[Ω]
V_a	Voltage amplitude	[V]
V_{act}	Actuation voltage	[V]
V_{cc}	Input voltage	[V]
V_{DB}	Dielectric breakdown voltage	[V]
$V(t)$	Voltage vector	[V]
Z_I	Reactance	[Ω]
Z_{Ln}	Microfluidic impedance	[Ω]
Z_R	Resistance	[Ω]
Z_{tot}	Total impedance	[Ω]

List of Abbreviations

3D: three dimensional

AC: alternating current

A/D: analog-to-digital

AFM: atomic force microscope

ALD: atomic layer deposition

AMP: antibody mimic protein

APTES: (3-amino-propyl)triethoxysilane

AR: aspect ratio

CFU: colony forming unit

CNT: carbon nano tube

DC: direct current

DEP: dielectrophoresis

DNA: deoxyribonucleic acid

E. coli: Escherichia coli

EIS: electrochemical impedance spectroscopy

ELISA: enzyme-linked immunosorbent assay

EW: evanescent wave

EWOD: electrowetting-on-dielectric

FET: field effect transistor

FFT: fast Fourier transform

FT: Fourier transform

FTIR: Fourier transform infrared

FOB: fiber optic biosensor

GA: glutaraldehyde

GPS: (3-glycidylxypropyl) trimethoxysilane

IME: interdigitated microelectrode

IR: infrared

ITO: indium tin oxide

I-V: current-voltage

LADM: light-actuated digital microfluidic

LB: Lysogeny Broth

LED: light emitting diode

LFA: lateral flow assay

LME: Lehrstuhl für Medizinelektronik

LOD: limit of detection

MTS: (3-mercaptopropyl) trimethoxysilane

NA: numerical aperture

PAb: primary antibody

PBS: phosphate-buffered saline

PCR: polymerase chain reaction

PCB: printed circuit board

PECVD: plasma enhanced chemical vapour deposition

PD: photodiode

PLD: plasma layer deposition

PVD: physical vapour deposition

RF: radio frequency RNA: ribonucleic acid

SAb: secondary antibody

SABS: South African Bureau of Standards

SANS: South African National Standard

SPR: surface plasmon resonance

SU: Stellenbosch University

TIR: total internal reflectance

TUM: Technical University of Munich

USB: universal serial bus

UV: ultra violet

UV-Vis: ultra violet visible

WHO: World Health Organisation

Chapter 1

Introduction

An investigation into low-cost, portable biosensors for the detection of *Escherichia coli* (*E. coli*) in water was proposed and conducted. This chapter introduces the various concepts to understand this investigation, as well as a motivation for why this work was completed. A biosensor is briefly defined, as well as the way in which biosensors work. The problems with current biosensors are discussed. A short synopsis of the literature review is provided. This contains the most relevant literature to this study, as well a critical evaluation of the publications relating to this investigation. The objectives of this investigation are clearly and succinctly set to ensure clear goals for the project. The contributions of this study to the current state of biosensor research is detailed. An overview of the work that has been completed i.e. the important results and conclusions are given. At the end of the introduction a clear formulation of the contents of the thesis, and how these contents progress through the thesis, is provided.

1.1 Background

A biosensor is defined as a device that can detect biological molecules or organisms in a sample or specific environment [1]. Biosensors play an important role in detecting these organisms, where other methods of detection are too laborious or expensive. The detection of biological contaminants is critically important for medical, pharmaceutical, agricultural and environmental fields, amongst others. A biosensor typically consists of a sample with the target analyte (e.g. microorganism, biological molecule) suspended in the sample. This comes into contact with a transducer (optical, electrochemical etc.) which reacts to the presence of the analyte. This reaction is then interpreted by a signal processing circuit. This signal can then be related to the concentration of the analyte in the sample. This is the basic working principle of a biosensor.

Biosensors typically use very specific biorecognition elements (e.g. enzymes, antibodies) to identify or label the targeted analyte. Antibodies are of particular interest. Antibodies are proteins formed by the body to target foreign matter, such as bacteria. The antibody typically attaches to the antigen (foreign matter) in a specific way. Certain antibodies only attach to certain antigens, making them highly specific to the target. This property can be

used in biosensors to ensure high specificity of detecting a certain antigen amongst other matter that may be present in the sample. This is due to their well defined chemical constituents, as well as protein structure. The attachment kinetics and mechanisms are well defined for antibodies. Antibodies for various antigens have been produced and are commercially available. Due to their well defined structures, antibodies can relatively easily be attached to inorganic surfaces such as glass.

Many authors have noted that biosensor development must focus on the application of the sensor. The application of the sensor, however, depends on the results obtained from manufacturing and testing in a laboratory setup. The application of developed sensors seem only to be clear at the end of a study. This is a problem when defining the goals of a single investigation into biosensors. By researching the most appropriate objectives and specifications for a biosensor, the research can be focussed on a certain area. The focus in this project is on low cost and portability. These form the single most important specifications for the development and implementation of the sensor. *E. coli* bacteria has been chosen as the analyte to focus on. In water quality testing the presence of bacteria can infer the presence of other harmful antigens, such as viruses, protozoa etc.

The World Health Organization and United Nations Children's Fund Joint Monitoring Programme for Water Supply and Sanitation (JMP) [2] and Plate et al. [3] noted that *Escherichia coli* is the preferred indicator of faecal contamination in water. Faecal contamination causes many problems in society. Ingestion of faecally contaminated water can lead to death due to the presence of pathogens. Crops that are watered with contaminated water can lead to widespread infections if the fruits or vegetables are not properly washed before consumption. Outbreaks of diseases, such as cholera and gastrointestinal diseases, can be limited when the contamination level of water and water sources is correctly monitored and controlled.

Biosensors are mostly developed for use in laboratories. The biosensors that are developed for outdoor use usually end up being limited to the laboratory due to various factors. There is, however, a major need for low cost sensors that can be used outside of laboratories. This need for low-cost and portability forms a central focus point in this study. This is due to the necessity for successful biosensor production and widespread use. The ease of manufacture, possibility to scale-up production, low-cost materials, robust design and sensing mechanisms all lead to lower total costs and more useful sensors that can be used in various situations.

Biosensors have the ability to determine the concentration of analytes in water samples at a high rate, in real-time and at a very low cost. Biosensors play

an increasingly important role in determining various pollutants in drinking water [4], but the focus in this project is on *Escherichia coli*. It is possible to develop biosensors with high sensitivity and accuracy. Biosensors can also be incorporated into portable sensing systems and be used to detect microbial water pollutants such as *E. coli* [5]. Another advantage of portable biosensors is that they can be used to determine spatio-temporal variations in water quality by deploying them in water sources or installing sensors at the point-of-source [5]. There is a great need for clean, safe drinking water. The investigation into portable biosensing devices for use in water quality determination at the point-of-source can help mitigate the challenges and problems faced in supplying clean and safe water.

1.2 Motivation

There is a global need for safe drinking water. The scarcity of water resources is a problem in rural areas and water-scarce nations such as South Africa. The increase in populations, industries and pollution have caused major stress on water supply networks, especially in developing nations. The Water Supply and Sanitation Technology Platform [6] notes that climate change, infrastructure change and globalisation are leading to increasing water scarcity and stress on water supplies. This level of safe water scarcity causes millions of deaths each year related to the consumption of unsafe drinking water [7], usually infected with pathogenic micro-organisms. 1.6 Million children, under the age of five, die each year due to water related deaths [8]. These children mostly live in rural and developing areas [8], where water quality is not properly monitored and access to healthcare is limited. It is also estimated that 1.7 billion rural dwellers will not have access to clean water and sanitation by 2015 [8].

Waterborne diseases are transmitted mostly by the consumption of infected water [9]. A possible solution to these problems is the investigation of effective water resource management techniques, advanced purification systems and effective monitoring and control systems. The cost-effective, efficient, point-of-source monitoring of this precious resource could lead to decreased mortality rates, especially in rural areas [9].

Rural areas are susceptible to natural water pollution due to the fact that most rural dwellers use rivers, open reservoirs, springs and open wells for fresh drinking water [10, 8, 11]. These are usually located close to contaminants, such as dug-out toilets, bathing and animal grazing areas [10, 8, 11]. This causes contamination and is especially prone to becoming faecally polluted. Water supplies tend to be very well controlled in the macro distribution system, but at a micro level (the point-of-origin or the point-of-source) there seems to be a major need to determine the quality of the water [11]. This is especially true

in rural areas where the impact is the most severe when waterborne diseases break-out, due to inadequate medical and sanitation infrastructure. There is a need to continuously monitor if the water is contaminated [11]. Constant monitoring could help prevent the outbreak of water related diseases [11] and ensure potable drinking water for all.

The Technical Research Centre of Finland's water research roadmap [12] discussed certain areas that must be investigated to improve water quality monitoring. These include the development of new tools for decentralised monitoring and control, investigation into the use of nanosensors, wireless sensors, selective fast measurements, microbiological sensors, biosensor applications, using nanotechnology and immobilisation techniques, and intelligent biosensors [12]. These tools, if developed, could greatly improve the health and well-being of many citizens in rural areas.

In many rural settings the determination of faecal pollutants will not rule out the consumption of the water. Effective and efficient water purification systems, that are portable, cost-effective and robust must be investigated. Rossouw [13] investigated modified track etched membranes for use in water treatment processes and found that it could be used for E.coli treatment of water due to the anti-microbial properties of certain metals used on the membranes. Rossouw [13] tested these membranes with Rhodamine 6G, an organic color dye, and the membranes showed good self-cleaning properties. It was recommended that the study of protein, virus and bacteria degradation of these membranes be extensively studied [14]. These membranes have the potential to be used in advanced water treatment processes where they can be used to produce pure drinking water at a significantly reduced cost [14]. These can then be installed at the point-of-source and an effective monitoring tool can be used to determine the efficiency of these membranes, as well as being used in rural settings with other purification devices. This tool also needs to determine the presence of faecal pollution when free-standing at the water source or with routine water field tests.

According to the Department of Water Affairs: Republic of South Africa [15], South Africa provides potable water to 95.2% of its citizens, but UNEP [16] noted that the negative impact level on the inhabitants is severe if freshwater supply in South Africa is limited. It is therefore necessary to investigate solutions for effective water quality monitoring.

Biosensors could play an important role in monitoring water quality. After evaluating literature there seems to be a need for low-cost, portable sensors. These sensors could be used in various applications depending on the results obtained in development. Investigating various detection techniques could narrow the focus of research and development in the field. It could also motivate

more investment into research in water quality monitoring. Developing low-cost biosensors is a priority for many research institutions and companies. The lower the cost of the sensors, the higher the use of these types of sensors will be. If inefficient and costly laboratory equipment can be bypassed, water testing could become decentralised from conventional laboratories. It could also mean that people with very little technical training could test their own water for contaminants. In a similar way that the litmus test is used to determine pH at a very low cost and high accuracy, biosensors need to be developed that offer a similar solution to determining bacterial concentration in samples. A focus on low-cost, portable biosensors for detecting *E. coli* is thus an important topic to investigate.

1.3 Literature synopsis

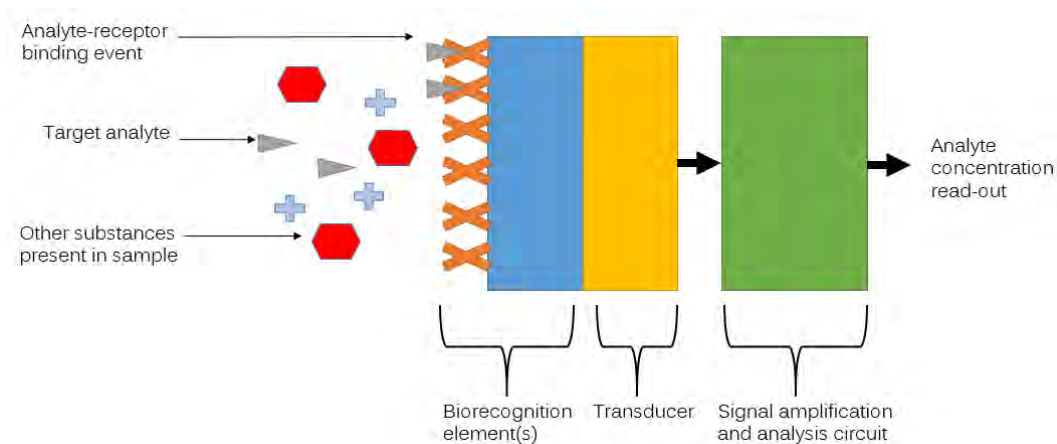


Figure 1.1: A biosensor model indicating the detection process

A study of the present state of relevant literature was conducted. The focus of the literature review was the use and definition of biosensors, bioreceptors, transducers and immobilisation methods. Water testing instrumentation and methods to detect bacteria were investigated, including a focus on fiber-optic and impedance based biosensors.

Figure 1.1 shows a typical biosensor model, indicating the most important elements of the sensor. A biosensor, as defined by Thévenot et al. [1], is "a self-contained, integrated device capable of providing specific quantitative or semi-quantitative analytical information" regarding the presence of a biological material. A biosensor can detect an analyte (the biological molecule or organism) in a sample. It does this by using a bioreceptor (the biorecognition element) or by using novel sensing mechanisms that detect certain bacterial

characteristics in a sample. The bioreceptor thus functions in two separate ways. It can function as a receptor that alters the ionic content of a sample, labels an analyte, or captures the analyte. It can also utilise certain unique features of bacteria, such as the insulative cell membrane in bacteria, ion channels etc. as detection method.

The analyte is dispersed in the sample among other molecules. The bioreceptor used must be highly selective to the specific analyte [17]. The transducer converts the signal from the analyte reacting with the biorecognition element and this signal is in turn interpreted by a signal analysis circuit [18]. The concentration of the analyte in the sample can then be calculated as the signal increases or decreases [18], depending on the biosensor's operational mechanism.

The most common bioreceptors used in biosensors are enzymes and antibodies [19, 20]. Enzymes are catalytic proteins that enhance certain reactions. In the case of biosensors enzymes typically consume/produce certain ions when reacting with analytes. This causes a change in the electron transfer characteristic of the sample. Antibodies, on the other hand, are proteins produced by the body to label foreign matter (antigens) [21]. Antibodies are used in biosensors as specific biorecognition elements due to their well defined binding and recognition domains [21]. There are various ways to attach these bioreceptors to surfaces. Immobilisation techniques vary and the method used depends on the biorecognition material and the operation principle of the sensor. This variation is due to the surface properties of the material, as well as the structure of the protein that is immobilised [22]. Different immobilisation methods have different properties depending on the adhesion method. Covalent attachment, crosslinking, self-assembled monolayers, and physical adhesion are some of the methods used to immobilise bioreceptors to inorganic surfaces/transducers.

The transducer governs the operation of a biosensor. A transducer is a device or material that converts one type of energy to another. The input and output forms of energy differ according to operation mechanism and method of detection. The types of energy input (used to classify transducers) include mechanical, magnetic, thermal, piezoelectric, optical and electrochemical [1]. The two types of transducers mostly studied and used are electrochemical and optical, due to their simple fabrication procedures, high sensitivities, robust sensing mechanisms, simple signal analysis circuits and relatively low cost [23].

Water testing is the eventual application of this project. Microbiological water quality, *E. coli*, water standards and *E. coli* testing methods are all relevant when discussing *E. coli* biosensors for water testing. Microbiological water quality is defined as the quality of water at the hand of knowing the amount of bacteria and viruses (among others) that are present. It is also relevant to

describe the amount of allowable contamination of bacteria in water to be safe for drinking. E.coli is the most significant indicator of faecal contamination of water supplies [24, 21]. E.coli can be found in the faeces of warm-blooded animals and humans [24]. When water is contaminated with E. coli, it infers that there may be other pathogens present. The concentration of E. coli can thus infer the safety of the water for consumption. According to South African [25] and World Health Organisation [26] standards the amount of E. coli in water to be completely safe for consumption should be 0 CFU/ml (colony forming units per milliliter). There must thus be no detectable amount of E. coli in any water sample. The concentration of E. coli in a sample can be determined by various methods.

Colony counting is the most common method of determining the concentration of bacteria in a sample. It has become the standard for counting bacteria. It entails plating bacteria samples of different dilutions onto nutrient plates. After incubating bacteria for 24 hours at 37.5 °C on nutrient plates, the colonies can be seen. When these are counted, and multiplied with the dilution factor, the amount of bacteria is known [27]. There are various laboratory instruments that can be used to count bacteria. Spectrophotometry is typically used to estimate the amount of bacteria in a sample. Light absorbance is used to quantify the concentration. This method also counts non-viable (dead) cells. This is not the ideal method for counting viable cells, but is useful when determining appropriate dilution factors.

Polymerase chain reaction (PCR) is a nucleic acid amplification technology used for bacterial detection [27]. It involves the exponential amplification of DNA from a single DNA strand. PCR can be used to determine the amount of bacteria, but may take 4-5 hours and requires specific training. PCR methods also count dead cells, seeing as DNA is not dependent on the viability of a cell.

An ELISA (enzyme-linked immunosorbent assay) is one of the most popular biosensors used in laboratories. An ELISA detects the presence of antigens using antibody-antigen-antibody binding. This results in a color change that can be used to quantify (using a photodiode) the amount of bacteria [28, 27]. Various water testing kits are commercially available. These are usually cumbersome, expensive and thus limited to laboratory use. Biosensors that detect E. coli with novel detection methods have been developed by research agencies and universities. Electrochemical and optical sensors are of particular interest.

Optical fibers have recently been used in novel ways to detect E. coli. Rijal et al. [29] used biconical tapered optical fibers to detect E. coli O157:H7. E. coli O157:H7 is a pathogenic strain of E.coli which is very dangerous if ingested. The fibers were tapered and then immobilized with antibodies [29] to capture bacteria. The pathogen was detected and then a pH buffer was used

to release it from the antibody surface, proposing the re-use of the sensor [29]. The sensor developed by Rijal et al. [29] was able to detect *E. coli* with a limit of detection (LOD) of 70 cells/ml. The LOD is a measure of the sensitivity of a sensor. Another unique method which uses a light source, optical fiber and a spectrophotometer was used to detect analytes [30] in a similar manner.

Light travels through an optical fiber by way of total internal reflection (TIR). Some of this light escapes the fiber and interacts with the environment (in the case of a bare fiber). The field in which the light interacts outside the fiber core is known as the evanescent field. DeMarco and Lim [31] developed an optical fiber-based biosensor to detect *E. coli* in ground beef samples using this evanescent wave. Others have also been successful in using optical fibers in bacterial detection [32, 33].

Novel electrochemical methods of detection, such as linear and non-linear impedance spectroscopy, have also been used to quantify bacteria. A linear electrical impedance spectroscopy (EIS) biosensor to detect *E. coli* O157:H7 was developed by Radke and Alocilja [34]. A high-density microelectrode array was immobilised with anti-*E. coli* antibodies [34]. The impedance change was measured and related to the concentration of the pathogen, resulting in a LOD of 10^6 CFU/ml [34]. Non-linear impedance spectroscopy has also proved successful in detecting bacteria. Above a certain excitation amplitude an electrochemical circuit starts to show non-linear behaviour. The non-linear effects caused by bacterial presence is not well known. These non-linear effects can be used to detect bacteria in water. Huzior et al. [35] and Ziemiecka et al. [36] used these effects to determine bacterial presence in teeth. The electrode material and geometry, as well as the excitation range and operation mechanism, need to be investigated for further non-linear AC impedance based biosensor development.

1.4 Objectives of the investigation

The following objectives have been set for the investigation:

- Describe the operation of a typical biosensor
- Find and evaluate different transducers and operation principles for a biosensor
- Compare South African and international standards for microbiological water quality
- Determine most appropriate biorecognition elements for an optical fiber biosensor to detect a wide range of *E. coli*

- Design an optical fiber based biosensor
- Develop and test a non-linear impedance based biosensor
- Develop and evaluate an operation method for a non-linear impedance based biosensor
- Develop a method in which to manufacture a low-cost optical fiber biosensor
- Develop a low-cost, robust testing method for an optical fiber biosensor
- Evaluate and compare the optical and electrochemical biosensors for use in a low-cost, portable biosensor
- Discuss possible applications for both optical fiber and non-linear impedance based biosensors
- Define a suitable high level biosensor prototype system layout
- Define the optimal specifications for a low-cost, portable biosensor
- Design a microfluidic platform to be used in a biosensor
- Discuss the EWOD operation principle in microfluidics, and evaluate its potential to be used in fluidic platforms
- Discuss the possible integration of the entire system, including microfluidic platform, into a biosensor prototype device

These objectives are the key focus areas of this investigation.

1.5 Contributions made

The main contributions made by this project are as follows:

- A review was supplied, concentrating on low-cost portable biosensors, their operation principles and the recent developments in detecting *E. coli*, using these types of sensors.
- Various *E. coli* testing methods were evaluated, which indicated that most methods are laborious and resource intensive. Many methods to detect *E. coli* are suitable for laboratory use, but there is a need for portable, low-cost sensors that can detect bacteria.
- A non-linear impedance biosensor was tested and evaluated. The method of determining bacteria using this sensor was developed, and bacteria was successfully detected (concentrations as low as 1.1×10^{10} CFU/ml were detected in less than 4 minutes). This sensor could be used in future testing and development of biosensor prototypes.

- A method to immobilise antibodies to optical fibers has been established.
- A fiber-optic sensor was manufactured that could detect *E. coli* during initial tests (3×10^7 CFU/ml was detected in less than 120 minutes).
- A low-cost testing method using optoelectronics and 3D printed parts was developed. This could be used for future biosensor testing and improvement.
- A non-linear EIS and fiber-optic biosensor were compared for use in a biosensing system. This could be used in further development and guide research efforts in the field.
- A simple PCB based microfluidic platform was designed. This could be used as a design for use in future portable sensing systems.
- The specifications and possible applications for a biosensor prototype, including a system model, have been provided. These could be used as the basis from which future biosensor development could start.

1.6 Summary

Low-cost, portable biosensors for the detection of *E. coli* in water is the focus of this thesis. Biosensors are reviewed, detailing the different types and operation principles. The detection of *E. coli* has been performed by various methods. Biosensors have been used to detect bacteria and these, including other detection methods, are reviewed. The theory concerning electrochemical impedance sensors, including non-linear harmonic sensing, is discussed. The evanescent wave principle is also described at the hand of a designed fiber-optic sensor.

Patterned electrode chips were tested for use in a non-linear EIS biosensor. *E. coli* was successfully detected using these chips. The method to immobilise antibodies as biorecognition element on fiber-optics was explored. The antibodies were successfully immobilised, imaged, and bacteria was adhered to the surface of these fibers. The fibers were successful in initial bacterial tests to detect *E. coli*. Recommendations on future development of a biosensor prototype was provided, including a system model, specifications and recommended applications.

Chapter 2

Literature Review

2.1 Biosensors

2.1.1 Introduction

Biosensors are devices that can detect biological molecules or microorganisms, such as bacteria, in a specific environment. Thévenot et al. [1] defines a biosensor as "a self-contained, integrated device capable of providing specific quantitative or semi-quantitative analytical information" regarding the presence of a biological material. They are used in various industries to detect biological analytes [37]. These industries include clinical diagnostics, bacterial and viral diagnostics, medical applications, process control applications, bioreactors, quality control applications, agricultural industries, veterinary medication development, pharmaceutical production, water treatment, mining industries, military defence and for environmental monitoring [38, 39]. In medical industries biosensors are used to help diagnose disease [22]. Pharmaceutical developers use biosensors to detect and test various compounds [22]. Biosensors also play a critical role in environmental monitoring [40, 5], where contaminants in water supplies cause many problems for the environment and could potentially harm humans [40, 41].

This section describes the way biosensors operate, as well as the relevant parts that make up a biosensor. This is done at the hand of a typical biosensor process model. Biosensors are capable of sensing a biological molecule's presence with the help of a biorecognition element [1], which is critical in many biosensor applications. The two most common biorecognition elements, enzymes and antibodies, are described as well as why they are used. Classification of biosensors is often done by the way in which they detect analytes, namely transducer types. The most frequently used transducer types, optical and electrochemical transducers [17, 42], are reviewed. Biorecognition elements are typically adhered to the surface of inorganic materials (used as transducers) through various immobilisation methods [40, 43, 42]. These methods are discussed, including a review of two common methods of immobilisation, namely physical adsorption and covalent attachment [17].

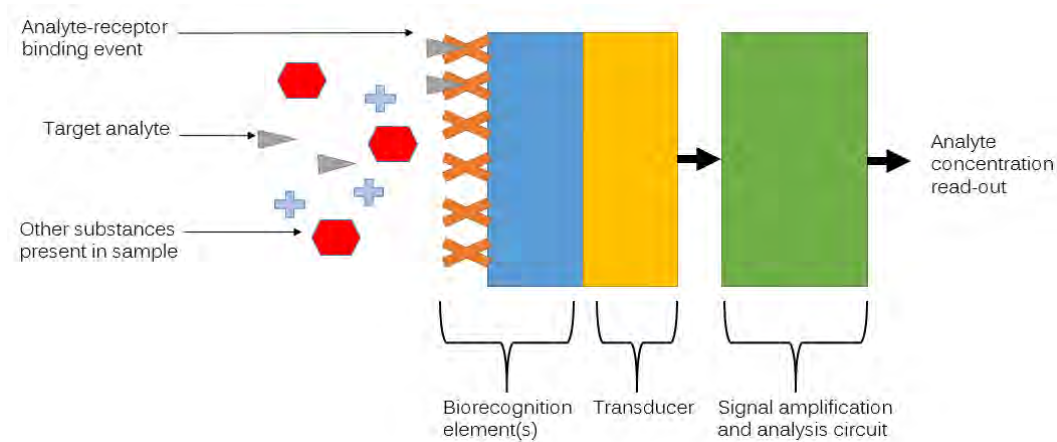


Figure 2.1: A biosensor model indicating the detection process

2.1.2 Biosensor model

A biosensor model is shown in Figure 2.1, indicating the basic process in which many biosensors operate. A biosensor can detect an analyte (the biological molecule or microorganism) in a sample using a bioreceptor (the biorecognition element). The analyte is dispersed in the sample, typically a fluid, among other substances. Receptors are typically immobilised onto a transducer surface [17]. The transducer converts the interaction of the analyte with receptor into a signal that is interpreted by the signal amplification and analysis circuit [17]. The concentration of the analyte in the sample can then be calculated as the signal increases or decreases [18]. This concentration is given as an output to the user in some format (electronic display, colour change etc.).

A biosensor is a complex system with many interactions and properties influencing its operation. The choice of analyte, environment of operation, biorecognition element interaction and transducer type are some of the most critical parts of the system to be considered [42].

2.1.3 Biorecognition elements

Biorecognition elements are biological substances used in biosensors to recognise analytes [44]. These elements allow accurate detection of specific analytes due to their inherent biological properties [44]. Biorecognition elements are typically protein-based [43] and transducer surfaces are often immobilised with these elements by various adhesion methods.

Biorecognition elements are found in nature, but are typically synthesised in laboratories [44]. These recognition elements can identify analytes in a few different ways. When a recognition element is used to bind to a target antigen, it is referred to as a bioaffinity recognition element [44, 22]. When a recognition

element is used to facilitate a chemical reaction, which may be detected with a transducer, it is referred to as a biocatalytic recognition element [44, 22]. Both bioaffinity and biocatalytic elements use the specificity of biological conjugates to create sensors that only recognise a desired analyte [17, 44]. The elements used in biosensors include enzymes, antibodies, aptamers, membrane pores and channels, ionophores and receptors [19, 20]. Antibodies (bioaffinity) and enzymes (biocatalytic) are mostly used as biorecognition elements due to their availability, well defined biomechanics and ability to specifically target certain antigens or molecules [42, 44] of interest.

2.1.3.1 Labelling vs non-labelling

Biorecognition elements can be used as labelling elements or in label-free biosensors. Labelled biosensors employ external methods of marking the analyte with for e.g. antibodies, fluorescent markers etc. This is done in a pre-processing step. This complicates the system, making it more expensive and time-consuming [22]. Non-specific signalling issues may also occur [22] due to labelling. Label-free sensors, on the other hand, do not require the labelling of target analytes. It excludes the use of a preprocessing step, and significantly simplifies biosensor development and lowers cost.

2.1.3.2 Important biorecognition element properties

Bioreceptors are adhered to surfaces via various methods referred to as immobilisation methods. These biorecognition elements are usually chosen on grounds of the analyte that is being detected [42], as well as the operating principle of the sensor. Certain properties, though, should be present in all biorecognition elements to ensure optimal operation and detection.

Biorecognition elements used *in vivo* (in a living organism) should always be biocompatible i.e. should not harm the host or invoke an immune response [45]. They should also be highly specific to the target analyte (a specific molecule, protein or antigen on the surface of an organism) [42]. The recognition element should invoke a binding event or reaction that is detectable by the specific transducer [42]. The properties of the recognition elements should also not change when it is immobilised onto transducer surfaces [42]. Biorecognition elements should have a high affinity for the target and should form a relatively stable complex with the target [42] when binding with it. For these reasons, biorecognition elements are typically engineered for their size, specificity, affinity, stability, and charge characteristics [46], all of which have an effect on the performance of the biosensor.

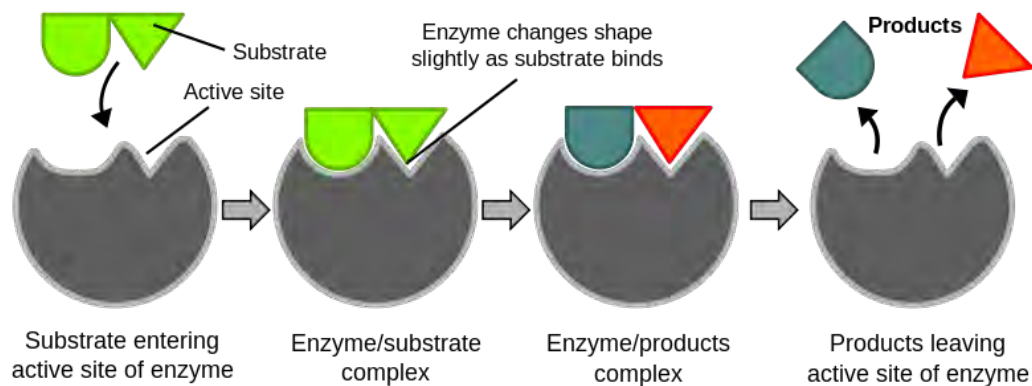


Figure 2.2: The induced fit model of a typical enzymatic reaction

2.1.3.3 Enzymes

An enzyme is defined as a biological substance that acts as a catalyst to bring about a specific biochemical reaction [44, 47, 1]. Enzymes are mostly used in biocatalytic biosensors [46] where certain reactions will cause interference with a transducer, that can in turn be related to the concentration of the specific analyte.

Figure 2.2 shows the induced fit model and the typical enzymatic reaction process. Enzymes are highly specific to the target (or better known as the substrate) due to the active site on the enzyme surface. This active site only accepts substrates of a certain shape and type, also known as the "lock and key" effect. When this substrate binds to the active site, a reaction occurs where the substrate is changed in a certain way [1]. The products are then released, and the enzyme is re-used [1]. These products and their reactions are typically used to detect analytes in the sample [1, 44], and their reaction rates are used to quantify the concentration of the analyte. Biosensors using enzymes can achieve high sensitivities and allow for a lower detection limit due to the efficient catalytic activity that enzymes provide [19].

Enzyme immobilisation on transducer surfaces, such as electrodes, have to result in an efficient electrical communication interface [48]. The electrode surface must retain or improve the biocatalytical effect of the enzyme [48]. Various materials have been successfully immobilised with enzymes including carbon nano tubes (CNTs) [49], semi-conductive materials such as zinc oxide (ZnO) nanowires [48], optical fibers [50], metal electrodes [51], etc. The use of enzymes as a biorecognition element depends on the biological material that needs to be detected, as well as the operation principle of the sensor.

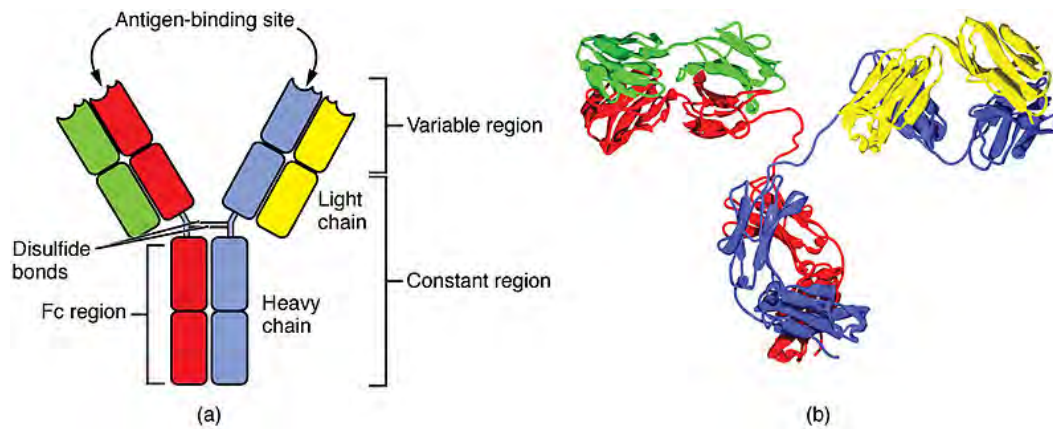


Figure 2.3: Antibody illustration indicating (a) the various regions and (b) the three-dimensional protein structure [52]

2.1.3.4 Antibodies

Antibodies (Abs) are proteins produced by mammals as part of their immune defence system against foreign matter [21]. They possess highly specific binding and recognition domains that can be targeted to specific antigens [21]. Figure 2.3 shows an illustration of an antibody, indicating its heavy and light chains, as well as its 3-D protein structure. There are five types of antibodies namely IgG, IgM, IgA, IgD and IgE. They are classified according to the heavy chain region of the antibody. The antibody type most commonly used in biosensors are IgG antibodies.

Antibodies are the most used affinity biorecognition elements. Others include aptamers, nucleic acids, and polymer antibodies [46]. They are mostly used, due to the simplicity of their biomechanics as well as cancelling pre-processing steps that are needed in for eg. deoxyribonucleic acid (DNA) and ribonucleic acid (RNA) based biosensors [22].

Antibodies can be subdivided into monoclonal and polyclonal antibodies. Table 2.1 shows a comparison between monoclonal and polyclonal antibodies. The use of both monoclonal and polyclonal antibodies are applicable to biosensors. The immobilisation method, analyte type and response must all be considered when selecting an appropriate antibody [53]. It is recommended by the World Health Organisation [21] that monoclonal antibodies be used in biosensing devices. Polyclonal antibodies, on the other hand, may produce better results when multiple epitopes on an antigen must be identified, or when the sensor must be more robust. Antibody immobilised sensors can be stored and transported at room temperature, but are very sensitive to temperature and humidity during immobilisation [54]. The denaturation of the proteins are also of concern, and thus storage environments must be carefully considered.

Table 2.1: A comparison between polyclonal and monoclonal antibodies [53]

Polyclonal	Monoclonal
Inexpensive to produce	Expensive to produce
Recognises multiple epitopes on any one antigen	Recognises only one epitope on an antigen
Can amplify signal from target protein with low expression level	Less likely to cross-react with other proteins
More tolerant to minor changes in the antigen	Highly reproducible results due to higher specificity
Multiple epitopes provide more robust detection	Higher homogeneity than polyclonal antibodies

2.1.4 Immobilisation methods

Immobilisation refers to the attachment kinetics of biorecognition elements to transducer surfaces [42]. Correct and effective immobilisation is important in creating high specificity and sensitivity in sensors [42]. The most popular methods of immobilisation include physical adsorption, covalent attachment and membrane entrapment, amongst others [17]. Physical adsorption and covalent linking techniques are mostly used due to their simplicity, well understood kinetics and bonds that are formed during immobilisation processes.

2.1.4.1 Physical adsorption methods

Adsorption refers to the adhesion of molecules to a transducer surface. The adhesion can be attributed to physical and chemical forces acting between the molecules and the solid surface [17]. The simplest form of immobilisation is physical (electrostatic or hydrophobic) interactions [22]. This is due to the fact that the transducer surface does not have to be prepared with other chemicals for immobilisation. Physical adsorption typically results in weak bonds formed between the molecule and the surface, resulting in a much smaller surface area being immobilised. A smaller area of immobilisation results in less interaction between the recognition elements and the transducer surface. The lower level of interaction between antigen and recognition element lowers the sensitivity of the sensor. These methods simplify the manufacturing process, but may result in poor sensor performance.

2.1.4.2 Covalent attachment

Covalent attachment is an effective immobilisation technique. Covalent bonds are strong and may result in good transducer coverage in recognition elements. Covalent attachment refers to the bonds being formed between the molecules on inorganic surfaces (transducers) and on recognition elements (e.g. antibodies).

Figure 2.4 shows an antibody structure, indicating the functional groups.

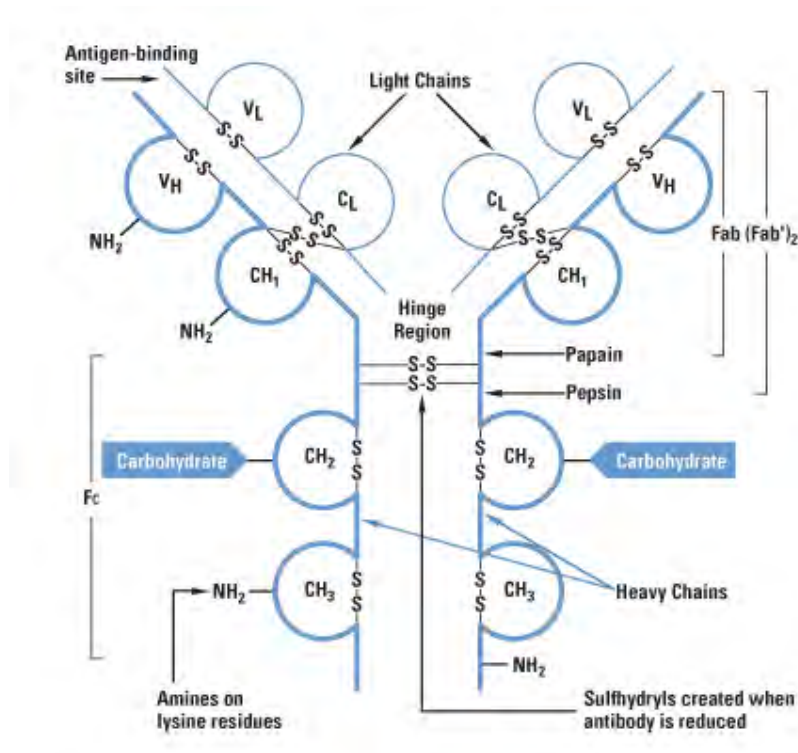


Figure 2.4: Antibody structure indicating the functional groups for covalent attachment [55]. Adhesion can occur between any of these groups and a range of crosslinking agents.

These groups can be used to create covalent bonds with inorganic surfaces. These conjugations are possible between the amino, carboxyl, aldehyde, or sulfhydryl groups [47] of the antibody. This forms a much stronger bond between the molecule and the solid surface than electrostatic or hydrophobic bonds. It typically requires surface preparation of the transducer, but results in much higher immobilisation efficiency (higher surface area covered) and higher sensor sensitivities. Immobilisation techniques are dependent on the physical and chemical characteristics of the transducer and the environment in which one seeks to operate the biosensor [22].

2.1.5 Transducers

A transducer is defined as a device that converts a signal from one type of energy to another. In the case of biosensors the amplification and transfer of the signal can also be facilitated by the transducer. The types of energy transduction include mechanical, magnetic, thermal, piezoelectric, optical and

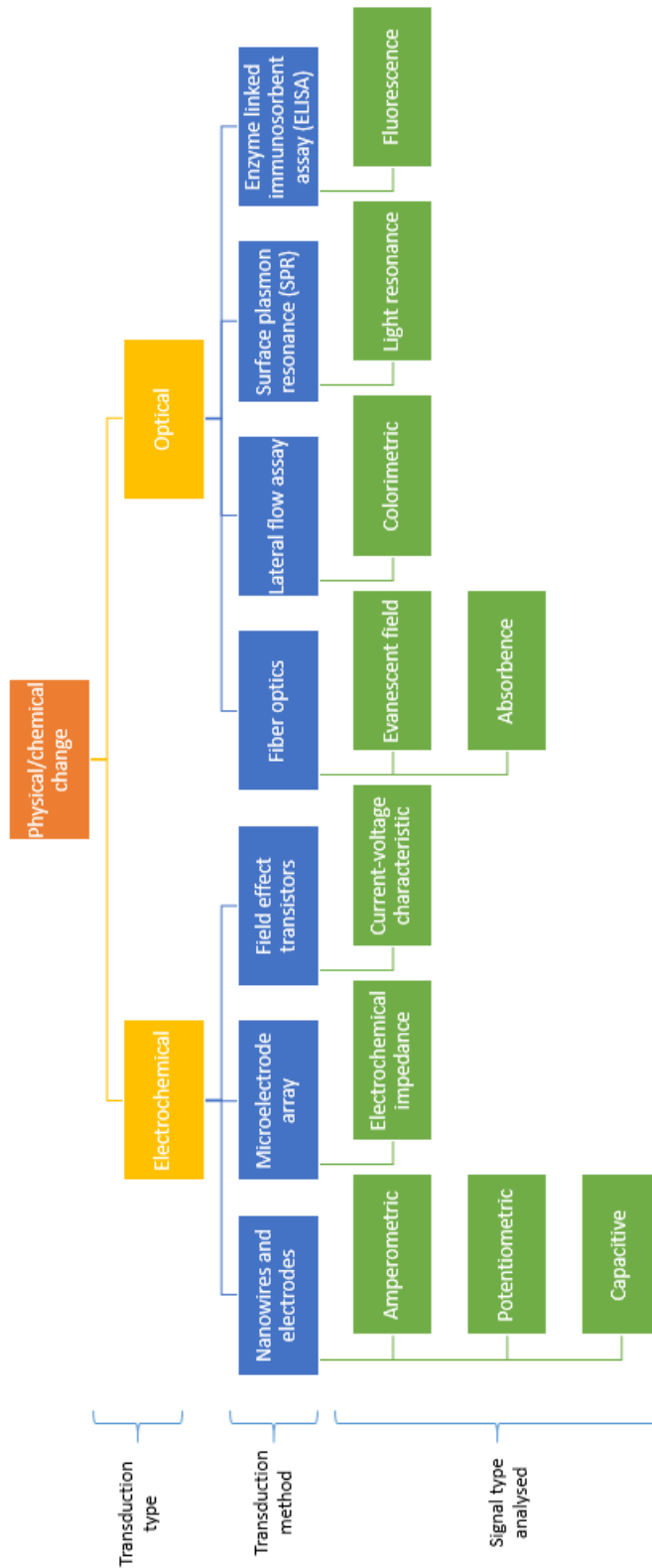


Figure 2.5: Chart indicating transducer types, methods and signals detected in biosensors

electrochemical [1]. The two types of transducers mostly studied and used are electrochemical and optical. This is due to their simple fabrication procedures, high sensitivities, robust sensing mechanisms, simple signal analysis circuits and lower cost [23]. Figure 2.5 shows a hierarchical structure of the transducer types (electrochemical and optical), the transducer method used in each type, and the type of signal that is analysed.

2.1.5.1 Electrochemical transducers

Electrochemistry is the field relating electricity and chemical reactions. Electrochemical transducers thus detect the electrical changes occurring in solutions. These electrical changes may occur due to certain reactions taking place (e.g. catalytic reactions due to enzymes) or due to electrical energy being applied to the system via electrodes. The electron transfer kinetics of reactions is very important in electrochemical biosensors. The sensors try to quantify the analytes by analysing the electrical characteristics of the electrochemical cell.

A bioelectrochemical reaction occurring between the bioreceptor and analyte may cause a change in current, potential or resistivity between electrodes [17]. Electrochemical biosensors can thus be categorised according to which type of signal is measured: potentiometric, amperometric, conductometric or capacitive [1]. Potentiometric sensors detect voltage signal changes, amperometric sensors detect current or charge transfer changes, conductometric sensors measure a change in resistance across electrodes or a surface and capacitive sensors detect a change in the dielectric constant of the material and sample being analysed [17].

Certain important characteristics of electrochemical biosensors include the detection mechanism, the selection of a bioreceptor that is specific to the target analyte, the correct immobilisation method and appropriate transducer selection [17]. The performance of the sensor is dependent on the electrode material, the surface modification of the electrode and the geometrical dimensions [17, 43].

Electrochemical impedance spectroscopy (EIS) techniques have been used in many biosensor designs, exploiting the characteristics of the interaction between electrodes and solutions. Three unique methods are highlighted due to their simple manufacturing techniques, simplicity of operation and relevance to low-cost sensors. These three methods are interdigitated microelectrodes (IMEs), capacitive sensors, and field effect transistor (FET) sensors.

Figure 2.6 shows an IME sensor diagram. These microelectrodes are manufactured from various materials, including platinum, titanium, aluminium,

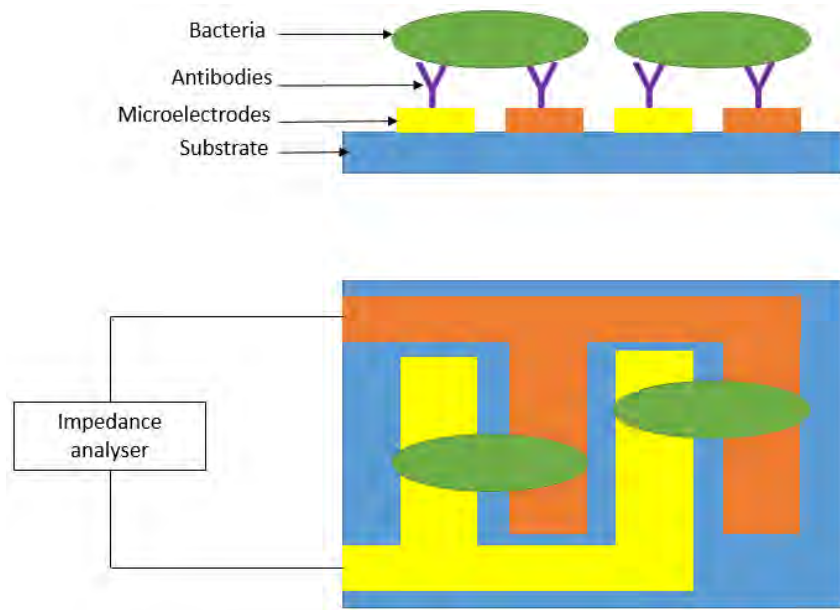


Figure 2.6: Interdigitated microelectrode biosensor diagram. Bacteria binds onto the antibodies, creating links between the electrodes. The bacteria can be quantified by measuring the impedance over the electrode array.

copper, gold, etc. The dimensions are usually in the micrometer range. Bioreceptors are immobilised onto these electrodes. When a target antigen binds to the receptor (an antibody in Figure 2.6), a bridge is formed between the electrodes. This causes a change in impedance due to a bioelectrical contact being formed between the electrodes. This can be measured using EIS. EIS is a method by which to characterise electrochemical cells by measuring the impedance while a voltage is applied over the electrodes [17, 22]. The concentration of the analyte can be quantified by comparing impedance spectra.

Capacitive sensors [56] operate in a similar manner, but by using different electrode geometries. When a reaction occurs in the solution, there is a change in the electric double layer at the surface of the electrodes [57]. An electric double layer schematic is shown in Figure 2.7. When an electrode has a certain applied potential, ions in the fluid are attracted to the surface. This layer of ions which adheres to the surface of the electrode, in turn, attracts ions of the opposite charge. This forms the electric double layer, which has a measurable capacitance. When this interfacial capacitance is modified by a binding event, a change in capacitance can be observed [58]. This may be due to charge transfer from the solution to the electrode, or vice versa, and by the electrochemical change that may occur in the solution due to redox reactions. This change in capacitance is used to quantify the concentration of the analyte.

Field effect transistors (FETs) have been used in electronic circuits for many

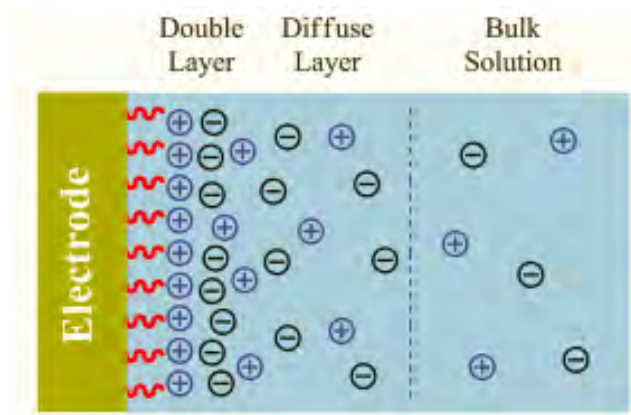


Figure 2.7: Electrical double layer schematic [22]

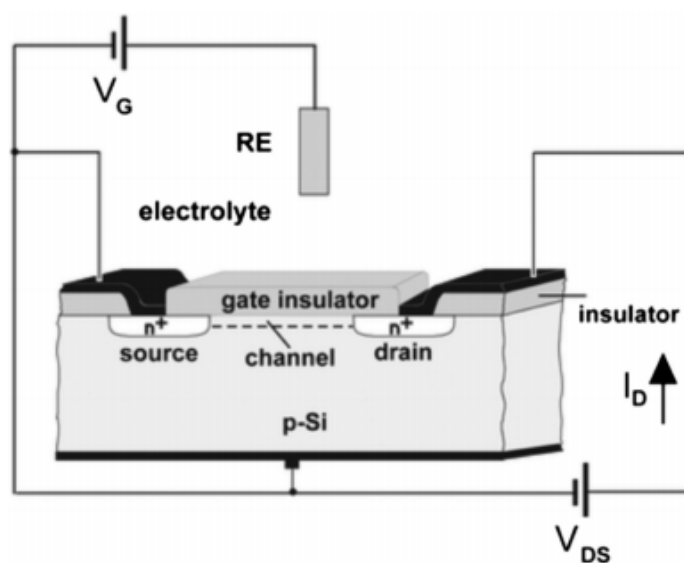


Figure 2.8: Field effect transistor schematic [22]

years. The current-voltage characteristics of a FET can be manipulated to create low-cost biosensors. This is done by modifying the gate surface of a FET. The interaction of biomolecules with the gate surface will result in a change in the current-voltage characteristics of the transistor. Figure 2.8 shows a FET schematic, indicating the positions of the source, drain, gate, reference electrode (RE), gate voltage (V_G), drain-source voltage (V_{DS}) and drain current (I_D). The I-V characteristic curve of the FET changes as the concentration of the target antigen changes. The method to analyse signals in this electrochemical circuit is relatively simple and FETs can be produced at a large scale using a mature electronic technology.

2.1.5.2 Optical transducers

Optical transducers use the properties of light to detect analytes. This is done in various ways and with various types of optical transducers. Optical transducers can be classified according to the type of light used and how it interacts with the analyte [59]. These include absorbance [60], reflectance, fluorescence [60, 27], chemiluminescence, evanescent wave, and bioluminescence optical sensors [61, 60]. There are other interesting methods of optical detection relating to this project, namely fiber optic sensors, lateral flow assays (LFAs), surface plasmon resonance (SPR) devices and enzyme-linked immunosorbent assays (ELISAs) [62]. There are also many different types of optical transducers used in innovative sensors [61, 60]. These types of sensors are discussed, because they can have the potential to be produced at a relatively low-cost, they can be simple to manufacture and have well established operation principles.

Fiber-optic biosensors (FOBs) operate by using light to interact with target

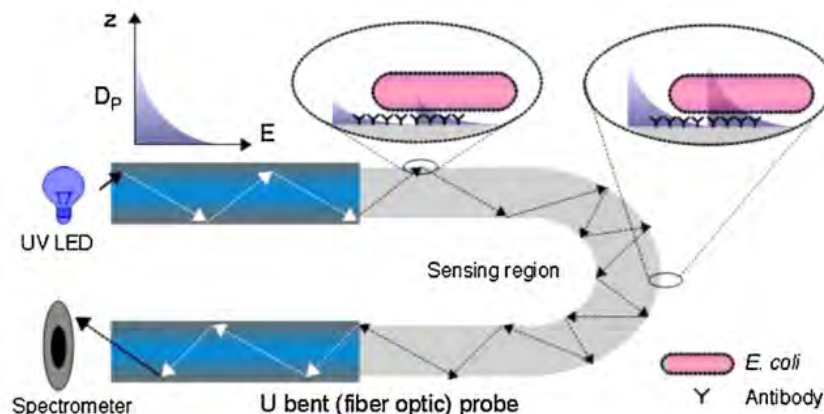


Figure 2.9: U-bent fiber-optic biosensor indicating the evanescent wave modulation during bacterial detection in the fiber [63]

antigens. Evanescent wave modulation is a promising method of employing fiber optics to detect analytes. Figure 2.9 shows a diagram of a fiber-optic biosensor developed by Bharadwaj et al. [63]. The light enters the fiber and is transported due to the total internal reflectance (TIR), the principle by which light travels in optical fibers. An evanescent wave, which penetrates the core of the fiber (indicated by D_P), interacts with an antibody immobilised surface. When more bacteria bind with the surface of the fiber the light intensity is altered and monitored by a spectrometer [63]. The fiber is U-bent to increase the penetration depth of the evanescent wave [63]. This can, however, be simplified by not bending the fiber and by using simpler electronics to monitor changes in the light intensity. Fiber optic biosensors can easily be miniaturised and the development of integrated biosensors onto portable devices is relatively

simple [59, 60, 64].

A lateral flow assay uses capillary forces to move liquid samples to a de-

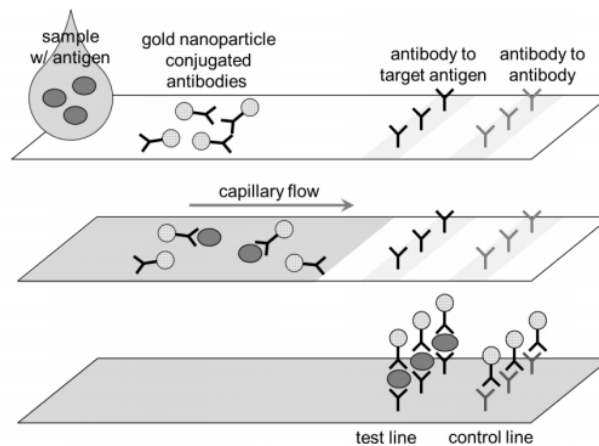


Figure 2.10: A lateral flow assay (LFA) [28]. Colour changes are used to indicate the presence of analytes.

tection region on the assay. The most famous LFA is the home pregnancy test. Figure 2.10 shows an example of an LFA and its detection method. LFAs are usually conjugated with a bioreceptor and a control line. When the analyte binds with the receptor, a colour change occurs indicating a positive result (due to fluorescent markers in the sample or the assay). This is a simple method for binary biosensor tests. The conjugation of the fluorescent marker, however, complicates the sensor. Quantification of the concentration can also be achieved when the assay is imaged (e.g. with a cellphone). The colour intensity of the binding event can be related to the concentration. This also complicates the system. Conjugation of bioreceptors to the assay may also require specialised equipment. Even though this technology has the possibility of enabling very low-cost sensors, the rapid development and testing of LFAs may not be feasible.

Figure 2.11 shows a schematic of a surface plasmon resonance (SPR) biosensor. SPR is a method in which the refractive index of a surface changes when an analyte binds onto the surface [59]. As light enters through a prism, the adhered analyte causes a shift in the light spectrum [59]. This shift can be detected by an optical detector (photodiode or phototransistor) [59]. This shift in spectrum can then be quantified and related to the concentration of the analyte.

Enzyme-linked immunosorbent assays (ELISAs) are a well established optical biosensor technology. ELISAs use antibodies and enzyme assays to provide

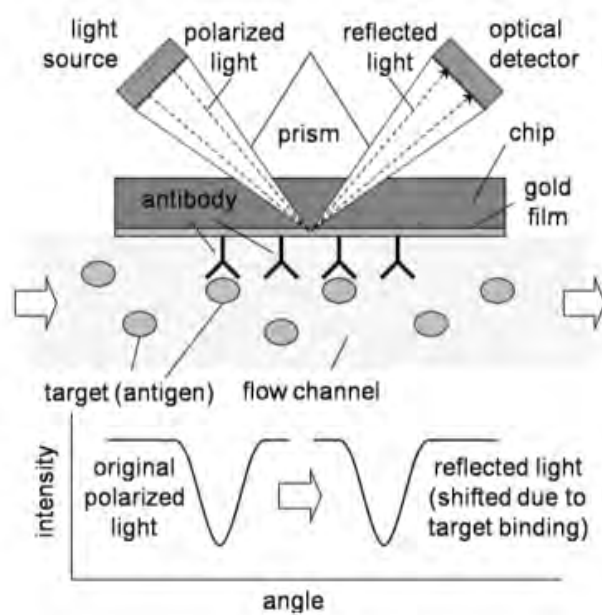


Figure 2.11: Surface plasmon resonance sensing mechanism [28]

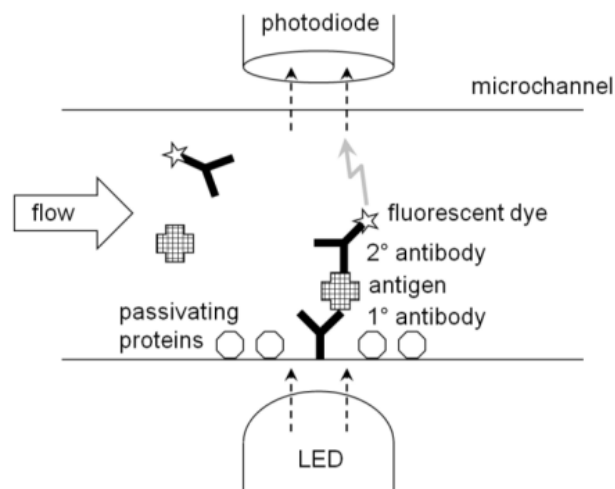


Figure 2.12: Enzyme-linked immuabsorbent assay (ELISA) schematic [28]

colorimetric results, as shown in Figure 2.12. An ELISA detects the presence of antigens using antibody-antigen-antibody binding, which results in a color change that can be quantified. A photodiode detects the color change and this can in turn be related to the concentration of a pathogen in a sample [28, 27]. ELISAs are typically used in laboratory setups, where commercial ELISAs are well established. The method of detection (using antibody-fluorescence conjugates) is still relevant, and may be simplified to create low-cost, portable optical biosensors.

2.1.6 Conclusion

Biosensors have been designed and developed for many applications. Various industries utilise the unique properties of biosensors and research institutions continuously develop new methods of detection. The basic biosensor operation principle was discussed at the hand of a simple biosensor model. The biorecognition elements used (focussing on enzymes and antibodies) were described. These receptors are continuously being synthesised and improved upon for various applications and different transducers. Immobilisation of these biorecognition elements are dependent on the choice of biorecognition element and properties of the transducer surface. Biosensors can be classified according to these transducer types. The review focussed on the use of electrochemical and optical transducers, due to their simplicity and well understood operation mechanisms. Examples of each method were given, focussing on the potential for developing low-cost and portable sensors. All these factors need to be considered when designing and developing a low-cost, portable biosensor.

2.2 Escherichia coli detection in water

2.2.1 Introduction

Escherichia coli (*E. coli*) is a well known bacterium that has been extensively studied in universities and research institutions worldwide. *E. coli* is of particular importance in water supplies. When *E. coli* is present in water, it can cause illness when this water is consumed [65]. *E. coli* also infers that the water may be polluted with other harmful pathogens [2, 3]. The rapid and low-cost detection of *E. coli* is thus of critical importance. Many international and local standards have been established to guide water services in the detection of this bacteria. These standards are only effective when appropriate testing procedures are conducted at regular intervals. This section will explore the relevant literature concerning microbiological water standards used. It describes the established methods of *E. coli* detection and refers to literature where novel biosensors have been used to detect bacteria.

2.2.2 Microbiological water standards

Pesticides, hormones, phenols, surfactants, toxins, metals and nitrate all pose a threat in drinking water supplies when the concentrations exceed safe limits for consumption [5]. It is important to monitor all of these compounds. Microbiological water quality, however, refers to the amount of microbes that are present in water. This includes bacteria, viruses, protozoa and helminths. *E. coli* bacteria count gives an indication of the general quality of the water, and is the most specific indicator of faecal contamination [2, 3]. According to the SABS [25] *E. coli* is the definitive, preferred indicator of faecal pollution and

the focus will thus be on this bacterium and the role it plays in water quality.

The other pathogens are also critical to monitor, but the detection of *E. coli* infers that other pathogens are present. Therefore it is of critical importance to monitor and detect the *E. coli* levels in water supplies to indicate when water may have been exposed to other harmful pathogens [11]. Most macro water distribution systems treat water with chlorine and other disinfectants, which kill most of the bacteria. At the point of source, however, this is not the case. Pathogenic *E. coli* (O157:H7) can lead to diarrhoea [65]. This is especially harmful to children and the elderly who have compromised immune systems and lack formal medical care (in developing nations) in case of infection. Many *E. coli* strains are not pathogenic but may still be present in water supplies.

The most appropriate guideline for microbiological water quality occurs in the specifications as set by national and international standards. The South African Bureau of Standards is responsible for aligning national standards for drinking water quality with international regulations. The SABS has to update the drinking water standard [25] every 5 years [66]. To be SABS [25] compliant water must be considered safe to consume over a lifetime without any adverse health effects [66]. The standards specify the amount of allowable contamination and methods by which water determinants must be tested with regard to trueness, precision and the limit of detection [66].

In 1984 and 1985 the first international guidelines for drinking water quality was published by the World Health Organisation (WHO) [24]. The WHO [26] stipulates the following risk standards for *E. coli* concentrations, as shown in Table 2.2. It must be noted that colony forming units (CFU) are a standard for counting and reporting the amount of microorganisms grown on a nutrient plate from a water sample [67]. This guideline can be used as a reference

Table 2.2: The World Health Organisation (WHO) *E. coli* concentration and risk guideline [26]

E. coli concentration (CFU/ml)	Risk
0	None
1 - 10	Low
10 - 100	Intermediate
100 - 1000	High
> 41 000	Very high

point for user interfaces (in electronic devices) and for indicating risk levels associated with consuming water that has been tested. It can be seen that the most appropriate concentration for safe drinking water consumption is 0

CFU/ml. The other concentrations can be seen as a guideline for the indication of the microbial quality of the water. These can also be used to specify the limit of detection for a sensor. The limit of detection (LOD) is defined as the smallest concentration that can be determined in a sample volume. The LOD of a sensor is the prime indication of the sensitivity of the sensor. A very low LOD will be able to determine if even a single CFU is present in a water sample. This can be a challenge for determining concentrations in large volumes of water, which is usually the case when working with water systems. When *E. coli* is unevenly spread across for example a lake, river or well, the capture and testing of small volumes will not give an acceptable concentration with which to judge the quality. Multiple samples will have to be tested in a timely fashion, which increases the need for fast, accurate biosensors that can detect *E. coli*.

SANS 241-1:2011 [25] and SANS 241-2:2011 [68] are the latest South African National Standards for drinking water. SABS [25] specifies that *E. coli* counts must be 0 CFU/ml for drinking water to be safe. SABS [68] specifies the sampling frequency and calculations for water supply networks and the necessary limits for compliance with the standard. The preferred testing methods for the microbiological quality of water are specified in SANS 5221 [69]. The two standard test methods specified by the SABS [69] for *E. coli* detection are the membrane filtration and colony counting methods. There are, however, other laboratory instruments, immunoassays, polymerase chain reaction (PCR) devices and biosensors for the detection of *E. coli* in water [65].

2.2.3 *Escherichia coli*

In biology a microorganism refers to a virus, bacterium or fungus. A bacterium is a unicellular microorganism which has cell walls, but lacks organelles and an organised nucleus. A strain is a genetic variant or subtype of a microorganism. Different strains of the same species can have different pathogenic properties. *E. coli* is a gram-negative, non-spore forming, rod-shaped bacterium [24]. Figure 2.13 shows an electron micrograph of a group of *E. coli* bacteria. *E. coli* typically have lengths of about 2 μm . Figure 2.14 shows a diagram of a single *E. coli* bacterium, indicating the structure of the organism. *E. coli* can be found in the faeces of warm-blooded animals and humans [24]. The ingestion of *E. coli* in an excessive amount will lead to gastro-intestinal disease. This can be lethal, especially to children under the age of five and the elderly [24, 70]. *E. coli* strains are categorised according to pathotype, six of which cause diarrhea: enteropathogenic, enteroinvasive, enterotoxigenic, verocytotoxin-producing, diffusely adherent and enteroaggregative [71]. Temperature, oxygen levels and acidity (pH) levels greatly influence the survival and growth of *E. coli* [72].



Figure 2.13: An electron micrograph of *E. coli* bacteria ($10\,000 \times$ magnification)

2.2.4 Established methods for *Escherichia coli* detection

2.2.4.1 Plate counting and membrane filtration

Bacteria is quantified by the amount of colony forming units (CFU) that are present within a sample. This can be determined by growing bacteria on a nutrient plate, counting the amount of viable colonies, and calculating the concentration in the sample [27]. Figure 2.15 shows an agar nutrient plate with *E. coli* colonies grown on top. Each "spot" is counted as a viable colony. Depending on the level of dilution, these colony counts can be related to the concentration of the original sample. This is the most reliable method to determine the amount of CFU in a sample.

Plate counting is seen as the golden standard for reporting bacteria colony counts (where the golden standard refers to the most accurate test, and a benchmark for determining CFU counts). This method, however accurate, is very time consuming [27]. To allow the colonies to grow, tests can take up to 24 hours [65]. The bacteria can grow at room temperature, but are usually grown in a 37°C environment. Plate counting also requires nutrient plates, microscopes and trained personnel, all of which increase the cost of determining the presence of bacteria in a sample.

Membrane filtration methods are similar to plate counts. By filtering a sample through a specific membrane, the amount of colonies can be grown and counted on the membrane [69]. This also requires specialised equipment, nutrient plates

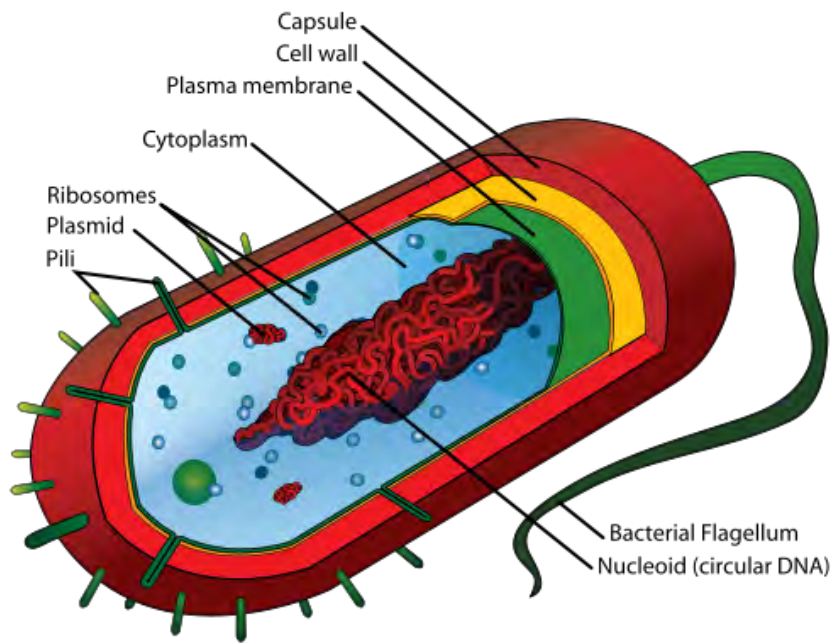


Figure 2.14: An *E. coli* bacterium diagram

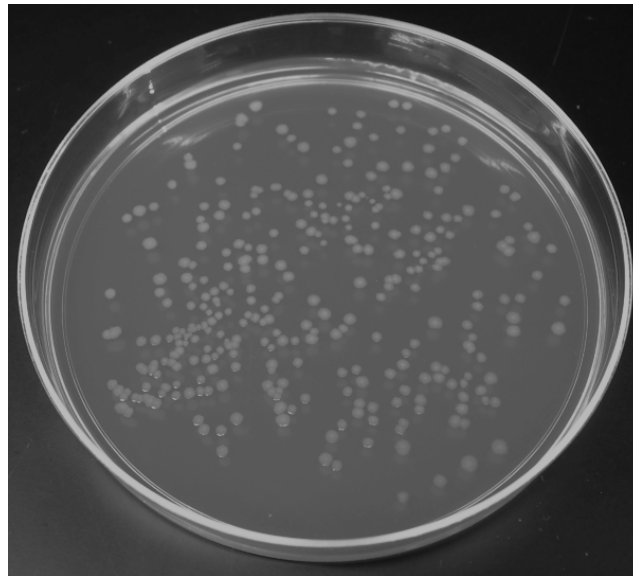


Figure 2.15: *E. coli* colonies grown on an agar nutrient plate

and time (24 hours). These methods (plate counting and membrane filtration) are thus laborious. Another disadvantage is that the concentration of *E. coli* at the source can not be determined in real-time. These methods must, however, be used to determine biosensor performance.

2.2.4.2 Polymerase chain reaction

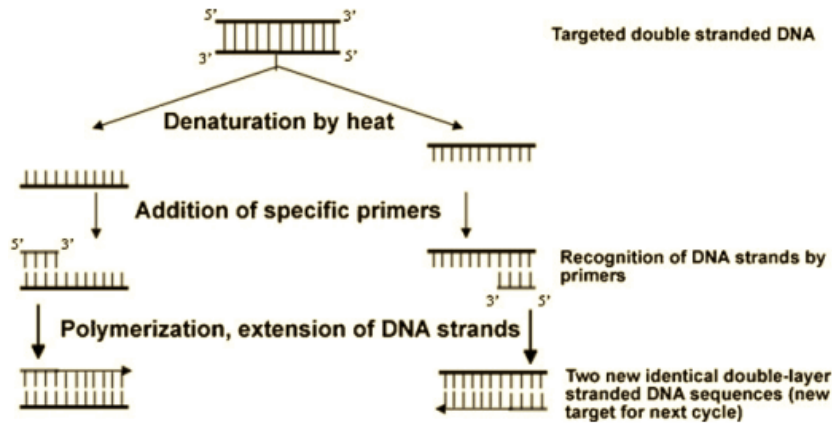


Figure 2.16: Polymerase chain reaction (PCR) cycle representation [27]

Polymerase chain reaction (PCR) is a nucleic acid amplification technology used for bacterial detection [27]. Figure 2.16 shows a schematic representation of a PCR cycle. Deoxyribonucleic acid (DNA) is extracted and purified by heat denaturation [27]. Each cycle, with the addition of primers and polymerisation, extend the DNA strands [27]. This causes an exponential amplification of the DNA [27]. A disadvantage of PCR is that the system can not discriminate between live and dead cells, because DNA is always present [27] in the biological matter. It is, however, less time consuming than culturing techniques (4-5 hours), depending on the type of PCR device used [27]. Theoretically PCR has a sensitivity of 10-100 CFU/ml [28], but this method of analysis is best suited to laboratory applications.

2.2.4.3 Enzyme-linked immunosorbent assay

There are various immunology based detection methods employing antibodies, enzymes, etc., in the detection of pathogens. The Enzyme-linked immunosorbent assay (ELISA), however, is the most established technique in biosensing [27]. ELISAs use antibodies and enzyme assays to provide colorimetric results, i.e. an ELISA detects the presence of antigens using antibody-antigen-antibody binding, which results in a color change that can be quantified. A photodiode detects the color change and this can be related to the concentration of an antigen in a sample [28, 27]. ELISA has been utilised with anti-E.coli antibodies to detect up to 32 CFU/ml of E.coli O157:H7 (a pathogenic strain of E. coli) in a sample [73].



Figure 2.17: Potaflex water testing kit [74]

2.2.4.4 Portable water test kits

There is a range of portable potable water testing kits on the market. A set of these test kits was developed by Wagtech WTD [74]. They can be used to test for a variety of water quality parameters, including microbiological quality [74]. The "Potaflex" kit, as seen in Figure 2.17, which can be used to test for the microbiological quality of the water, was designed specifically for laboratory use [74]. Wilhelmsen Ships Service [75] developed another potable water test kit which can test for total bacteria count accurate to 100 CFU/ml. It can also be used to specifically test for *E.coli* and *Legionella* [75], another pathogenic bacterium. This kit contains various instruments, chemicals, incubators and UV lights and can also be used to test for turbidity, pH, chlorine, and water colour [75].

These kits can determine *E.coli* concentrations at a relatively low level, but are often bulky, expensive and difficult to handle in a field setting. They are also time-consuming and the results can not be interpreted electronically.

2.2.5 Biosensors for *Escherichia coli* detection

Biosensors show numerous advantages to other established methods of detection [17]. This includes the measurement of non-polar molecules, high speci-

ficity due to the use of biorecognition elements and short response times [17]. The advantages of high specificity and sensitivity can be integrated to create highly robust, low-cost, and portable devices. Real-time monitoring of the microbiological quality of water sources is made possible with the use of biosensors, and can thus be used in advanced water treatment processes to monitor efficiency and degradation of filters/membranes. Various kinds of biosensors have been developed by research groups and universities that detect *E. coli* in water samples.

Bridle et al. [76] reviewed microfluidic based biosensors and lists the relative literature for various kinds of sensors for the detection of *E. coli*. Immunosensors for the rapid detection of *E. coli* O157:H7, for use in the meat processing industry, was reviewed by Tokarsky and Marshall [77]. Costa et al. [78] reviewed low-cost biopaper sensors for use in pathogen sensing, showing promising examples of pathogen sensing using bio-conjugated paper sensors that can be mass produced at a very low cost. Advances in cellphone-based devices for the detection of pathogens was reviewed by Vashist et al. [79]. Sicard and Brennan [80] presented a summary of current methods for immobilisation of biorecognition elements onto bioactive paper for use in environmental monitoring and discussed a few examples of biosensors using these novel and low-cost methods. These reviews detail various biosensors and the way they operate. The following section will review electrochemical, optical and biopaper biosensors used to detect *E. coli*. The focus has been on sensors that could be produced at a low-cost, provide high sensitivity and could easily be integrated into portable systems.

2.2.5.1 Electrochemical biosensors

A good example of a biosensor based on EIS was developed by Radke and Alocilja [34]. A high-density microelectrode array was manufactured and immobilised with polyclonal antibodies [34]. *E. coli* cells bonded with the antibody, as can be seen in Figure 2.18, creating a reduction in impedance [34]. The impedance change was then related to the concentration of the pathogen resulting in a detection limit of 10^5 CFU/ml [34].

García-Aljaro et al. [81] reported on a carbon nanotube (CNT) chemiresistive biosensor for the detection of *E. coli* O157:H7. Single-walled CNTs were functionalized with antibodies, and an increase in the resistance of the device was observed with the addition of the pathogen [81]. A LOD of 10^5 CFU/ml for whole cells was achieved [81]. This sensor is an example of the innovative use of carbon nanotubes in biosensors.

Other nanotechnologies have been employed in the development of biosensors. A system was developed by Teng et al. [82] for the detection of *E. coli* using

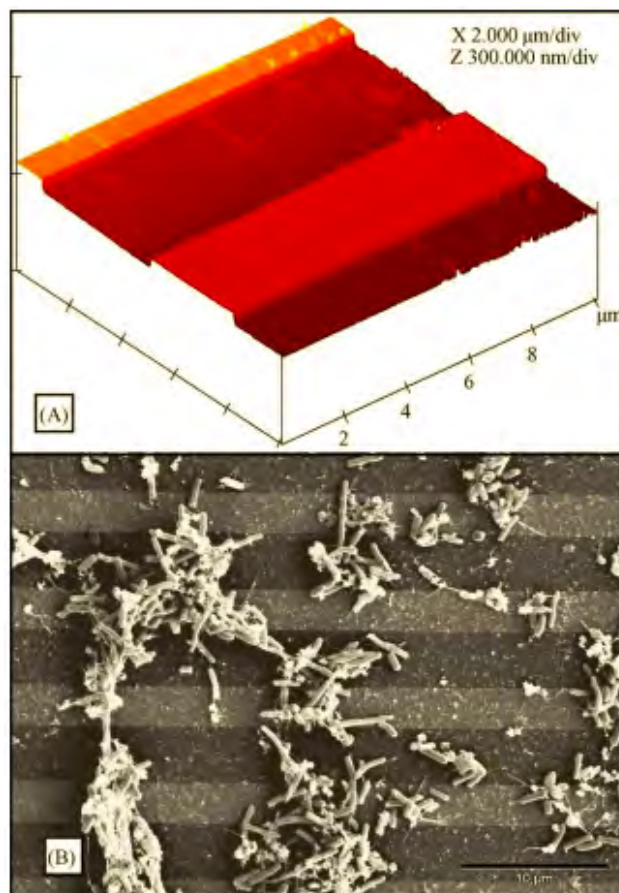


Figure 2.18: (a) AFM scan of microelectrode array and (b) SEM image of *E. coli* bacteria creating links between electrodes [34]

ferrocene-functionalized ZnO nanorods. A change in current was observed, which could be related to the concentration of the pathogen in the samples [82]. A LOD of 50 CFU/ml was achieved with this biosensor [82].

A potentiometric alternating biosensor for the detection of *E. coli* was developed by Ercole et al. [83]. The sensor used polyclonal rabbit antibodies in conjunction with a light addressable potentiometric sensor, and could detect *E. coli* at a LOD of 10 CFU/ml in an assay time of 90 minutes [83]. A change in the red-ox potential was observed by an electrode due to the production of NH_3 by a urease-*E. coli* antibody-conjugate linked with the *E. coli* cells in the water samples [83].

These sensors have the potential to be used in integrated portable systems. The cost, however, is dependant on the equipment used in conjunction with these sensors. During laboratory setups it is common to use the most appropriate equipment (e.g. signal generators, oscilloscopes, impedance analysers

etc.), but this is only applicable when developing the sensors and their operating principles. Very few of the sensors developed have been realised into a portable, low-cost prototype. This is due to many reasons, one of which is the complexity of the sensors. Simplification of these sensors is a necessity to develop low-cost, portable devices. There will be a limit to the sensitivities that will be achieved, but low-cost and portability must form the central focus point of the study.

2.2.5.2 Optical biosensors

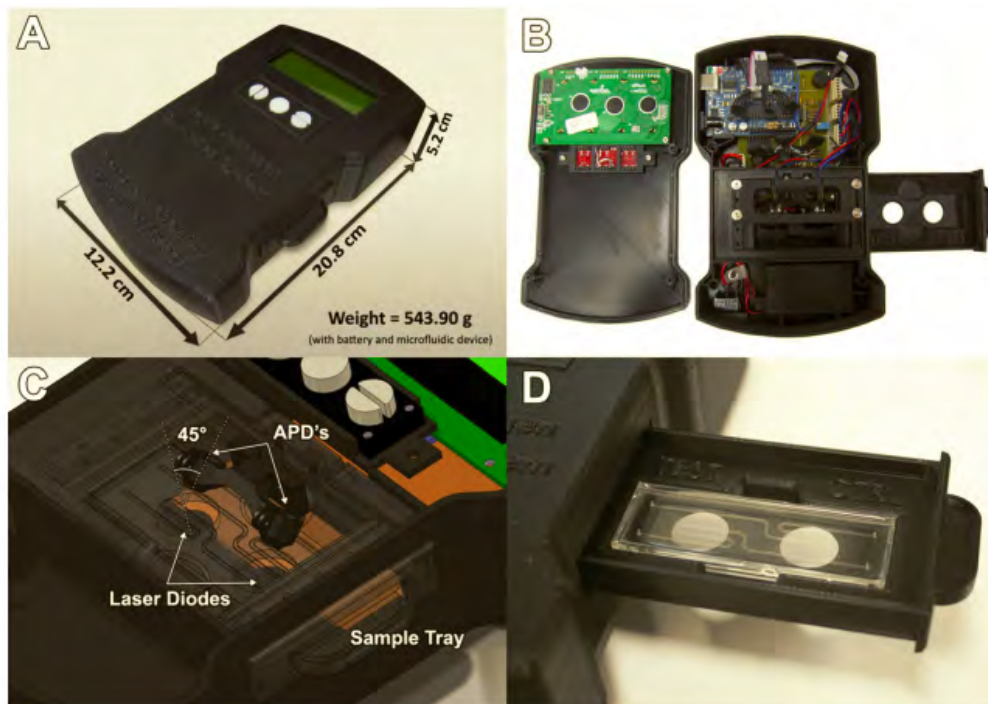


Figure 2.19: Battery-operated mobile device developed by You et al. [84]

Optical transducers have been used in many portable biosensors. You et al. [84] achieved sensitive detection of *E. coli* using a handheld lab-on-a-chip device, as can be seen in Figure 2.19. The detection of *E. coli* K12 and O157:H7 strains, at a LOD of 10 CFU/ml in 6 minutes, was achieved in lettuce samples [84]. This device showcases a good example of the integration of a biosensor into a fully portable device. The biosensor, circuitry and fluid manipulation subsystems have all been incorporated to complete the portable biosensing system. Very high sensitivities and response times have been achieved, but the cost-effectiveness of the system is debatable. The specifications for sensitivity, response time, portability and cost (amongst others) are dependant on the application, and changes for every biosensor.

Some novel biosensors have been developed that use optical fibers as transducers. Rijal et al. [29] developed a biosensor using tapered optical fibers immobilized with antibodies. The sensor was able to achieve a LOD of 70 CFU/ml [29]. The pathogen was detected and then a pH buffer was used to release it from the antibody surface, proposing the re-use of the sensor [29]. A unique method using a light source, optical fiber and a spectrophotometer was used to detect analytes [30] in a similar manner. DeMarco and Lim [31] developed an optical fiber-based biosensor to detect *E. coli* in ground beef samples using evanescent wave modulation. Ohk and Bhunia [85] used a multiplex of fiber optic cables to develop a biosensor for the detection of multiple microorganisms, including *E. coli* O157:H7, in meat samples. By immobilizing antibodies on optical fibers the fluorescence intensity for each fiber was measured and related to the concentration of the pathogens [85].

Other optical biosensors have been developed using interesting methods of detection [86, 87]. Optical biosensors could possibly be manufactured using smaller components (light sources, optical detectors etc.), but the performance of such sensors is unknown. Fiber optics could be used, but to create robust sensors these fibers have to be cost-effective. This may influence the sensitivity of sensors. The operating principle of optical sensors, especially fiber optics, is relatively simple. The detection of other substances other than the analyte may interfere with signals. The utilisation of biorecognition elements in conjunction with optical biosensors may increase specificity among other biomolecules.

2.2.5.3 Biopaper biosensors



Figure 2.20: A lateral flow assay (LFA) of bioactive paper for the detection of *E. coli* [88]

Hossain et al. [88] reported on the use of bioactive paper for the detection of β -glucuronidase (an indicator of *E. coli* presence) using a paper strip that could achieve a LOD of 5 CFU/ml for *E. coli* O157:H7. This novel paper strip is fabricated using ink-jet printing techniques and the use of a preconcentration step involving immunomagnetic nanoparticles [88]. The quantification of *E. coli* bacteria was done by lateral flow chromatography. An increase in colour intensity is noted as the concentration of the pathogen increases, as shown in Figure 2.20 [88]. These strips can be stored for a period of weeks without losing effectiveness and are able to be mass produced at a very low cost [88]. The materials and equipment to develop such biopaper biosensors are not readily available, and may complicate the development process.

2.2.6 Conclusion

E. coli plays an important role in microbiological water quality. International and local standards stipulate how *E. coli* must be tested. Various established methods are used to detect *E. coli*. Plate counting and membrane filtration methods are the most used, due to their sensitivity. Other methods include the use of laboratory based devices such as PCR, ELISA and potable water testing kits. Many biosensors have been developed to detect *E. coli*. Electrochemical and optical biosensors have the potential to be used in low-cost, portable sensors.

Chapter 3

Theory

3.1 Electrochemical impedance biosensor

3.1.1 Introduction

An electrochemical cell relates chemical reactions with electrical energy. Impedance is the effective resistance of a circuit element due to alternating currents (AC), consisting of both real resistance and reactance. Electrochemical impedance spectroscopy is the measurement of impedance over an electrochemical cell. This method of analysis is useful for characterising the change in impedance caused by enzymatic reactions, chemical reactions between the surface of the electrodes and biomaterials and changes in impedance due to the presence of bacteria.

This section will explore the relevant theory concerning electrochemical cells at the hand of circuit models. This is related to the impedance in the cell, and how it can be used to detect bacteria using a novel method (non-linear EIS). A short discussion on the interface interactions between bacteria and electrodes is given. This theory is used to describe the non-linear EIS biosensor.

3.1.2 Impedance spectroscopy

Impedance is defined by

$$Z_{tot} = Z_R + Z_I \quad (3.1.1)$$

where Z_R is the real part of impedance and Z_I the imaginary part (reactance). This is due to AC voltages (or currents) being applied over a circuit element, typically resistors, capacitors and inductances. Electrical impedance can be related to voltage by

$$V(t) = Z_{tot}(t)I(t) \quad (3.1.2)$$

where $I(t)$ is the current and Z_{tot} is the total impedance. It must be noted that (3.1.2) is described in the time domain. The excitation signal (voltage) can be written in the time domain as

$$V(t) = V_a \sin(\omega t) \quad (3.1.3)$$

where ω is the excitation frequency and V_a is the excitation amplitude. EIS typically sweeps numerous frequencies to create a spectrum of the electrochemical cell (i.e. to see the frequency dependant behaviour of electrochemical

cells).

A Fourier transform is used to change a function from the time domain to the frequency domain. This is defined by

$$\mathcal{F}\{f(t)\} = F(\omega) = \int_{-\infty}^{\infty} f(t)e^{-i\omega t} dt. \quad (3.1.4)$$

where $f(t)$ is the time domain signal and ω is defined as

$$\omega = 2\pi f \quad (3.1.5)$$

where f is the frequency of excitation. These transforms provide harmonic spectra which can be evaluated.

3.1.3 Equivalent circuits

Electrochemical cells typically consist of electrodes emerged in a liquid sample. The sample contains the analyte (bacteria) and, depending on the operating mechanism, biorecognition elements, e.g. enzymes. The chemical reactions occurring in the sample due to bacterial presence, or due to electrical energy being added to the cell, change the impedance of the cell. These complex interactions can be described by equivalent circuit models. These models use electrical circuit elements to represent the presence of analytes in the sample, including certain phenomena occurring in the cell.

Yang and Bashir [89] derived an equivalent circuit for a two electrode (bipo-

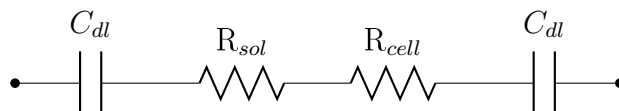


Figure 3.1: Equivalent circuit diagram of a bipolar electrochemical cell setup

lar) electrochemical cell, shown in Figure 3.1. The circuit consists of a double layer capacitance (C_{dl}) at each of the electrode surfaces, bulk resistance of the fluid (R_{sol}) and the bulk resistance of the bacteria (R_{cell}). This circuit assumes that there is no bulk capacitance in the solution. This circuit, however, is only representative of a bipolar electrochemical cell setup. When working with interdigitated microelectrodes (IMEs), this model changes. IMEs have many advantages. They have lower resistances, higher signal-to-noise ratios and enable the use of much smaller sample volumes [89]. This increases the sensitivity of the sensor. Large bulky electrodes can also be eliminated with the use of small patterned electrodes. The typical bipolar setup measures

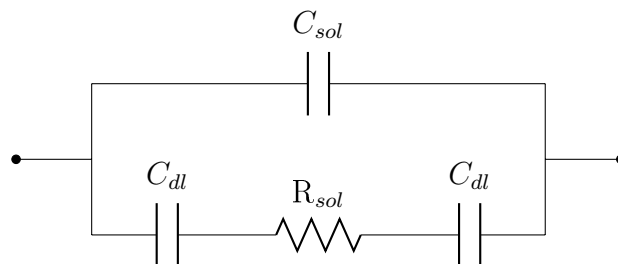


Figure 3.2: Equivalent circuit diagram of an IME array electrochemical cell setup

changes in the bulk solution resistance, where IMEs predominantly measure the changes in double layer capacitance [89]. This is influenced by the ionic composition of the solution, as well as cells that adhere to the surface of the electrodes.

Yang et al. [90] derived the equivalent circuit diagram for an electrochemical cell using IME arrays, shown in Figure 3.2. The double layer capacitances (C_{dl}), solution resistance (R_{sol}) and solution capacitance (C_{sol}) are shown in the circuit diagram. Yang et al. [90] showed that IMEs are better represented by using a parallel capacitance for the bulk solution. The circuit's total impedance magnitude can be calculated by using two parallel impedances

$$\frac{1}{Z_{tot}} = \frac{1}{Z_1} + \frac{1}{Z_2} \quad (3.1.6)$$

where the magnitude of the first impedance is described by

$$|Z_1| = \sqrt{(R_{sol})^2 + \frac{1}{(\pi f C_{dl})^2}} \quad (3.1.7)$$

and the magnitude of the second impedance is described by

$$|Z_2| = \sqrt{\frac{1}{(2\pi f C_{sol})^2}} \quad (3.1.8)$$

where R_{sol} is the equivalent of the solution resistance, C_{dl} the double layer capacitance, C_{sol} the solution capacitance and f the frequency of excitation.

3.1.4 Harmonic spectra

When discussing impedance spectroscopy of electrochemical cells the input range of the excitation voltage is important. Excitation voltage amplitudes are typically less than 30 mV. This results in linear current-voltage (IV) curves

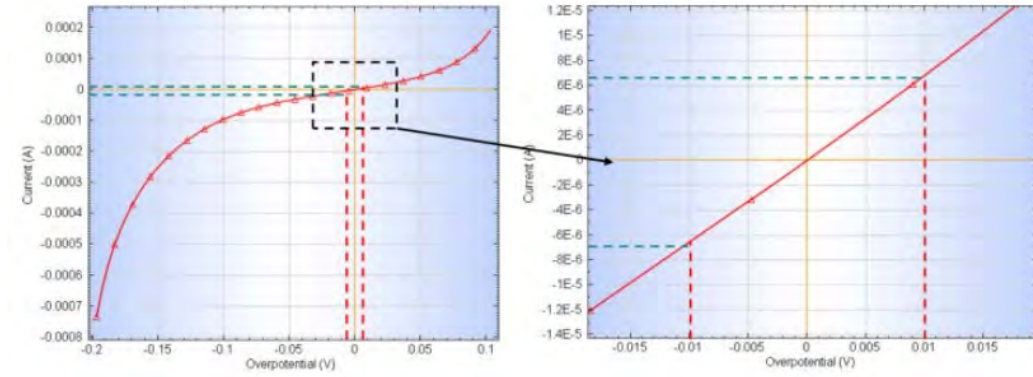


Figure 3.3: Current-voltage (IV) characteristic curve indicating the linear range [91]

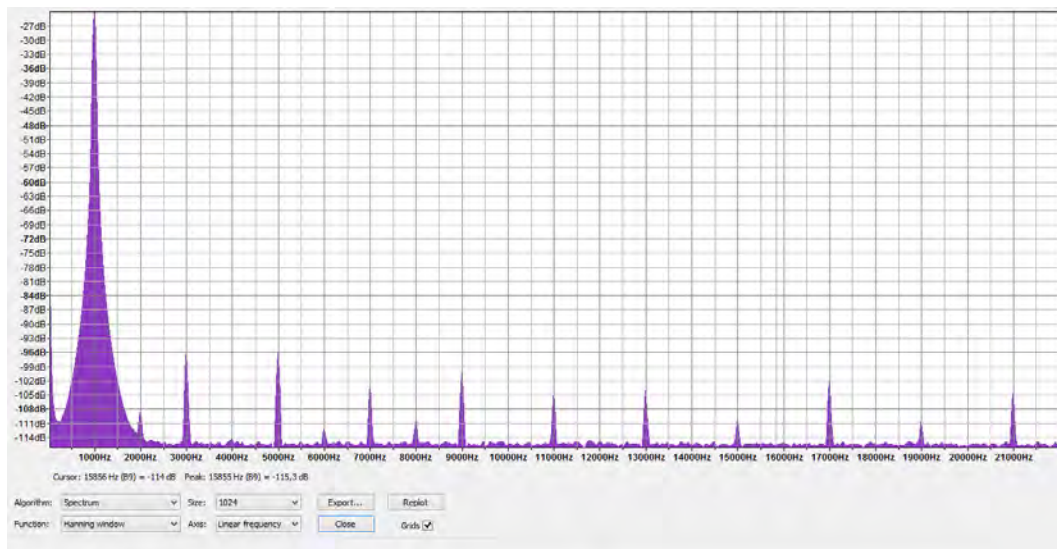


Figure 3.4: Harmonic spectrum of an electrochemical cell ($V_{p-p} = 3$ V, $f = 1$ kHz)

when measuring the impedance. Figure 3.3 shows a current-voltage (I-V) characteristic curve indicating the linear range assumption. It can be seen that a linear range exists around the crossing point (where $I = 0$ mA). Non-linear behaviour can be seen at higher excitation voltages.

When signals are excited, they are in the time domain. Software can be used to transform these time domain signals to the frequency domain, using fast Fourier transform (FFT) analysis. When an excitation wave is used, the first harmonic is known as the fundamental frequency. If the fundamental frequency is

$$f_{Fund} = f_x \quad (3.1.9)$$

then harmonics excited by bacteria or ions can be described by

$$f_N = Nf_x \quad (3.1.10)$$

where N denotes the first, second, third, etc., harmonic being excited. These harmonics are thus integer multiples of the fundamental frequency. Figure 3.4 shows a harmonic spectrum, indicating the fundamental frequency (1 kHz) and the harmonic frequencies excited. A harmonic spectrum is thus a spectrum showing only multiples of the fundamental frequency of excitation. A harmonic spectrum can be used to show non-linear behaviour due to modulation of a sinusoidal signal at a single harmonic frequency. When, for example, a signal interacts with an electrochemical cell, non-linear harmonics can be present that can indicate the presence of bacteria, ions, or other analytes. Huzior et al. [35] used non-linear impedance spectroscopy to detect bacteria (*Lactobacillus acidophilus* and *Streptococcus mutans*) in human teeth. This method can be adapted to measure bacterial and ionic presence in water.

3.1.5 Electrode material, geometry and interfacial effects

Various parameters have an effect on the operation and performance of a non-linear electrochemical impedance biosensor. The choice of electrodes and electrode geometry has an influence on the performance. The use of interdigitated microelectrode (IME) arrays have recently been used to improve the sensitivity of EIS biosensors. Other parameters include the electrode material being used. Metals like platinum (Pt), gold (Au), copper (Cu), titanium (Ti) and aluminium (Al), amongst others, have been used as electrode materials.

Electrode geometry also has an effect on the output. Ahmed and Reifsnider [92] noted that the impedance of an electrochemical cell decreases as the surface area of electrodes are increased. It was also noted that the lower range of the frequency spectrum ($f < 10$ kHz) is more reliant on geometry changes than higher frequency responses [92].

Interfacial effects must also be considered when using EIS methods of detection. Bacterial metabolism changes the impedance of the bulk medium [89]. This is due to the release of ions by the energy production system of cells as well as by ion exchange through the cell membrane [89]. These energy metabolism and ion exchange processes cause a change in the ionic composition of the bulk medium (sample) and thus the electrical conductivity of the sample.

3.1.6 Conclusion

EIS uses the impedance characteristics of electrochemical cells to detect changes in the cell. These changes can be due to ionic composition, bacterial presence and interface interaction (with electrodes). These can be measured using this relatively simple method. When the input to the system is pushed beyond the linear range, non-linear harmonics can be seen (using FFT of the time domain signal). This has the potential to be used to detect bacterial changes, and can thus be used as a biosensor to detect *E. coli*. Electrode geometry, material and interfacial effects all need to be considered when evaluating EIS based biosensors.

3.2 Fiber optic biosensor

3.2.1 Introduction

Fiber optic sensors have been used in many ways to detect bacteria. The focus in this project is on an evanescent wave biosensor using simplified fiber optics. This is due to the relative simplicity of fiber-optic sensors, potential low cost and high performance. The basic operating principle of a simplified fiber optic biosensor will be described. Fiber optics transport light due to an effect known as total internal reflection (TIR). This effect, using the Ray Tracing model, is used to describe the important parameters related to the evanescent field. Antibodies were chosen as the biorecognition element for this sensor. The method in which it was immobilised to the inorganic fiber surface through covalent attachment is described. All calculations and additional figures are included in Appendix C and D.

3.2.2 Biosensor model

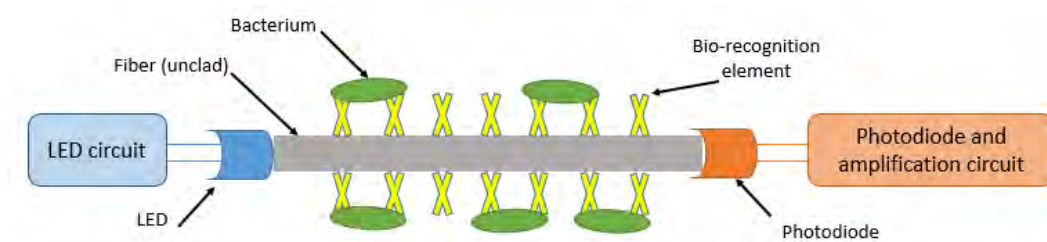


Figure 3.5: Simplified fiber optic biosensor schematic

A schematic of the simplified fiber optic biosensor is shown in Figure 3.5. When light from an LED enters the optical fiber, the light is transmitted by the principle of total internal reflection (TIR). The light wave propagates through the fiber, but an evanescent field exists outside the fiber core. This

evanescent field penetrates and interacts with the surrounding material (usually a cladding around the fiber). The fiber can be unclad, and thus allow for adhesion of other materials to the surface of the fiber core. The unclad optical fiber is then immobilised with antibodies (the biorecognition element) that are specifically manufactured to target E. coli.

When the fiber is exposed to a sample containing E. coli, antigen-antibody interaction takes place between the bacteria and immobilised antibodies. The light in the evanescent field interacts with the bacteria. This causes a loss in power (light intensity) due to two effects, namely absorption and a change in the bulk refractive index. This intensity change is detected by a photodiode at the other end of the fiber. A change in the output power is related to the concentration of bacteria in the sample.

3.2.3 Ray tracing model

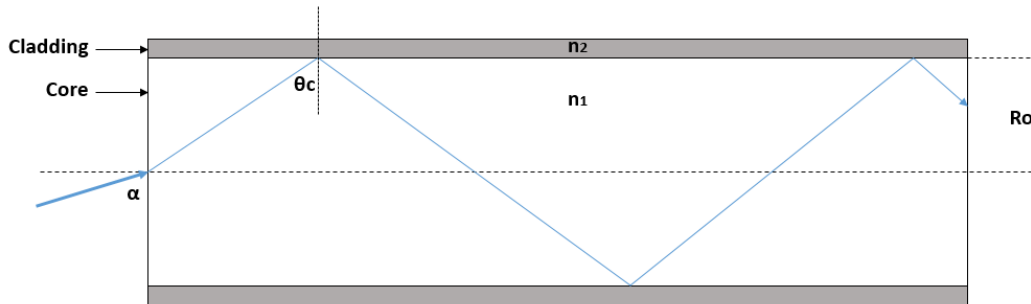


Figure 3.6: Ray tracing model of light travelling in an optical fiber

Figure 3.6 shows the Ray Tracing model of light travelling through an optical fiber, where R_o is the fiber core radius, n_1 the refractive index of the core material, n_2 the refractive index of the cladding (surrounding medium), θ_c the critical angle and α the angle of incidence.

The numerical aperture of an optical fiber is described by

$$NA = \sqrt{n_1^2 - n_2^2} \quad (3.2.1)$$

where n_1 and n_2 are the two respective refractive indices. The critical angle of light entering and exiting the fiber is described by

$$\theta_c = \arcsin\left(\frac{n_2}{n_1}\right) \quad (3.2.2)$$

where n_1 and n_2 are the two respective refractive indices. The angle of incidence of the fiber (α) must satisfy the equation

$$\alpha > \theta_c \quad (3.2.3)$$

for total internal reflection (TIR) to occur in the fiber. The V -number, an important parameter in calculating the power in the evanescent field, is described by

$$V = \frac{2\pi R_0 NA}{\lambda} \quad (3.2.4)$$

where R_0 is the core radius of the fiber, NA the numerical aperture, as described by (3.2.1) and λ the wavelength of light used. The Ray Tracing model [93] describes the penetration depth of the evanescent field outside the fiber core as

$$d_p = \frac{\lambda}{2\pi \sqrt{n_1^2 (\sin(\alpha))^2 - n_2^2}} \quad (3.2.5)$$

where λ is the wavelength of light, n_1 is the refractive index of the fiber, n_2 is the refractive index of the surrounding medium and α is the angle of incidence of light as described by (3.2.3). The optical power [94] in the evanescent field, as a percentage of the total power in the evanescent field and the core, is described by

$$P_{EW\%} = \frac{1.89}{V} \quad (3.2.6)$$

where V is the V -number as described by (3.2.4).

A simplified optic fiber circuit was designed. Borosilicate glass fibers were chosen (due to availability and cost effectiveness). Water and bacteria is the surrounding mediums, but the refractive index of water was chosen for the calculations. The angle of incidence was assumed as varying due to the fact that the optical fiber will be placed directly on top of an LED (thus eliminating expensive focal lenses and simplifying the manufacturing process).

From (3.2.5) (Figure C.1 in Appendix C) it can be seen that the penetration depth is proportionally related to the wavelength of light entering the fiber. It can be seen from (3.2.6) that the power in the evanescent field is inversely proportional to the V -number. From (3.2.4) it can be seen that the V -number is proportionally related to the core radius of the optical fiber and inversely proportional to the wavelength of light. The relation between the V -number and the core radius for a constant wavelength of light is shown in Figure C.2 (Appendix C). The relation between the V -number and the excitation wavelength of light for a constant core radius is shown in Figure 3.7. The optimum point would thus be to use the longest wavelength of light available and the minimum fiber core radius.

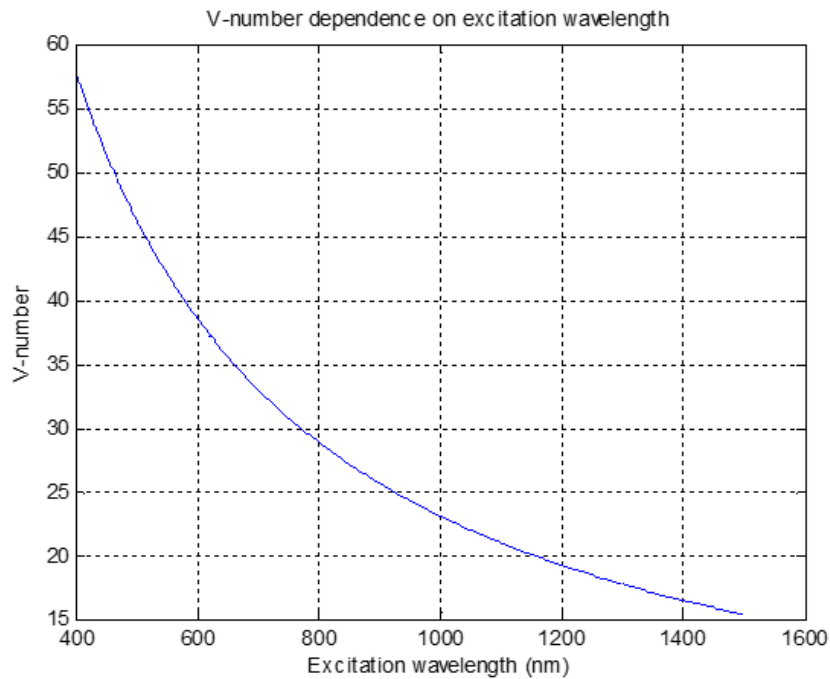


Figure 3.7: V -number vs excitation wavelength. As the excitation wavelength increases, the V -number decreases, resulting in more power present in the evanescent field.

Figure 3.8 shows the penetration depth of the evanescent wave related to the angle of incidence i.e. the angle of light entering the fiber. When (3.2.3) is not satisfied, it can be seen that all the light entering the fiber is transmitted i.e. TIR does not occur. When the angle of incidence approaches the critical angle, the penetration depth of the evanescent wave spikes.

3.2.4 Antibody immobilisation

Figure 3.9 shows a representation of the antibody immobilised optical fiber indicating the evanescent field. The elements linking the surface of the optical fiber (borosilicate glass) core to the anti-*E. coli* antibody is represented in Figure 3.10 and Figure 3.11. The organosilane, (3-glycidyloxypropyl) trimethoxysilane (GPS), was chosen as an appropriate crosslinker. The surface of the optical fiber will be prepared to increase the presence of hydroxyl (OH) molecules. It will be treated with GPS to form a stable covalent bond between the silicon and oxygen molecules. An IgG anti-*E. coli* antibody (Ab) that binds with the antigens of a wide variety of *E. coli* strains was chosen as an appropriate biorecognition element. All IgG antibodies have an amine ($-\text{NH}_2$) group on the end of its heavy chain. This amine group creates a stable covalent bond with GPS, resulting in a covalently attached Ab to the fiber surface.

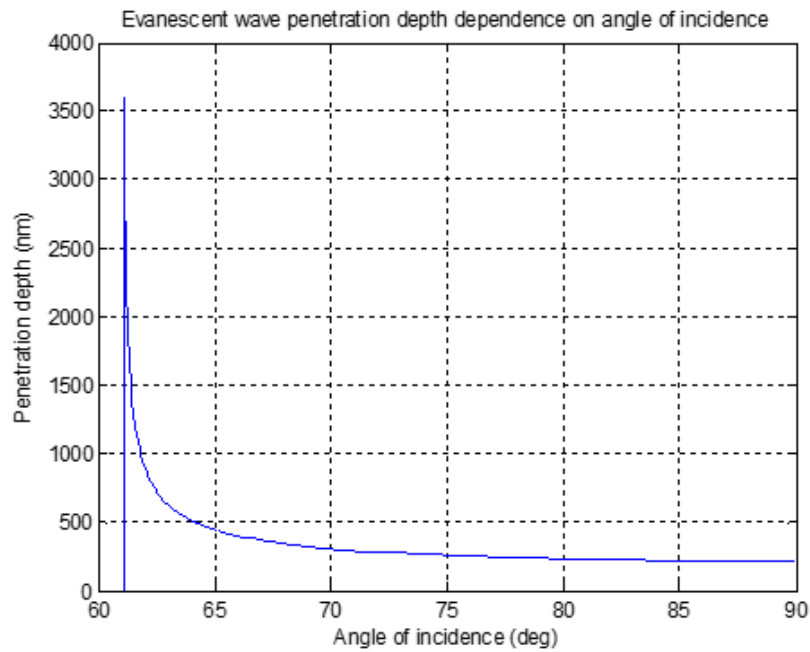


Figure 3.8: Evanescent wave vs angle of incidence. As the angle of incidence increases above the critical angle, the penetration depth of the evanescent wave increases.

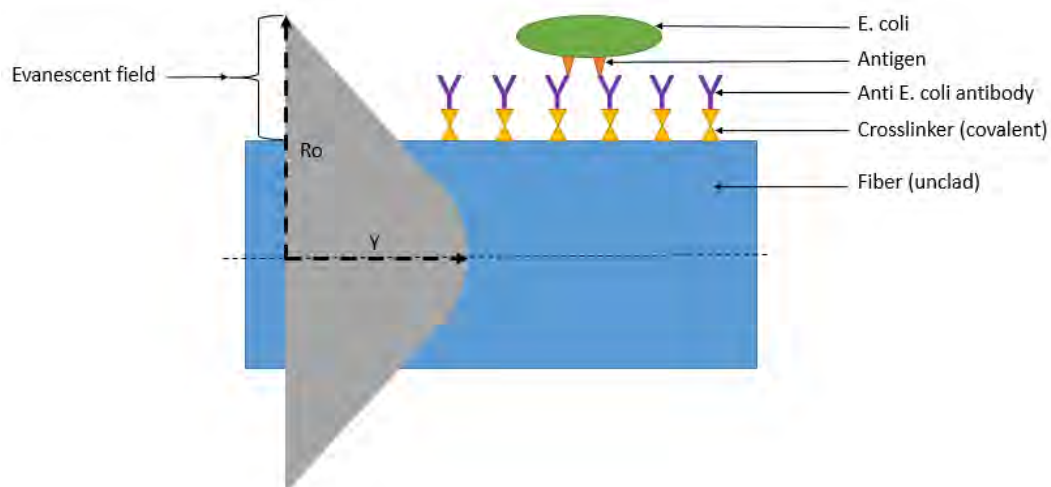


Figure 3.9: Antibody immobilised optical fiber model indicating the evanescent field. As the light travels through the fiber, the evanescent field interacts with the material/bacteria on the surface of the fiber.

3.2.5 Conclusion

Optical fibers have been thoroughly studied for use in biosensors. The use of novel biorecognition elements, such as antibodies, have also been used to "cap-

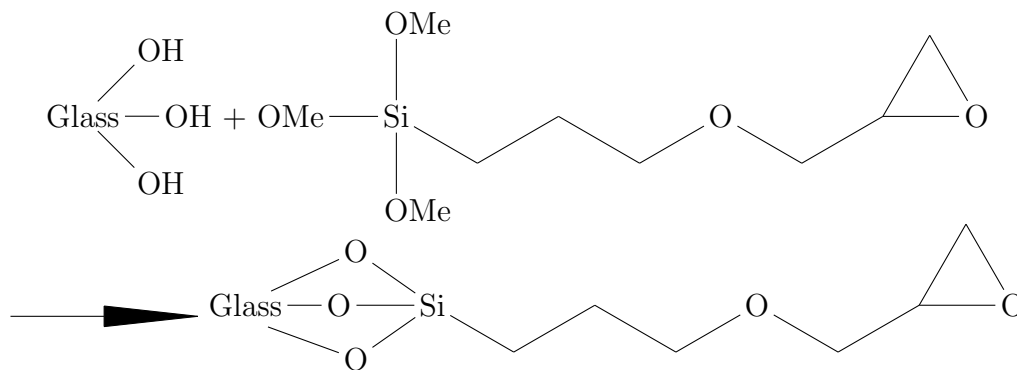


Figure 3.10: Covalent bonding of borosilicate glass fiber with GPS crosslinker

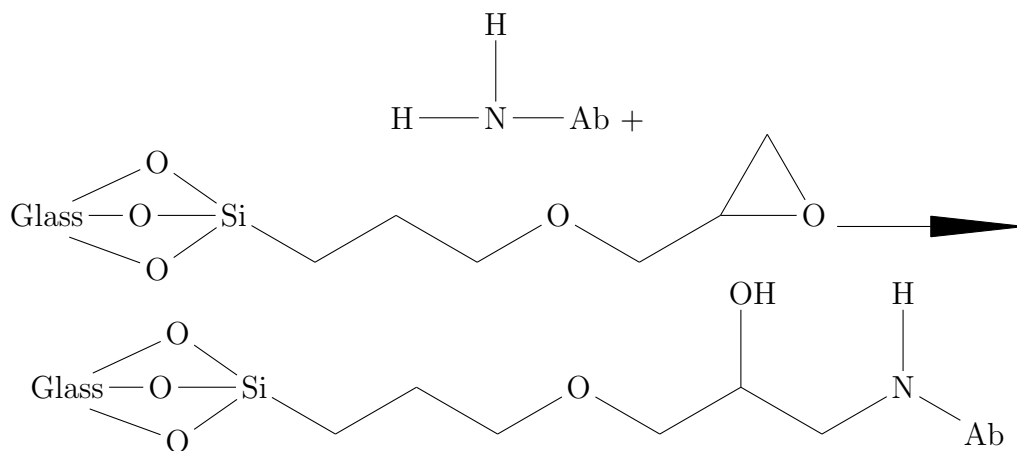


Figure 3.11: Crosslinking IgG antibody to borosilicate glass fiber and GPS crosslinker

ture" bacteria to the surface of optical fibers. Most fiber optic sensors, however, use expensive lenses and measurement devices to monitor these changes. They could also only be limited to laboratory set-ups, and were not designed or suited to be used in a portable sensor system. These methods of detection, such as evanescent field absorbance, and refractive index change, can be very powerful when trying to detect low levels of bacteria in a sample.

To develop low-cost sensors, with a focus on portability, fiber-optic sensors have to be simplified. Modern optoelectronics (LEDs and PDs) allow for this simplification. The method of manufacturing and testing this simplified fiber optic sensor, as well its various components (fiber, optoelectronics, antibody immobilisation), need to be established.

Chapter 4

Electrochemical Impedance Biosensor

4.1 Introduction

An electrochemical impedance biosensor was evaluated for use as a low-cost, portable sensor. Electrodes patterned on glass chips were provided by the Technical University of Munich (TUM). The electrodes were patterned in various geometries and made from different materials. Non-linear impedance spectroscopy was used as the method to detect bacteria. The appropriate testing method, electrodes and signal analysis method are discussed. The influence of ionic solutions on the bacteria was observed. Various concentrations of bacterial solution were tested. The concentration curves and results were evaluated. The effect of viable and non-viable bacteria was observed. The use of this setup and detection method is evaluated for use in a low-cost, portable biosensor setup.

4.2 Test protocols

4.2.1 Electrodes

Three chips with different electrode patterns were tested. Figure 4.1 shows the IntelliTUM chip with patterned electrodes. The other chips are seen in Figure D.1 and Figure D.2 in Appendix D. The IntelliTUM chip electrodes were manufactured from platinum or titanium. The two large electrodes (right and top of Figure 4.1) were mostly used due to their notable performance.

4.2.2 Impedance spectra

Impedance spectra were observed by performing a frequency sweep over the electrodes with a Solartron SI 1260 Impedance/Gain-Phase Analyser. A chip was placed in a holder (Figure D.3 in Appendix D) with an opening. The method for testing was as follows:

- Insert 50 μl of distilled water into holder
- Test spectrum

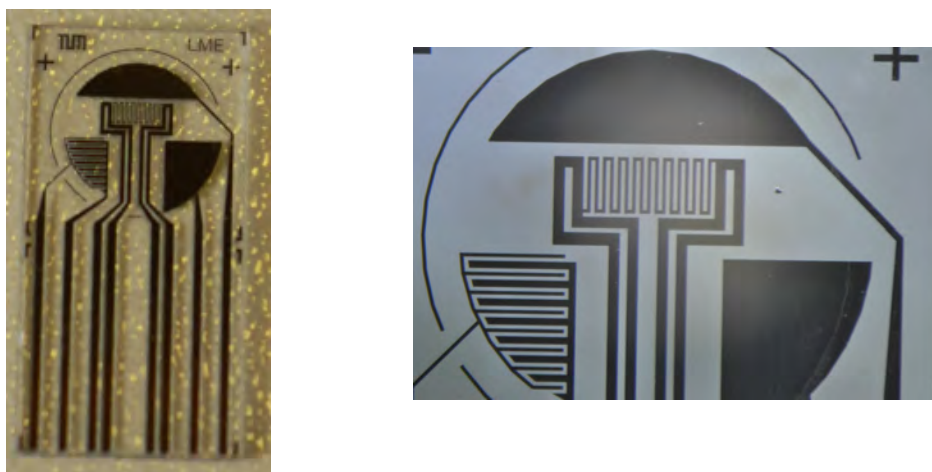


Figure 4.1: IntelliTUM chip with patterned electrodes as provided by TUM (Pt or Ti, 7.5 mm×15 mm)

- Remove distilled water, and insert 50 μl of analyte (liquid sample)
- Test spectrum
- Remove analyte
- Wash 3 \times , by adding and removing 50 μl of distilled water

The washing steps are included to ensure that a baseline measurement (distilled water) is repeated, that there is no adhesion and fouling on the chip surface and ensuring repeatable results. This method was repeated for each chip and for each analyte. The spectra were analysed using Z-plot and Z-view (Schriber Associates, Inc.) software.

4.2.3 Harmonic spectra

Figure 4.2 shows the setup for measuring harmonic spectra. The y-axis shows a $\text{dB}\mu$ value, which is relative to 1 μW . A signal generator, a chip inside a chip holder (Figure D.3 in Appendix D) and a Steinberg UR22 USB audio interface was used to measure spectra. The following method was used to acquire spectra:

- Insert 50 μl of distilled water into holder
- Test spectrum (4 seconds)
- Remove distilled water, and insert 50 μl of analyte (liquid sample)
- Test spectrum (4 seconds)
- Remove analyte

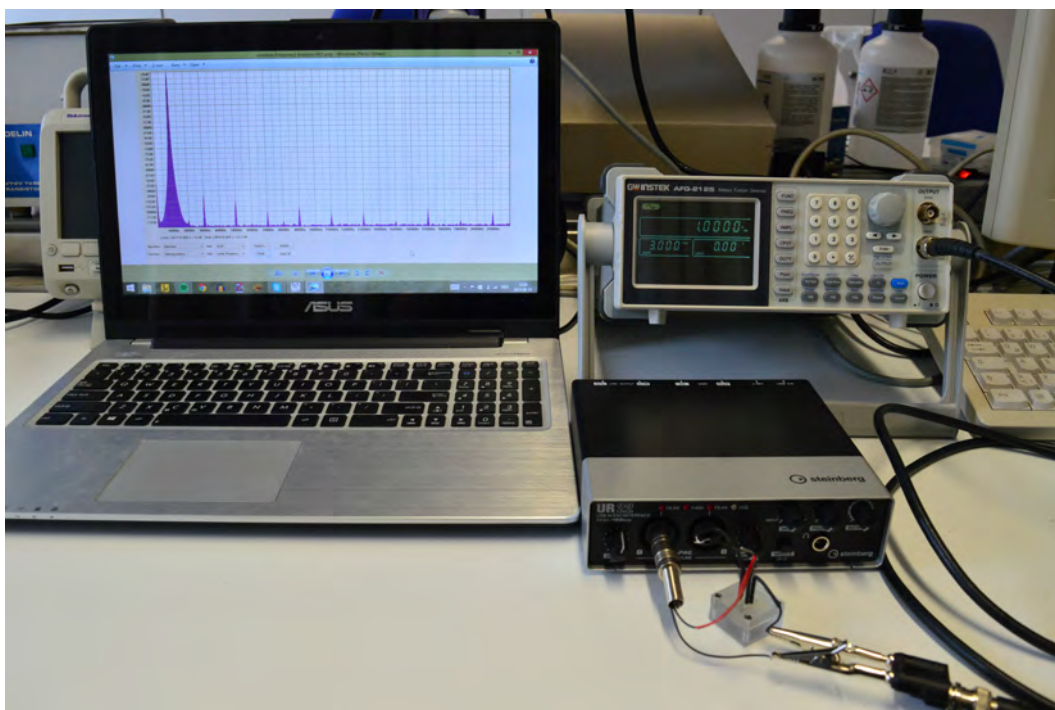


Figure 4.2: Measurement setup for measuring harmonic spectra. The electrode chip was placed in a holder, and connected to a UR 22 audio interface. Spectra were measured using a computer.

- Wash 3 \times , by adding and removing 50 μ l of distilled water
- Insert 50 μ l of distilled water into holder
- Test spectrum (4 seconds)

This was repeated for each chip and liquid sample tested. The spectra were analysed using Audacity (Freeware) audio software.

4.2.4 Electrode re-usability

The patterned chips could be reused after testing. This was done by removing the chips, and cleaning them with the following method:

- Use a soft cotton swab, and wipe surface with distilled water
- Repeat with 70 vol % ethanol
- Repeat with distilled water
- Dry using pressurised air

Chips were cleaned at the beginning of each day of testing.

4.2.5 Bacterial suspensions

E. coli B44 was grown in a nutrient broth. A bacterial suspension for testing was prepared in the following way:

- Pipette 3 ml of bacterial nutrient solution into a vial
- Centrifuge for 90 seconds at 7000 rpm
- Remove nutrient broth from vial (leaving centrifuged bacterial pellet)
- Pipette 1.5 ml of distilled water into the vial
- Vortex for 10 seconds
- Centrifuge for 90 seconds at 7000 rpm
- Remove distilled water from vial
- Pipette 1.5 ml of distilled water into vial
- Vortex for 20 seconds

Bacterial concentrations were determined by diluting the bacterial suspension, pipetting onto agar nutrient plates and growing for 24 hours at 37.5°C. The viable colonies were then counted to determine the concentration (CFU/ml).

4.2.6 Non-viable bacteria

Bacterial suspensions were prepared for testing viable (live) bacteria. To test non-viable (dead) bacteria, the following method was used to heat-kill the bacteria:

- Bacterial suspension in a vial was placed in a heat bath
- The suspension vial was boiled at 100°C for 30 minutes

The following method was used to kill the bacteria with ethanol:

- Pipette 3 ml of bacterial nutrient solution into a vial
- Centrifuge for 90 seconds at 7000 rpm
- Remove nutrient broth from vial (leaving centrifuged bacterial pellet)
- Pipette 1.5 ml of distilled water into the vial
- Vortex for 10 seconds
- Centrifuge for 90 seconds at 7000 rpm

- Remove distilled water from vial
- Pipette 1.5 ml of 70 volume % ethanol into vial
- Vortex for 20 seconds

4.3 Impedance spectra

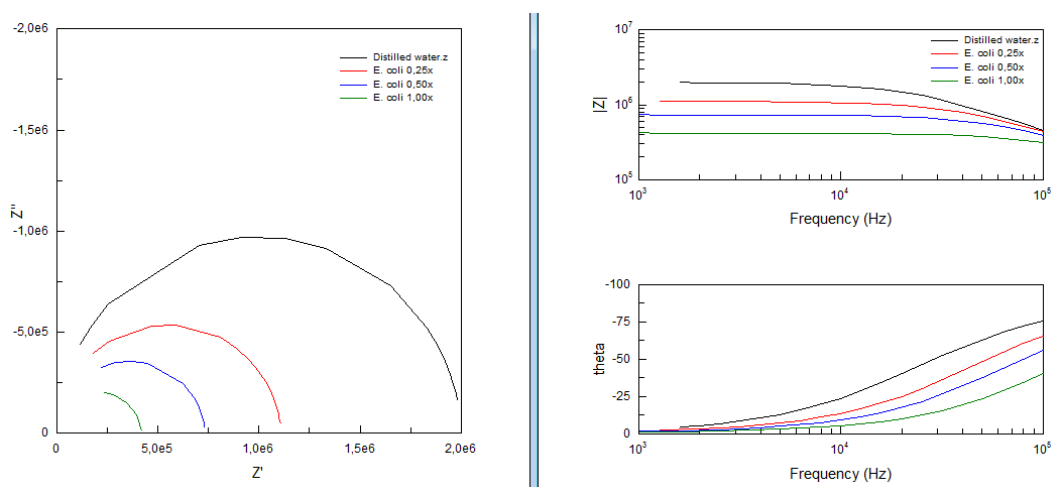


Figure 4.3: Impedance spectrum at varying bacterial concentrations (Pt electrodes) showing the a.) complex impedance diagram and b.) the bode plot. As the bacterial concentration increased, the impedance decreased.

Impedance spectra of the chips were recorded. A frequency sweep from 100 to 100 000 Hz, at an amplitude of 1.5 V was performed. The impedance spectra for the platinum chip (IntelliTUM), showing different bacterial concentrations, is seen in Figure 4.3. As can be seen, there is a decrease in impedance for higher concentrations of bacteria in the samples. This indicates an increase in conductivity as the bacterial concentration increases. The spectra for the Ti IntelliTUM chip and the symmetrical electrodes chip is provided in Appendix D (Figure D.4 and Figure D.5 respectively).

4.4 *E. coli* detection

To ensure detection of analytes with non-linear EIS, a baseline measurement had to be made. Distilled water is the most appropriate baseline, as it contains almost no ions or other foreign species. It is also used to determine the amount of gain (set on the Steinberg UR 22). The gain is increased until harmonics are present. This is the threshold gain. Figure 4.4 shows the harmonic spectrum of distilled water. As can be seen, the fundamental frequency (excitation

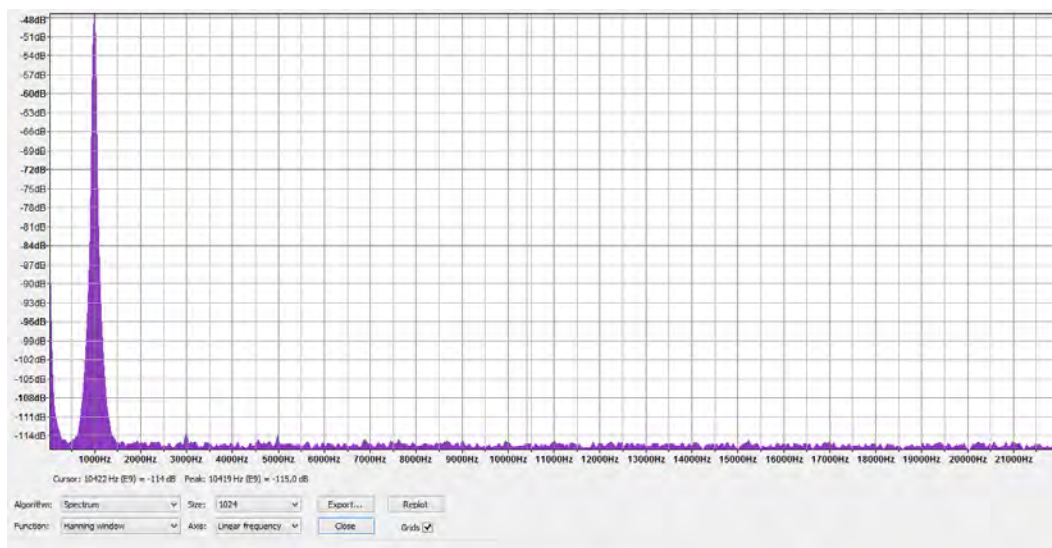


Figure 4.4: Harmonic spectrum of distilled water ($V_{p-p} = 2.987$ V, $f = 1$ kHz, Gain = 0.6), indicating only the fundamental frequency.

frequency) is always present. There are, however, no other harmonics present. This spectrum was tested before and after each analyte test to ensure no adhesion or contamination of the electrode surfaces.

Using bacterial suspensions, the effects of amplitude, gain and frequency were tested. Higher gains and excitation amplitudes have similar effects i.e. the input voltage is increased. With higher voltages, harmonics start to emerge. This voltage is limited by the threshold voltage of distilled water. The threshold input voltage is 3 V, with a gain of 0.6 (for the large electrodes on the IntelliTUM chips). When lower frequencies are used, it has the same effect as higher voltages i.e. harmonics emerge. 1 kHz was chosen as the excitation frequency, seeing that smaller frequencies did not give much more of an advantage to sensor performance.

4.4.1 Ionic solutions

The following ionic species were tested: NaCl, KCl and $MgCl_2$. Various concentrations (10 mg/L, 1 mg/L, 0.1 mg/L and 0.01 mg/L) were tested. These were tested on the large electrode surfaces of the IntelliTUM chips, using both Ti and Pt electrodes.

Both Pt and Ti electrodes could detect a change as small as 0.01 mg/L of salt solution (relative to the spectrum of distilled water). The higher the concentration of salt, the more harmonics are present. The amplitude of the harmonics are also higher. Figure 4.5 and Figure 4.6 show the harmonic spectrum for 0.01 mg/L and 10 mg/L of NaCl tested on Pt electrodes respectively.

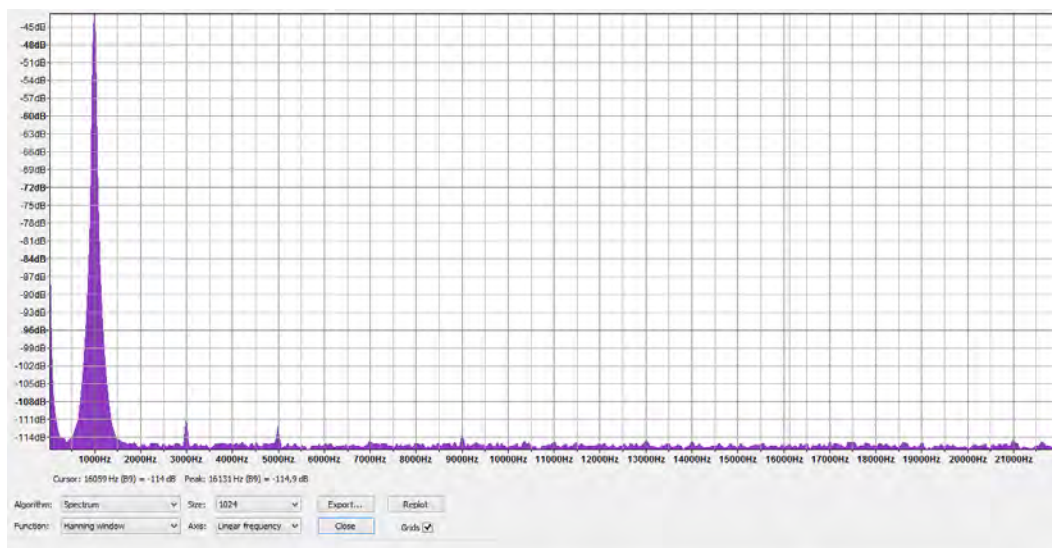


Figure 4.5: Harmonic spectrum of NaCl ($V_{p-p} = 2.987$ V, $f = 1$ kHz, Gain = 0.6, 0.01 mg/L). Increases in the harmonics are clearly seen.

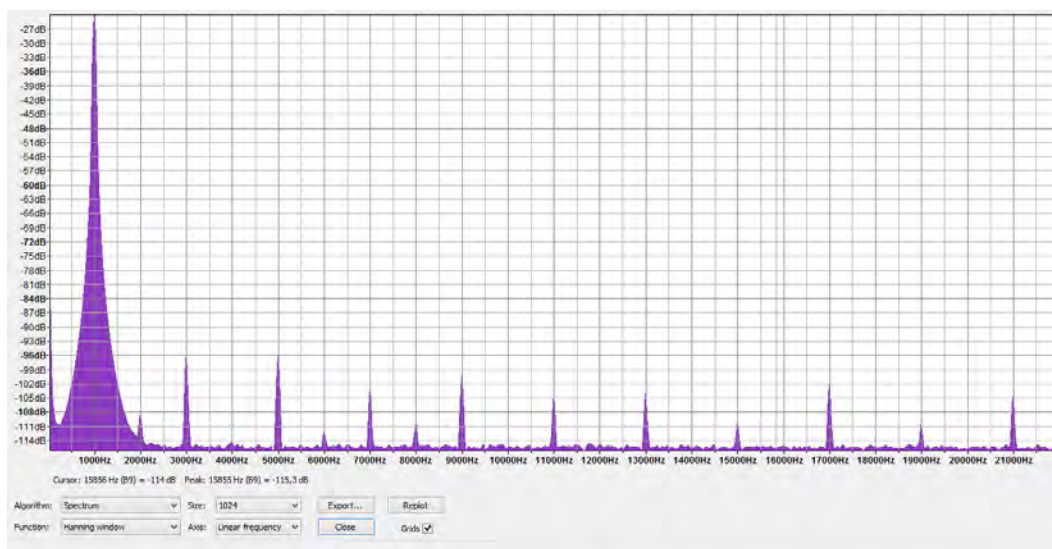


Figure 4.6: Harmonic spectrum of NaCl ($V_{p-p} = 2.987$ V, $f = 1$ kHz, Gain = 0.6, 10 mg/L). As the concentration of ionic solutions increased, the harmonic peaks increased.

There was no significant difference in the harmonic spectra between NaCl and KCl. The amplitudes for $MgCl_2$ (both on Ti and Pt electrodes) were lower than that of NaCl and KCl. This might be explained by the strength of the Mg ion dominating in the ionic solution, due to its higher molar concentration. This lowers the conductivity of the sample, and thus also the harmonic amplitudes.

The most significant difference between Ti and Pt electrodes is that Pt electrodes had higher amplitudes (approximately +4 dB) for most harmonics. This infers that Pt electrodes are more sensitive than Ti electrodes. This may be due to the insulative effect of an oxide layer that is on the Ti surface.

The concentration curves for NaCl on Pt and Ti electrodes are shown in

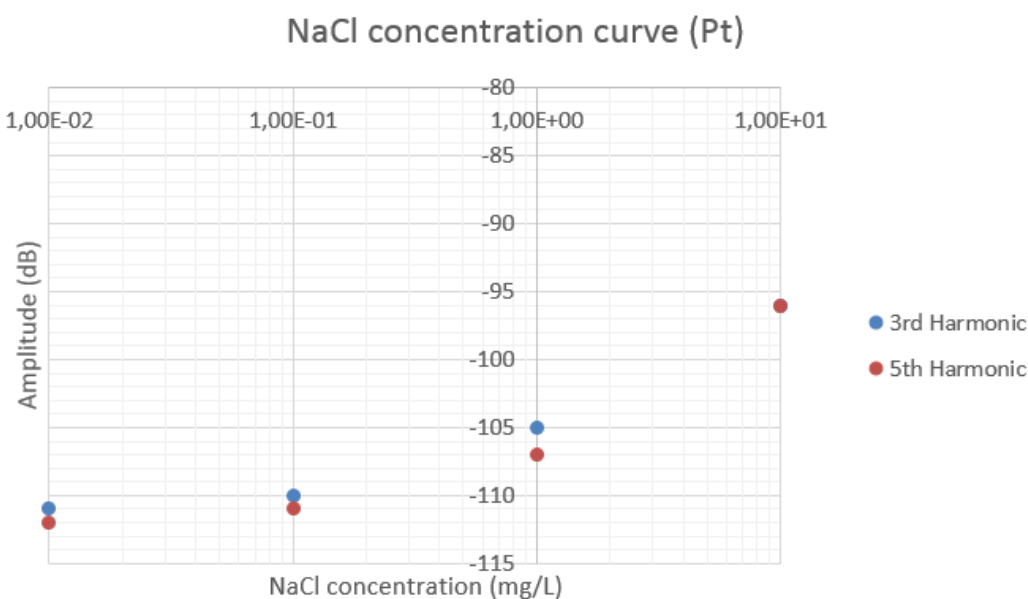


Figure 4.7: Concentration curve of NaCl on Pt electrodes ($V_{p-p} = 2.987$ V, $f = 1$ kHz, Gain = 0.6)

Figure D.9 and Figure D.6 respectively. The concentration curves for each salt solution, on both Pt and Ti electrodes, are included in the Appendix D.

4.4.2 E. coli suspensions

E. coli B44 was grown in nutrient broth. Bacterial suspensions in distilled water were tested. These suspensions were diluted ($0.5\times$, $0.25\times$, $0.1\times$, $0.01\times$) and the bacteria were grown and counted on agar nutrient plates. These were used to determine the bacterial concentration in the undiluted sample.

Bacterial concentrations as little as 1.1×10^{10} CFU/ml was detected. Bacterial peaks at the 3rd and 5th harmonic are present. As the bacterial concentration increases, the amplitude of the harmonics increase. More harmonics also emerge. This may be due to various reasons (conductivity, bacterial membranes, ionic channels etc.). Figure 4.9 and Figure 4.10 show the harmonic spectra for E. coli at various concentrations on Pt electrodes. Figure D.12 and

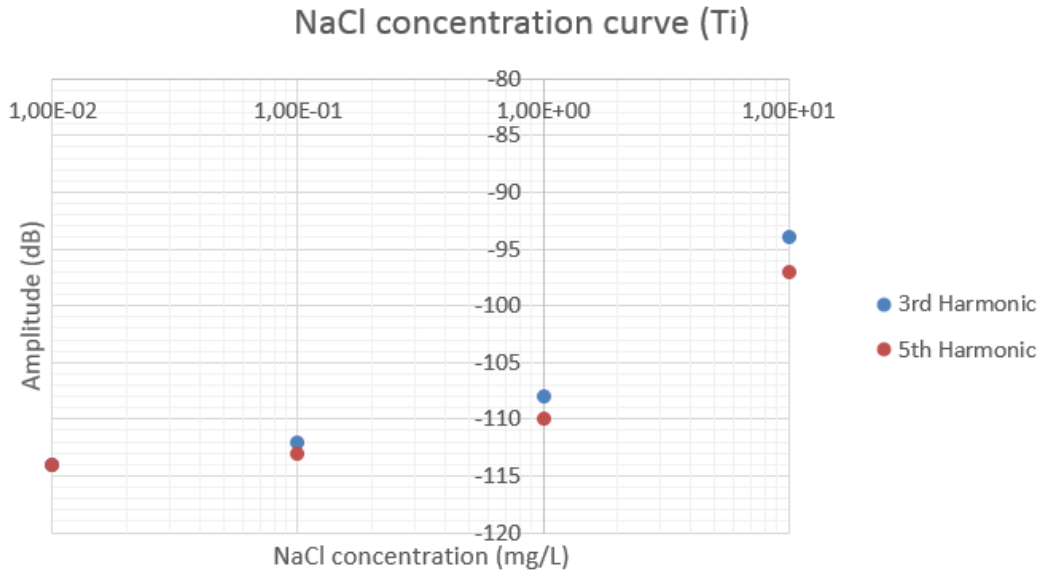


Figure 4.8: Concentration curve of NaCl on Ti electrodes ($V_{p-p} = 2.987$ V, $f = 1$ kHz, Gain = 0.6)

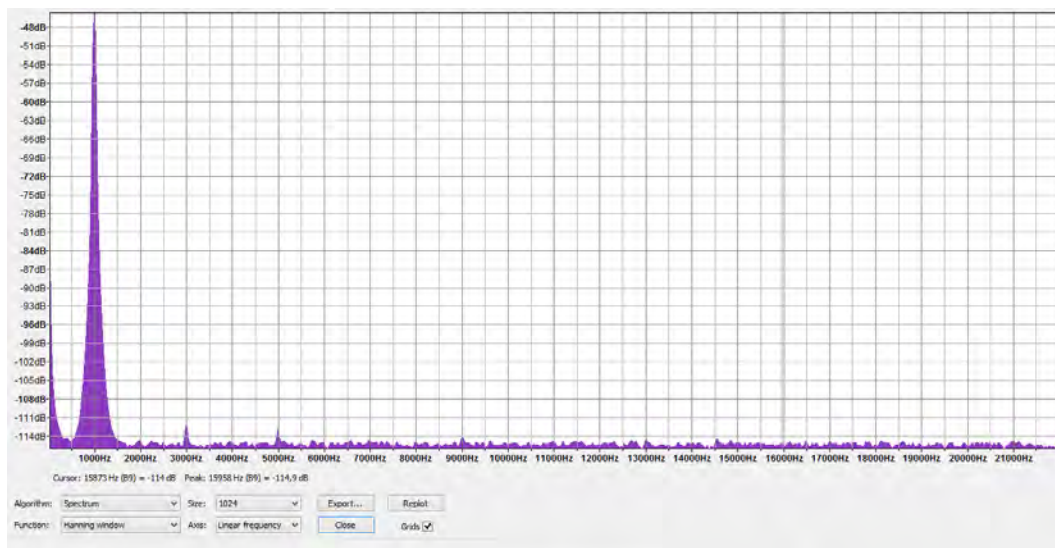


Figure 4.9: Harmonic spectrum of *E. coli* on Pt electrodes (1.1×10^{10} CFU/ml). The presence of bacteria is clearly seen due to the presence of harmonics.

D.13 (Appendix D) show the harmonic spectra for *E. coli* at various concentrations on Ti electrodes. As can be seen, there is an emergence of harmonic peaks. As the concentration increases, many more harmonic peaks are present.

Tests were performed on Pt and Ti electrodes. Varying concentrations were tested, and the tests were repeated 3 times. The amplitudes (dB) were recorded

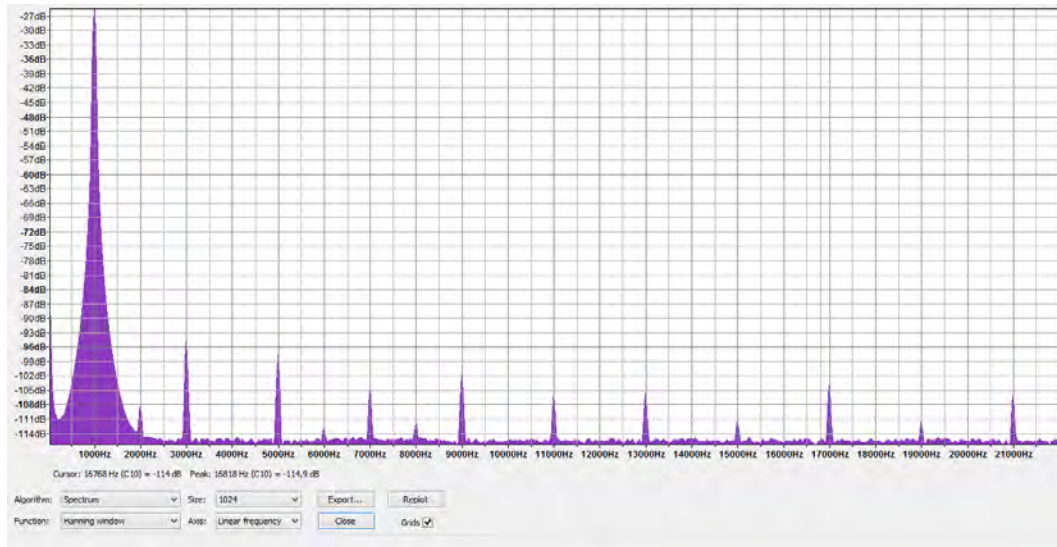


Figure 4.10: Harmonic spectrum of *E. coli* on Pt electrodes (1.1×10^{12} CFU/ml). As the bacterial concentration increased, the harmonic amplitudes increased as well as more harmonics emerging in the spectrum.

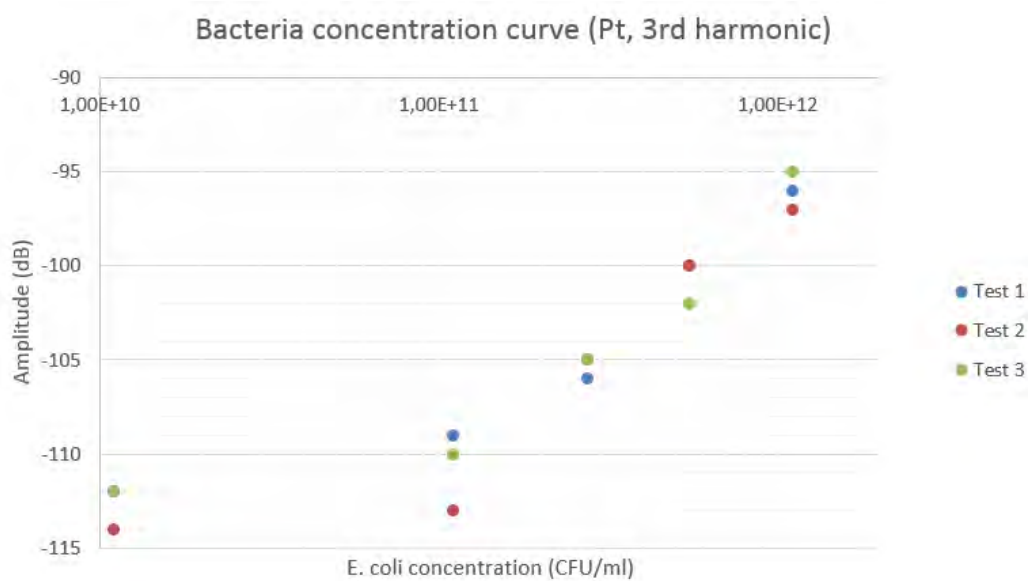


Figure 4.11: Concentration curve for Pt electrodes (3rd harmonic)

and concentration curves of the 3rd and 5th harmonics were plotted. Figure 4.11 and Figure 4.12 show the concentration curves for tests performed on Pt and Ti electrodes respectively. The concentration curves for both Pt and Ti are shown in Figure D.14 and Figure D.15 (Appendix D).

It can be seen that there is less variation in results for Pt electrodes than

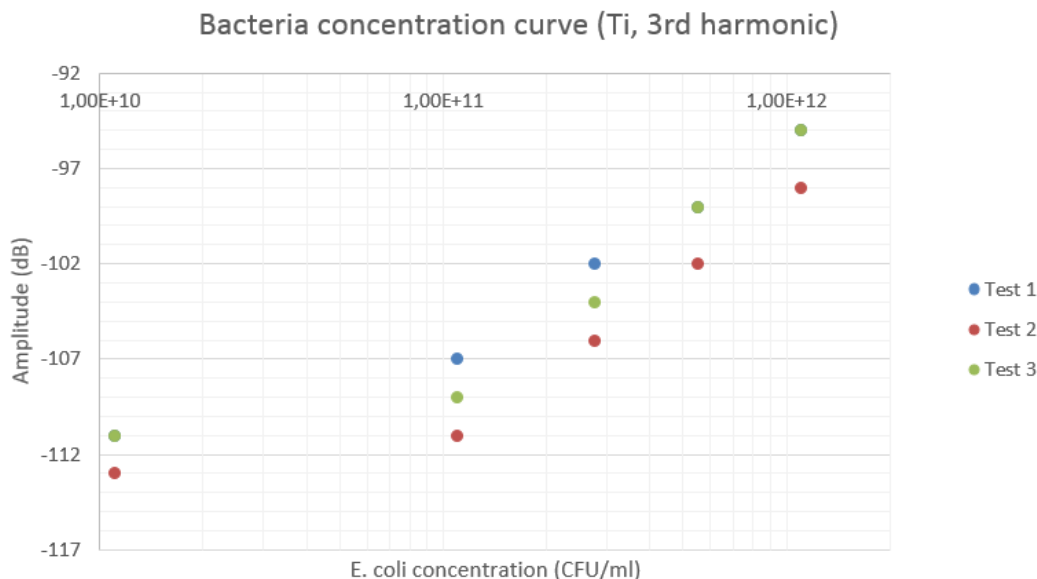


Figure 4.12: Concentration curve for Ti electrodes (3rd harmonic)

for Ti electrodes (present at both the 3rd and 5th harmonic). There is also a higher response (amplitude) for Pt electrodes. The higher amplitude may be due to the insulative effect of the oxide layer present on the Ti electrodes. The higher variation can be attributed to the non-uniformity of the oxide layer on the Ti electrode surfaces.

The testing process showed that the sensors had a response time in as little as 4 seconds. If a calibration step (with distilled water) and washing steps are included, tests per sample only took approximately 4 minutes.

4.4.3 Viable vs non-viable E. coli

The difference in non-linear harmonics of viable and non-viable bacteria was tested. Bacteria was killed by heat or using ethanol sterilisation. These samples were plated (on agar nutrient plates), which showed that most of the bacteria died (< 1000 CFU/ml).

The heat-killed bacteria were tested first. The most significant change was that there was a rise in the harmonic amplitude (+ 2-4 dB) for each peak when testing non-viable bacteria. This rise can be attributed to the way in which the bacteria were killed. The bacterial membrane may have ruptured, allowing the protein rich plasma to be exposed in the sample. This may have increased the conductivity, thus explaining the rise in the harmonics.

Another method of killing bacteria was tested. Bacteria was sterilised by

using 70 % ethanol. This suspension was plated onto an agar nutrient plate, proving that there were very few viable bacteria left (< 200 CFU/ml).

After three consecutive tests, it was seen that there was no increase in harmonics. The harmonics disappeared, and the sample showed results similar to that of distilled water. This shows that the plasma (or other bacterial proteins) that increased the conductivity in heat killing, was completely denatured by the alcohol. The bacteria may also be intact, but that the ion channels (which may be the cause of the non-linear harmonics) are blocked in some way by the addition of alcohol. This indicates a clear difference indicating that the way in which bacteria is killed, using heat or alcohol, changes the non-linear spectra.

4.4.4 Electrode geometry effects

The large planar electrodes were compared with the IME electrodes on the IntelliTUM chip. The working and measuring electrodes were switched. This gave similar results i.e. there were no significant changes in the harmonic spectra. This shows that the imbalance in electrode surface areas does not have much of an effect on the results in a bipolar setup (this was present in both IME and large electrodes).

The most significant difference when measuring with IME electrodes is that there is a more significant peak on the second harmonic. This is also present during testing for the threshold input voltage for distilled water. EIS tests with the IME chip have shown that the tests are not reproducible.

A symmetrical electrode setup was tested (Figure D.2 in Appendix D). The chip consisted of two sets of electrodes: an inner and outer small electrode pair, and an inner and outer large electrode pair.

The smaller electrodes gave no significant advantage compared to the IntelliTUM Pt chip. The large electrode pair gave similar results to the Pt IntelliTUM chip. This is due to similar surface areas and distance between electrodes. After consecutive tests on both sets of electrodes, it was seen that by increasing the distance of the electrodes, the sensitivity decreased. This may be due to the current density vector having a longer distance to reach the counter electrode, resulting in higher impedance. This higher impedance lowers the sensitivity of the sensor.

4.5 Conclusion

Non-linear electrochemical impedance spectroscopy (EIS) was used to detect bacteria. Various electrode geometries on glass chips were tested. Platinum

and titanium electrode materials were compared for ionic solutions, bacterial concentrations, non-viable bacteria and electrode geometries. Impedance spectra and harmonic spectra were recorded and compared.

The sensitivity achieved with this method was 1.1×10^{10} CFU/ml for bacteria, and 0.01 mg/L for ionic solutions. Response times for the detection of the analytes was less than 4 minutes (including calibration and washing steps). After testing it is recommended that the large planar electrodes (on the IntelliTUM chips) are to be used for further development. Platinum was the most successful material, showing the highest sensitivity and have the lowest variance in the results. This may have been due to the higher impedance caused by the oxide layer formed on top of the Ti chips.

The setup and measurement protocols for testing this method have been established (a bipolar electrode setup, with a gain of 0.6, input voltage of $3 V_{p-p}$ and frequency of 1 kHz). Geometrical effects were also tested. Using these methods, it was seen that IME arrays do not give any advantage than larger planar electrodes.

The actual cause of these harmonics is not well studied. The presence of bacteria causes these effects, and it is speculated that the bacterial membrane, ionic pores in this membrane or bacterial plasma may cause these harmonics to emerge. It was seen after testing non-viable bacteria that this may have been the case. After denaturing the bacteria (using ethanol) these harmonics disappeared. This gives a clear indication that the bulk conductivity of the sample increases when bacteria is heat-killed, due to some form of plasma being released due to the denaturation of the bacterial membrane. These effects, however, must be further investigated to determine the true cause of the non-linear harmonics due to bacterial presence.

Some improvements can be made to the detection method and setup. The measuring setup (using a voltage source and Steinberg UR 22 audio interface) can be improved by filtering the input from the signal generator. This could decrease the presence of ghost harmonics seen when determining the threshold voltage, thus increasing sensitivity. Testing for specificity has to be confirmed in future development, by testing the chips with other bacterial strains. This is a promising method for determining *E. coli* concentrations in water using a relatively simple and low-cost detection method, resulting in good sensitivity and excellent response times.

Chapter 5

Fiber-Optic Biosensor

5.1 Introduction

Fiber-optic biosensors have been used to detect bacteria with high sensitivities and with good response times. These sensors usually employ complicated lenses, detection setups and expensive equipment to detect the bacteria. A simplified fiber-optic biosensor is investigated. Hand-made fibers were manufactured for use in the setup. The test protocol, using simple optoelectronics, is discussed in detail. The fibers were immobilised with anti-E. coli antibodies. Fluorescence microscopy is used to determine the immobilisation efficiency of antibodies on the fibers. Fluorescence microscopy is also used to detect the attachment of bacteria on the fiber surface. The results of initial bacterial tests are also discussed in detail.

5.2 Test protocols

5.2.1 Optical fibers

Optical fibers were manufactured from borosilicate glass (of which the main constituents are SiO_2 and B_2O_3 with a molar percentage of approximately 84% and 11% respectively) at Glasschem CC (Stellenbosch, South Africa). This was done in the following manner:

- Heat borosilicate glass staff with a gas flame
- Tap end of melted staff with a metal rod
- Extrude the glass by moving the rod away from the melted glass staff
- Allow the fiber to cool
- Cut fibers to desired length using a scalpel

This method was used due to its simplicity, and the availability to manufacture many fibers at virtually no cost. The optical fibers typically used in biosensors are precision designed and manufactured, with smooth surfaces and perpendicularly flat planar edges. This method, however cost effective, resulted in fibers of varying diameters. The method of cutting the fibers (with a surgical

scalpel) also resulted in rough edges. This could influence light entering and exiting the fiber, as well as immobilisation efficiencies.

5.2.2 Surface hydroxylation

The method used by Corso et al. [95] was modified and used to modify the surface of the glass fibers and to covalently immobilise antibodies to the surface. The borosilicate glass fiber has naturally occurring hydroxyl molecules on the surface. In order to optimise the immobilisation efficiency of the antibody to the fiber surface, the concentration of hydroxyl molecules had to be increased. The following method was used to increase the amount of hydroxyl molecules on the surface of the fiber:

- Place fiber in a 3:1 Piranha solution (Sulfuric acid:Hydrogen peroxide) for 10 seconds
- Fiber was removed and placed on a Petri dish
- Fiber was placed in a 1.5 ml vial with toluene (99.8%, Sigma-Aldrich)
- Fiber was rinsed (turning the vial two times) in the toluene vial
- Fiber was removed and placed in 1.5 ml vial

This method removed all unwanted chemical species from the surface of the fibers and increased the amount of OH molecules for crosslinker attachment.

5.2.3 Antibody immobilisation

A method had to be developed to properly immobilise antibodies to the surface of the fibers. A method used to immobilise antibodies onto the surfaces of planar ZnO substrates was developed by Corso et al. [95]. Two different crosslinkers ((3-Glycidyloxypropyl) trimethoxysilane (GPS) and (3-mercaptopropyl) trimethoxysilane (MTS)) were compared. Both linkers acted by binding with activated hydroxyl groups on the surface of the substrate. The crosslinkers then covalently linked the surface of the substrate and an amine group on the antibody surface. GPS had a lower immobilisation efficiency, but required less processing steps. Less processing steps infer less processing costs when the sensor is to be manufactured. For this reason only GPS (Sigma-Aldrich) was used.

Using the method developed by Corso et al. [95] for ZnO surfaces, a GPS solution with toluene (99.8%, Sigma-Aldrich) was prepared. A 4% solution of GPS with toluene was prepared. The fibers were placed in a 1.5 ml vial containing the solution, placed in a nitrogen environment, sealed and left for 22 hours. Afterwards the fibers were treated in the following manner:

- Place fiber on Petri dish
- Place fiber in a 1.5 ml vial with phosphate-buffered saline (PBS) solution (pH of 7.4)
- Fiber was rinsed (turning two times) in the PBS vial
- Fiber was removed and placed in 1.5 ml vial

The fibers, now coated with the GPS crosslinker, were placed in a (2mg/ml antibody diluted in PBS, 750 ml total) 200 μ g/ml polyclonal anti-E. coli antibody (Abcam) solution with PBS (pH of 7.4). The primary antibody (Abcam, Anti-E.coli antibody, polyclonal goat, wide species range of E.coli (95 % homology between strains)) was bought. The fibers were left in the antibody solution for 4 hours in an opaque container in a nitrogen environment. The fibers were removed and rinsed with PBS solution.

After primary antibody (PAb) immobilisation the efficiency of the crosslinker had to be confirmed. Borosilicate glass slides were used to test the binding efficiency. These slides were processed in the method described above for primary antibody immobilisation. In addition these slides were then exposed to secondary antibodies (Donkey polyclonal Secondary Antibody to Goat IgG - H and L (Alexa Fluor 488, EX at 495 nm and EM at 519 nm)), to indicate fluorescence, in the following way:

- Glass slides were placed in a Petri dish
- Secondary antibody solution was pipetted onto the surface
- Slide was placed in a light-proof container
- Container was placed in a fridge for 2 hours at 4°C
- Slides were rinsed with aliquots of PBS

All these processing steps were conducted in a dark room to avoid denaturation of the fluorescence molecules that form part of the secondary antibody.

5.2.4 Bacterial suspensions

E. coli DH5 α was grown in a nutrient broth. A bacterial suspension for testing was prepared in the following way:

- Pipette 3 ml of bacterial nutrient solution into a vial
- Centrifuge for 90 seconds at 7000 rpm
- Remove nutrient broth from vial (leaving centrifuged bacterial pellet)

- Pipette 1.5 ml of PBS into the vial
- Vortex for 10 seconds
- Centrifuge for 90 seconds at 7000 rpm
- Remove PBS from vial
- Pipette 1.5 ml of PBS into vial
- Vortex for 20 seconds

Bacterial concentrations were determined by diluting the bacterial suspension, pipetting onto agar nutrient plates and growing for 24 hours at 37.5°C. The viable colonies were then counted to determine the concentration (CFU/ml).

5.2.5 Measurement setup

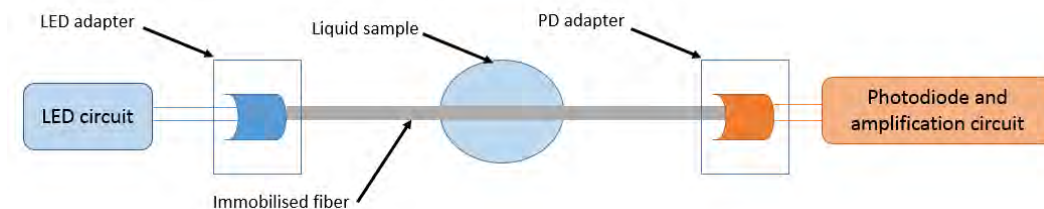


Figure 5.1: Fiber-optic biosensor measurement setup

Figure 5.1 shows the measurement setup used. The sensor was tested using an LED and photodiode. Two adapters were designed and 3-D printed to house the LED (datasheet in Appendix E) and PD (datasheet in Appendix E), and to allow space for the optical fiber to be inserted (small connecting hole). 3D Printing is a flexible technique that allows rapid prototyping due to its fast production time and low cost. The LED was connected to an LED circuit consisting of a power source, a resistor and an LED (circuit diagram is seen in Figure C.3 in Appendix C). The photodiode output current was converted to a voltage and amplified (circuit diagram is seen in Figure C.4 in Appendix C). This was connected to an Agilent 6.5 digit Digital Multimeter. The setup was placed in a darkroom and covered with a light shield. Liquid samples (250 μ l) were pipetted onto the fiber, suspended above a glass slide. Voltage measurements were taken approximately every 15 minutes for 2 hours.

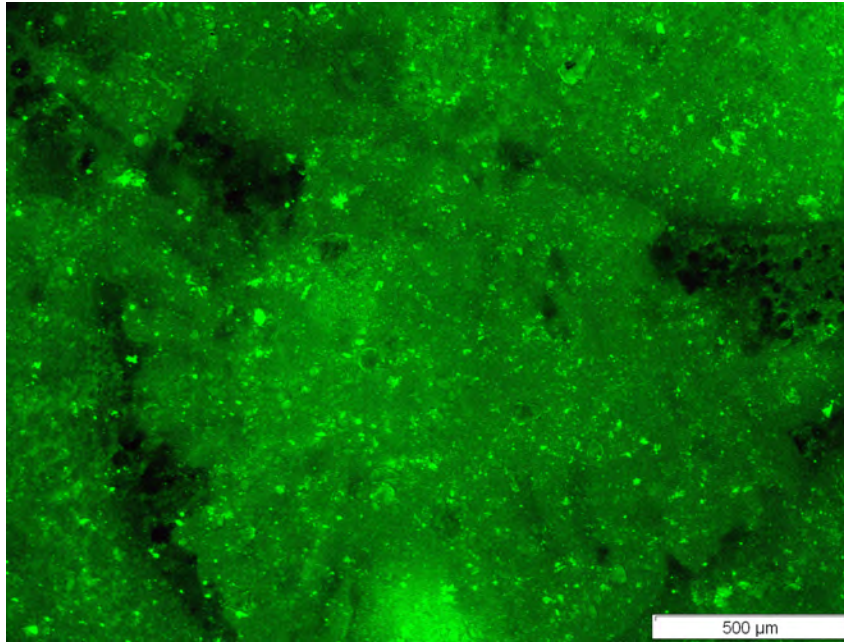


Figure 5.2: Fluorescence image of glass slide (Glass + GPS + PAb + SAb). The slide was immobilised with the crosslinker, primary antibody and secondary fluorescence antibody. The fluorescence indicates that successful immobilisation took place.

5.3 Antibody immobilisation on glass slides

Borosilicate glass slides were used to establish the immobilisation method before using glass fibers. The slides were hydroxylated and primary antibodies were immobilised. Thereafter secondary fluorescence antibodies were adhered to test immobilisation efficiency. These slides were placed in a Wide field fluorescence microscope (Olympus IX81 with UBG excitation filter excited at 492 nm) and imaged. Figure 5.2 shows a glass slide covered with primary and secondary antibodies, at $4\times$ magnification. Figure D.16 shows the glass slide covered in secondary antibodies at $20\times$ magnification (Appendix D). It can be seen that the secondary antibodies cover a great part of the surface. The attachment of the crosslinker (GPS), primary antibody (PAb) and secondary antibody (SAb) had to be investigated.

Figure 5.3 shows a glass slide that has not been treated with the GPS crosslinker or the primary antibody. It was treated with the secondary antibody. As can be seen, very little fluorescence is shown in the image. This is due to the little to no binding that occurs between the glass slide and the secondary antibody. The small amount of fluorescence indicates that a negligible amount of SAb may have bound to some surface molecules.

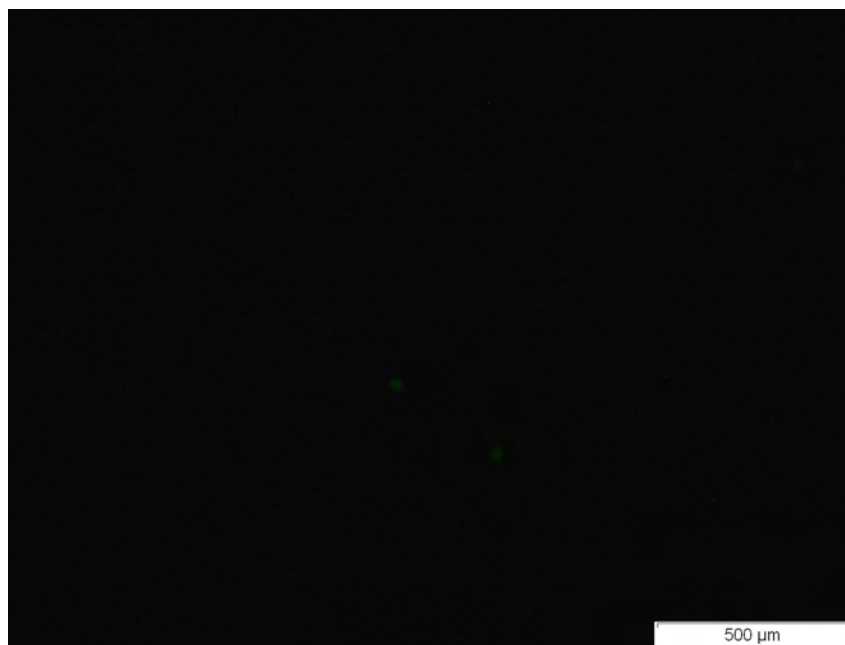


Figure 5.3: Fluorescence image of glass slide (Glass + SAB). The slide was only exposed to the secondary antibody, resulting in very low fluorescence levels.

Figure 5.4 shows a glass slide that has been covered with the crosslinker,

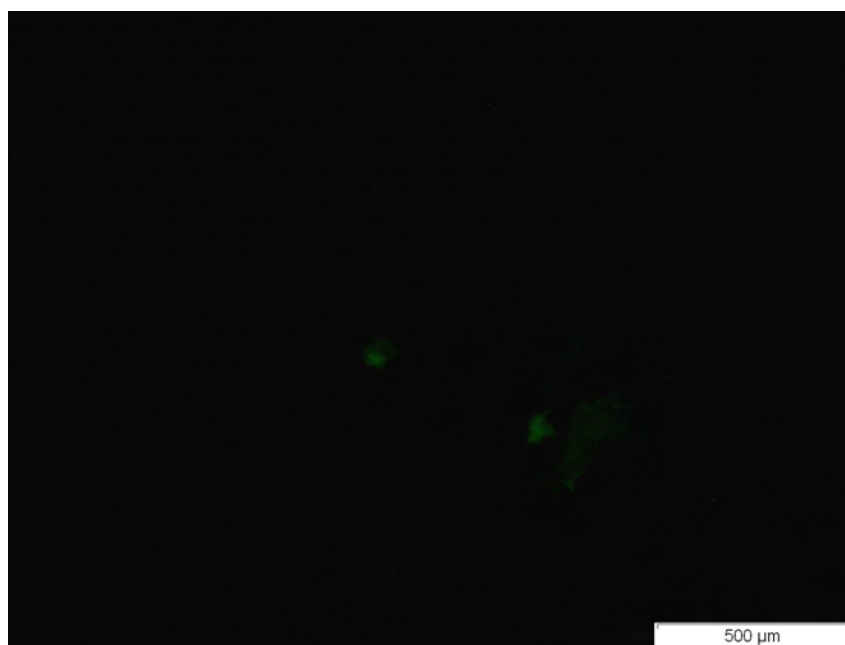


Figure 5.4: Fluorescence image of glass slide (Glass + GPS + Sab). The slide was exposed to the secondary antibody and the crosslinker. This resulted in very low fluorescence levels.

but no PAb. The glass slide has been treated with the secondary antibody to indicate possible fluorescence. It can be seen that, as in Figure 5.3, there is very little to no fluorescence in the image. This indicates that the secondary antibody does not efficiently bind with the crosslinker. This is the preferred state, as only primary antibody binding is required.

Figure 5.5 shows a glass slide covered with crosslinker, PAb and secondary

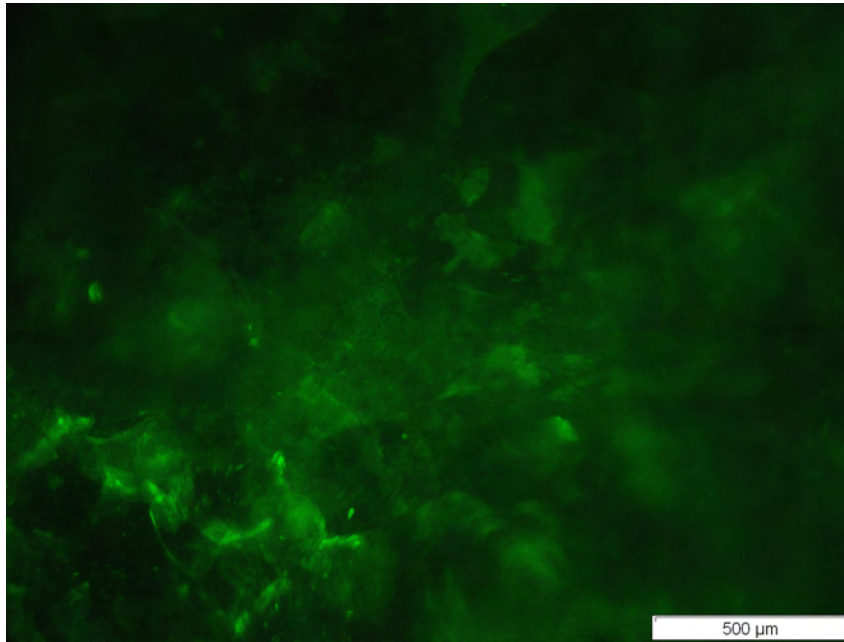


Figure 5.5: Fluorescence image of glass slide (Glass + GPS + PAb + SAb). The primary antibody was covalently immobilised onto the glass slide. The high level of fluorescence indicates that successful antibody immobilisation took place.

antibodies. The high fluorescence intensity indicates that the SAb successfully bonded with the PAb. As seen in the image, the coverage is quite uniform over the area, with slight intensity changes. This may be due to the imperfections caused by the crosslinker binding steps. This is, however, a successful binding result. The SAb can only bind to the two light chains of the primary antibody. A self assembled monolayer is formed due to the covalent attachment of the PAb amine group to the GPS crosslinker. This allows the two light chains of the PAb to be open for secondary antibody attachment. The fluorescence images indicate that this had occurred.

Figure D.17a and Figure D.17b (Appendix D) show two more images of a glass slide covered with the antibodies. It can be seen that there is fluorescence coverage over most of the surface, but that there are certain areas (clearly seen

in Figure D.17a) that cause "clumping" of the secondary antibodies. This may be due to a few reasons. The first is that the crosslinker is binding onto itself in certain areas. This causes the PAb to group together on a point, and thus also the SAb. The second reason may be that the PAb group together at a certain point. The grouping of the crosslinker is more likely, due to it being visually confirmed during the immobilisation of the crosslinker onto the surface. Some crystal structures form on the surface of the slides, which can indicate that there is some grouping of the crosslinkers at certain points. This may be due to long deposition time (22 hours) and can be improved for future applications. The overall attachment of secondary antibodies, however, indicate that the bacteria will bind to a great area of the fiber surface.

5.4 Antibody immobilisation on fibers

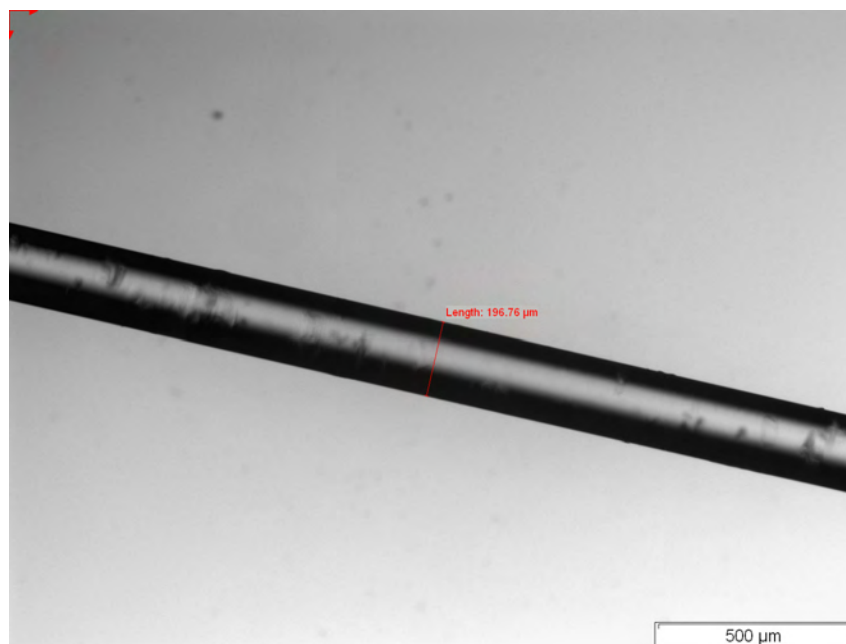


Figure 5.6: Micrograph of an optical fiber

Fibers were imaged with a Wide field fluorescence microscope (Olympus IX81 with UBG excitation filter excited at 492 nm). Figure 5.6 shows an optical fiber micrograph. The thickness of the hand-made fibers vary. When a random sample of 10 fibers were measured, the mean diameter was $243 \mu\text{m}$ with a standard deviation of $45 \mu\text{m}$. Imperfections in the fiber surface can also be seen. This may be due to the extrusion process (non-precise) or due to particles (dust) that may have attached after extrusion.

Figure 5.7 shows a fiber that has no crosslinker (GPS) and no PAb. It

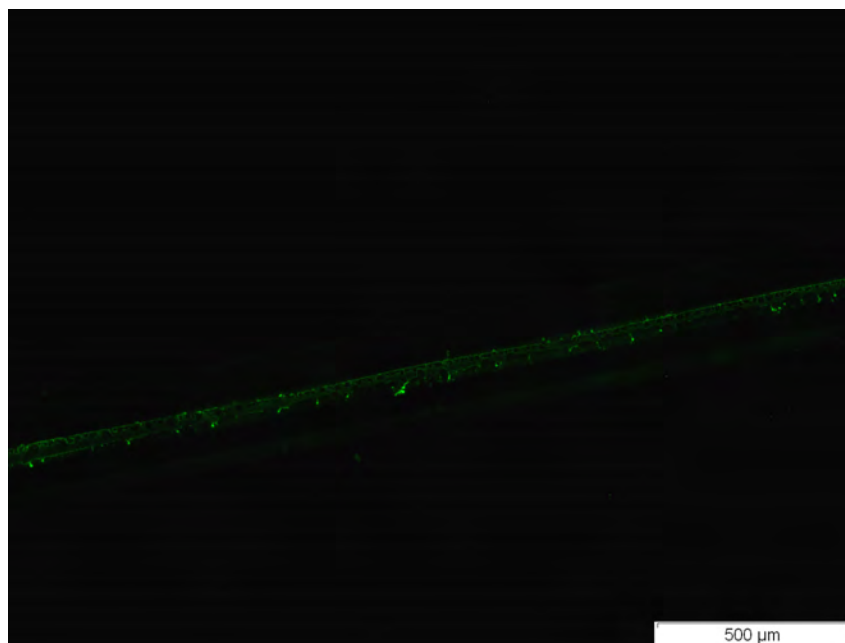


Figure 5.7: Fluorescence micrograph of a fiber (Glass + SAb). The fiber was only exposed to secondary antibodies, resulting in low levels of fluorescence.

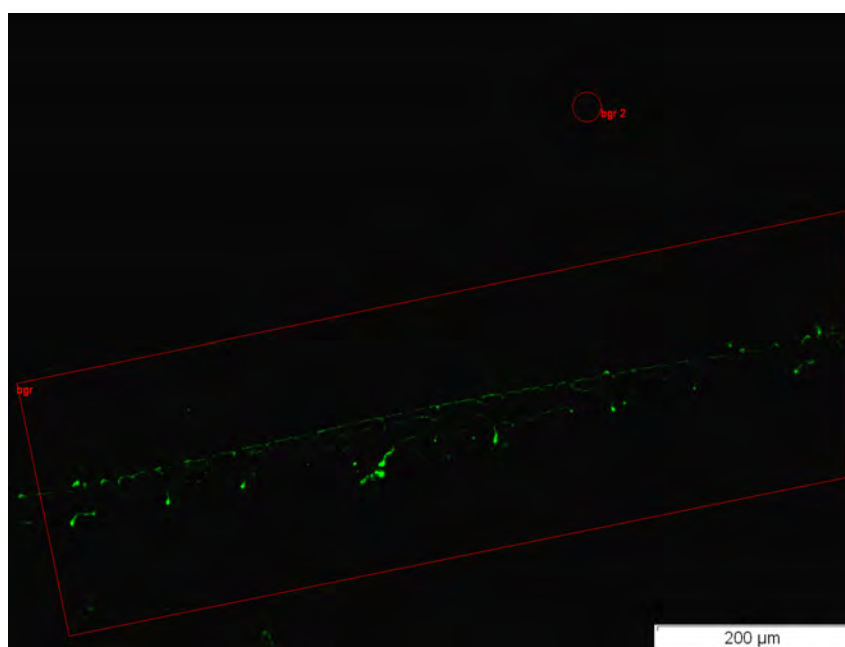


Figure 5.8: Z-stack fluorescence micrograph of a fiber (Glass + SAb)

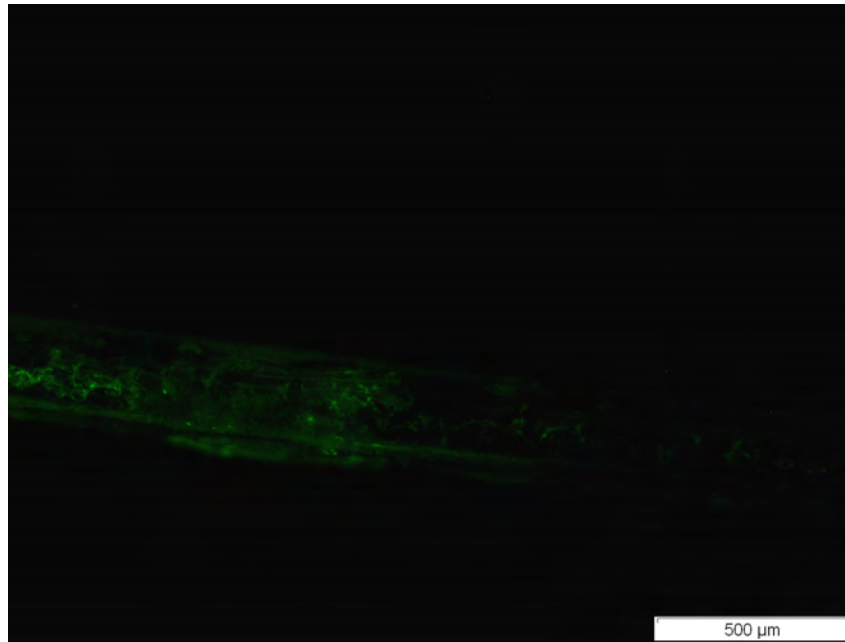


Figure 5.9: Fluorescence micrograph of a fiber (Glass + GPS + SAb). The fiber was exposed to the secondary antibody, after crosslinker adhesion. This resulted in low levels of fluorescence.

has been treated with the secondary antibody. The fluorescence image indicates that almost none of the SAb has attached to the surface of the fiber. The fluorescence seen on the image may be due to some of the unwashed SAb that have gathered at the bottom of the fiber. A Z-stack image is a compilation of cross sectional fluorescence micrographs, indicating fluorescence over the 3D surface of the fiber. A Z-stack is made to indicate the maximum intensity projection of all the images in the Z-direction. Figure 5.8 confirms that there was almost no SAb binding.

Figure 5.9 shows a fiber that has been covered with the crosslinker but no primary antibodies. Similar to Figure 5.7 there was little to no fluorescence present. This indicates similar results to the glass slides that were treated in the same manner. This indicates that the cylindrical surface of the fibers are immobilised in a similar manner to that of the planar glass surface. Figure 5.10 shows a Z-stack image of a fiber treated with crosslinkers but with no PAb. The Z-stack indicates that there are more SAb on the surface of the fiber than the initial image only indicating one Z-level. There is still, however, very little fluorescence. The images indicate that there might be some non-uniformity in the deposition of the crosslinker.

Using transmitted light images the fiber, with the covalently attached crosslinker, can be seen in a different view highlighting the physical fiber. Figure 5.11 shows

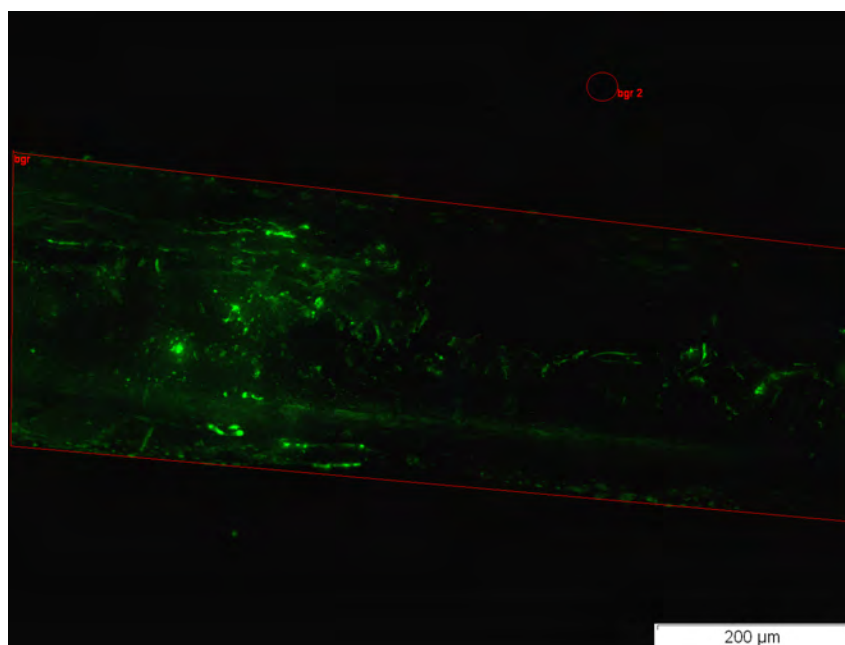


Figure 5.10: Z-stack fluorescence micrograph of a fiber (Glass + GPS + SAb)



Figure 5.11: Transmitted light image of a fiber (Glass + GPS, 4× magnification). The image indicates some non-uniformity in the surface after crosslinker attachment.

an image of the fiber with immobilised crosslinker. It can be seen that there is a non-uniformity in the deposition of the crosslinker, seen as a rough surface on the fiber. These irregularities occur due to the surface of the fiber not being

polished, or due to the long deposition time of the crosslinker. The longer the crosslinker is deposited, the more non-specific binding in a single crosslinking layer occurs. The crosslinker then binds to itself, forming in clumps as can be seen on the image. These effects can be seen on various transmitted light images included in Appendix D (Figure D.18, Figure D.19 and Figure D.20).

Figure 5.12 shows a fiber that has been immobilised with the crosslinker

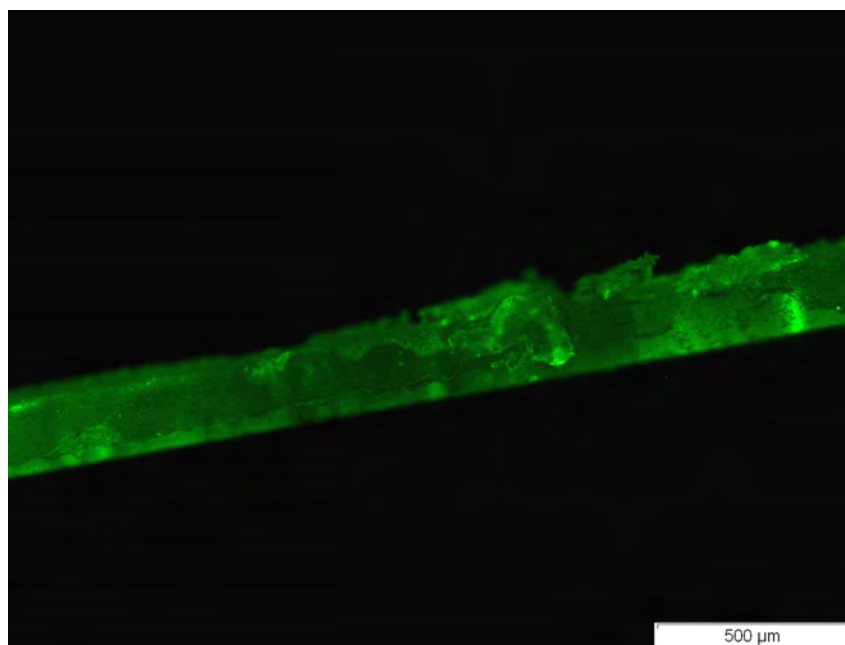


Figure 5.12: Fluorescence micrograph of a fiber (Glass + GPS + PAb + SAb). The high level of fluorescence indicates that successful primary antibody immobilisation occurred.

and PAb. This shows that the binding of the secondary antibodies are similar to that in the previous experiments with the planar glass slides. The fluorescence is clearly much brighter. It can be seen that the fiber has some 3D non-uniformities and clumping of the crosslinker (GPS) occurs. This, however, does not affect the binding of PAb or fluorescent SAb. This entire surface is covered in PAb which infers a successful covalent attachment technique. Z-stack images were taken to confirm that the fluorescence is present on the entire surface of the fiber. Figure 5.13 shows a Z-stack image of the fiber. Bright fluorescence can be seen, indicating that the entire 3D surface of the fiber has been covered with SAb, which indicates that the surface was immobilised with PAb.

Figure 5.14 and Figure 5.15 compare relative fluorescence values for glass slides and optical fibers. This was measured using the Wide field fluorescent

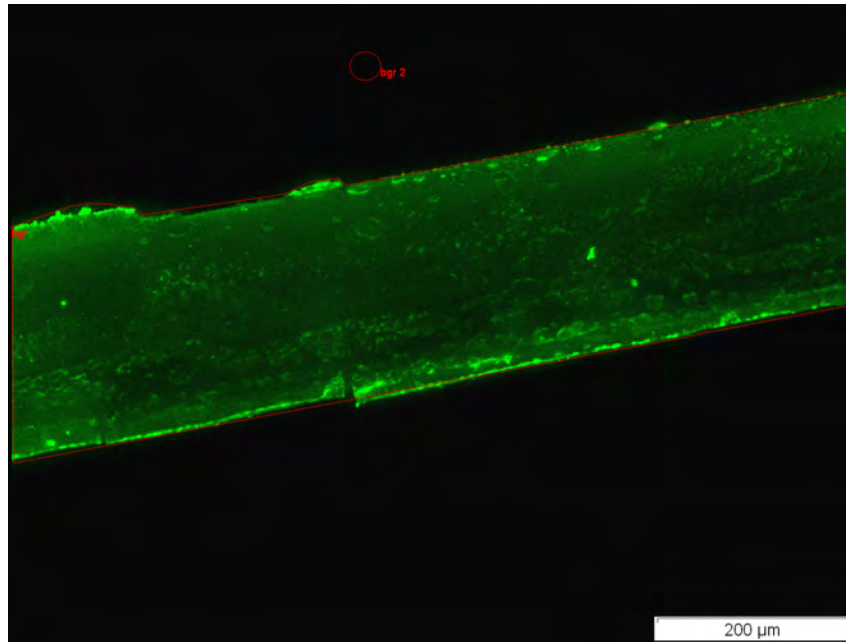


Figure 5.13: Z-stack fluorescence micrograph of a fiber (Glass + GPS + PAb + SAb)

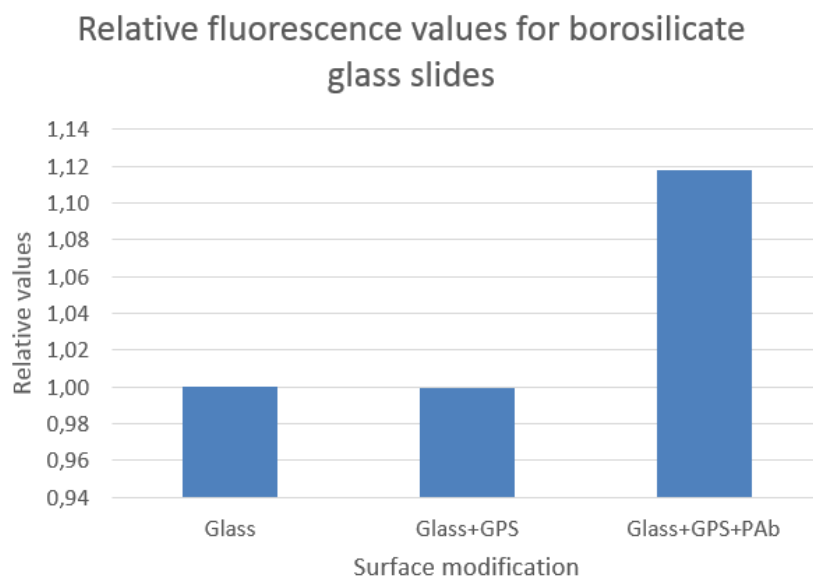


Figure 5.14: Relative fluorescence values (glass slides). The level of fluorescence drastically increases after primary antibody immobilisation.

microscope. The areas of fluorescence for the fibers was cropped and measured. The background was subtracted. As can be seen there is little to no change in both the glass and fiber fluorescence when only the GPS crosslinker is added. The fluorescence due to the presence of the PAb indicates that the

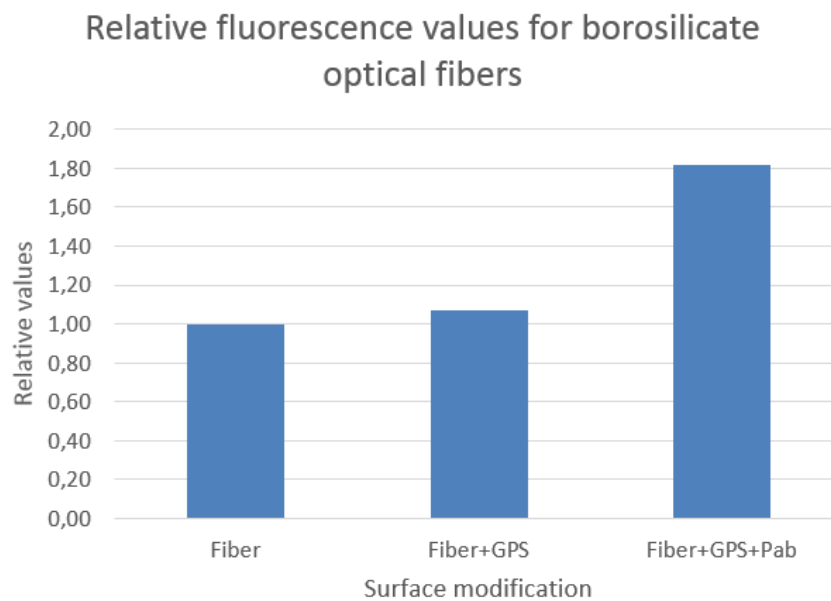


Figure 5.15: Relative fluorescence values (optical fibers). The level of fluorescence drastically increases after primary antibody immobilisation, similar to that on glass slides.

SAb only binds to the PAb.

5.5 E. coli binding on fiber surfaces

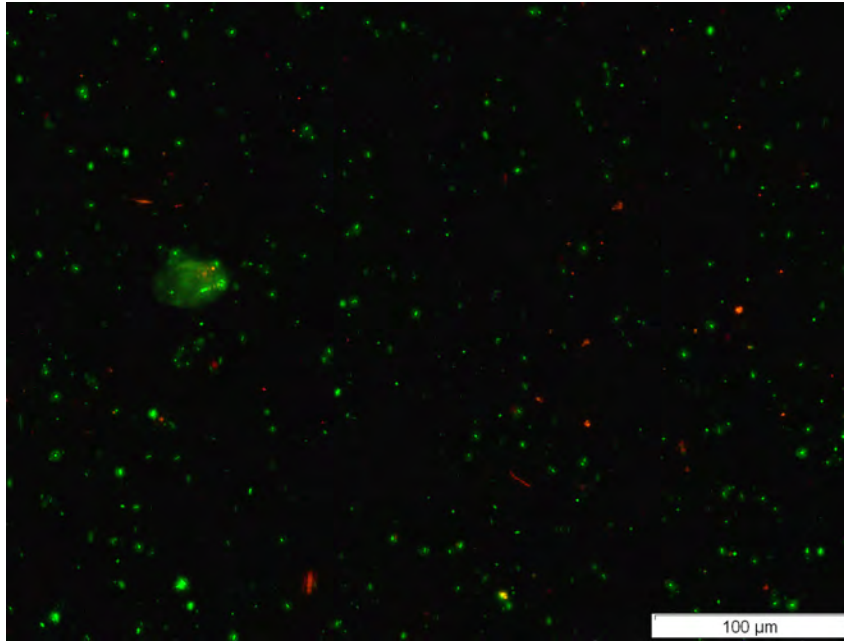


Figure 5.16: Glass surface with immobilised PAb and stained to indicate bacteria movement and adhesion

The bacteria attachment to the surface of the fibers is one of the critical mechanisms for the operation of this biosensor. The effect of bacteria adhesion to the PAb (on the surface of the fiber) had to be determined. The time for adhesion was also unknown. The position of the bacteria in the 3D matrix of the water droplet relative to the fiber can lengthen the adhesion time. Bacteria that are closer to the fiber will bind first. The health of the bacteria (vitality) will also have an effect. Bacteria seem to move through water droplets randomly. This random movement may cause certain bacteria to be captured by the fiber sooner and others later. Bacteria had to be imaged. This required staining of the bacteria and fluorescent imaging with a Wide field optical microscope. The bacterial stain, BacLight LIVE/DEAD Bacterial viability and Counting kit, was used to stain the bacteria. Propidium iodide was used to stain the dead cells (red) and Syto9 was used to stain the live cells (green). A Wide field fluorescence microscope (Olympus IX81 with UBG excitation filter) was used to image the cells. Excitation wavelengths between 492 nm and 572 nm were used.

An important consideration was the movement of the bacteria. Consequent images were taken over a period (2-5 minutes) and edited to make a video. This would indicate the movement of the bacteria and any other effects over

time. Figure 5.16 shows a planar glass surface that has been treated with the crosslinker and PAb. This PBS-bacteria suspension was pipetted onto the glass surface. After 1 hour the surface was imaged. A video was taken which showed the movement of the bacteria. Some bacteria had adhered to the surface, but many bacteria were free to move. The video shows that the bacteria moved in all three directions (X, Y and Z axis) in a seemingly random pattern. This indicated that unbound bacteria had to be removed from the surface. Washing with PBS aliquots was the most effective method.

Fibers were immobilised with the PAb. The fibers were placed in a vial and bacteria suspension was then pipetted onto the fibers and left for 1 hour, 4 hours and 5 hours. These were then washed by removing the fibers from the bacterial vial, placing in a vial with 1 ml of PBS and turning the vial twice. This removed all unbound bacteria from the fiber surface.

Figure 5.17 shows a fluorescent image of bacteria on the fiber after be-

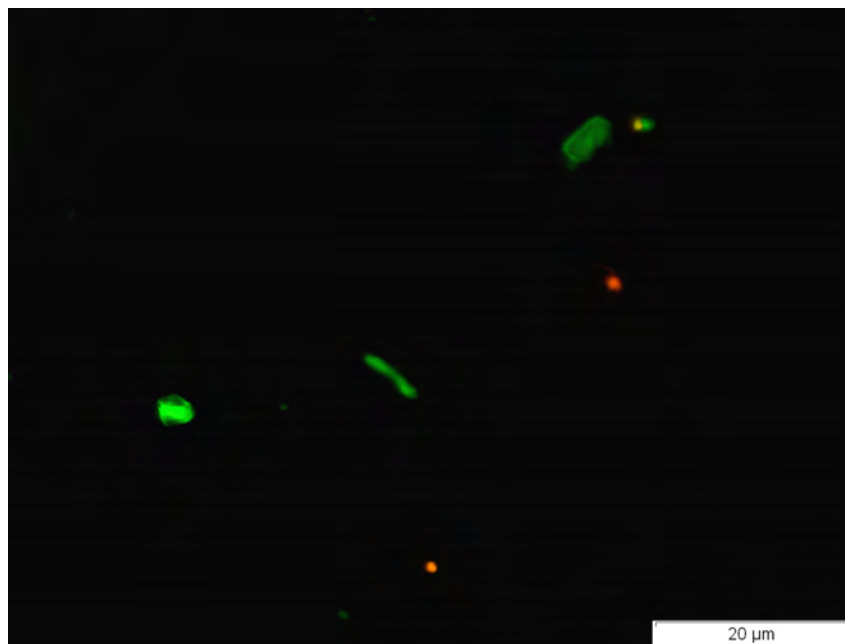


Figure 5.17: Optical fiber immobilised with PAb and exposed to bacterial suspension (1 hour). A few bacteria can be seen on the surface of the fiber.

ing exposed to the bacterial suspension for 1 hour. After a range of images was taken over 2 minutes, it was seen that the bacteria imaged were stationary. This is due to their adhesion onto the fiber surface through antibody capture. The live cells can be seen in green and the dead cells in red. It can be seen that some of the bacteria form small clusters that consist of more than one bacterium.

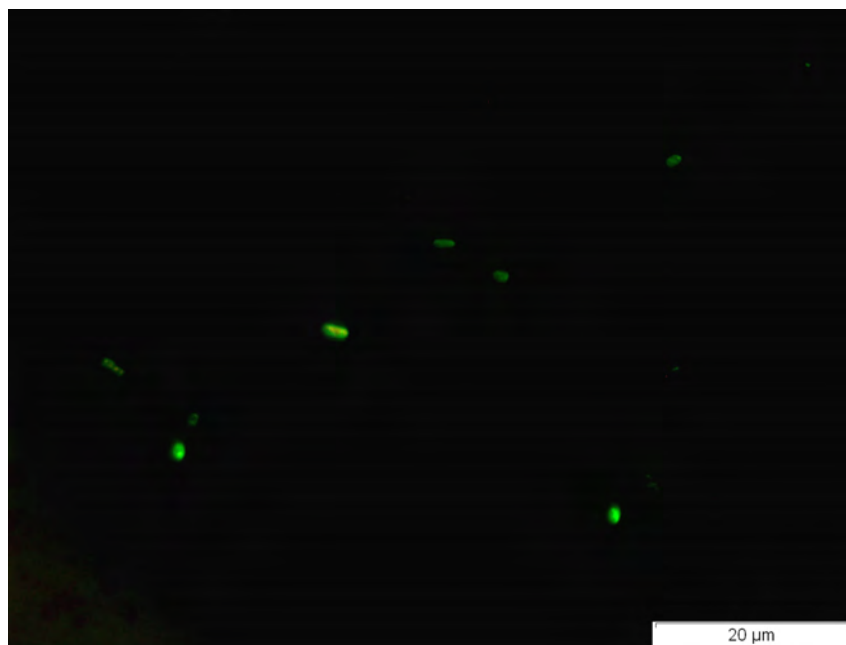


Figure 5.18: Optical fiber immobilised with PAb and exposed to bacterial suspension (4 hours). As the exposure time increases, the amount of bacteria adhered on the fiber increased.

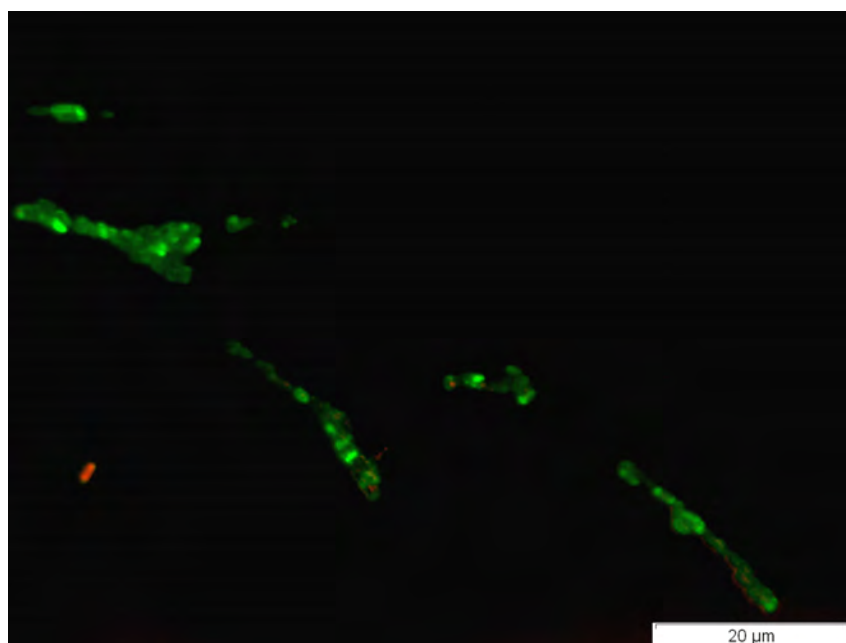


Figure 5.19: Optical fiber immobilised with PAb and exposed to bacterial suspension (5 hours). After a few more hours many bacteria can be seen adhered to the surface of the fiber.

When comparing Figure 5.17 with Figure 5.18 (4 hour exposure) and Figure 5.19 (5 hour exposure) it can be seen that the amount of bacteria attached increases. This can clearly be seen in Figure 5.19 where the bacteria are lying on the fiber surface. This may be due to a few reasons. The first is that antibody-antigen binding takes time. The bacteria move around the sample and may take a time to come into contact with the fiber, or be close enough to attach to the antibody. Due to this random behaviour of the bacteria moving around the sample (due to their flagella) as the exposure time increases, the more bacteria adhere to the surface. This has proven that the immobilisation method for adhering PAb to the surface was effective. It also showed that the bacteria bind to the PAb.

5.6 E. coli detection

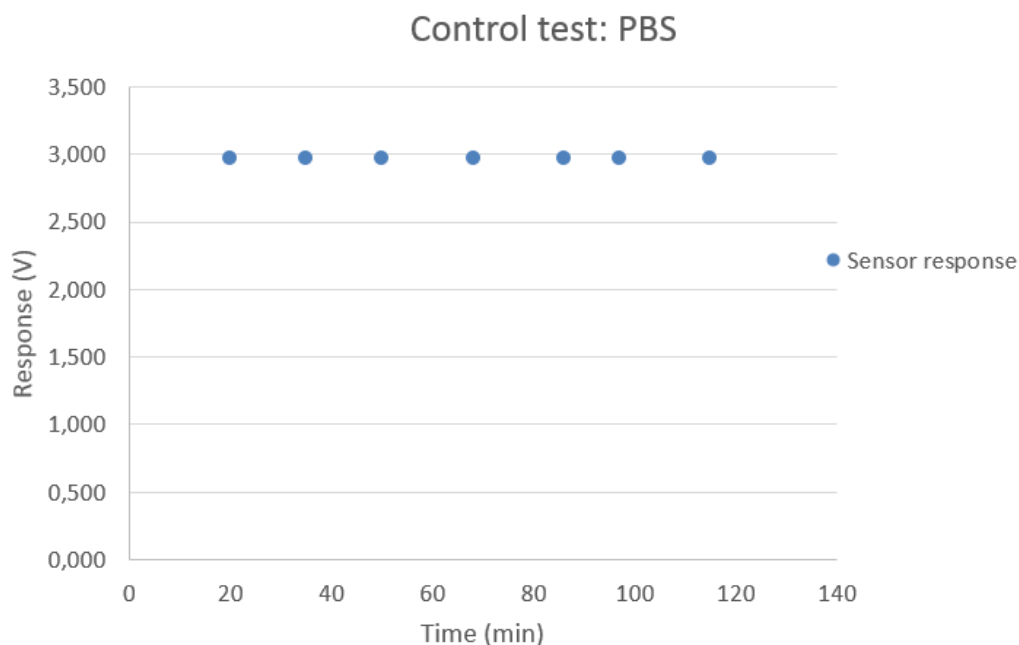


Figure 5.20: PBS control test

Three fiber-optic biosensor tests were successful in indicating bacterial presence. Figure 5.20 shows the control test using PBS and Figure 5.21 shows the bacterial test response for a concentration of 3×10^7 CFU/ml. The control values never change over time. There is a clear increase when bacteria is present in the sample. This clearly shows that when adding bacteria to a sample, there is a clear response.

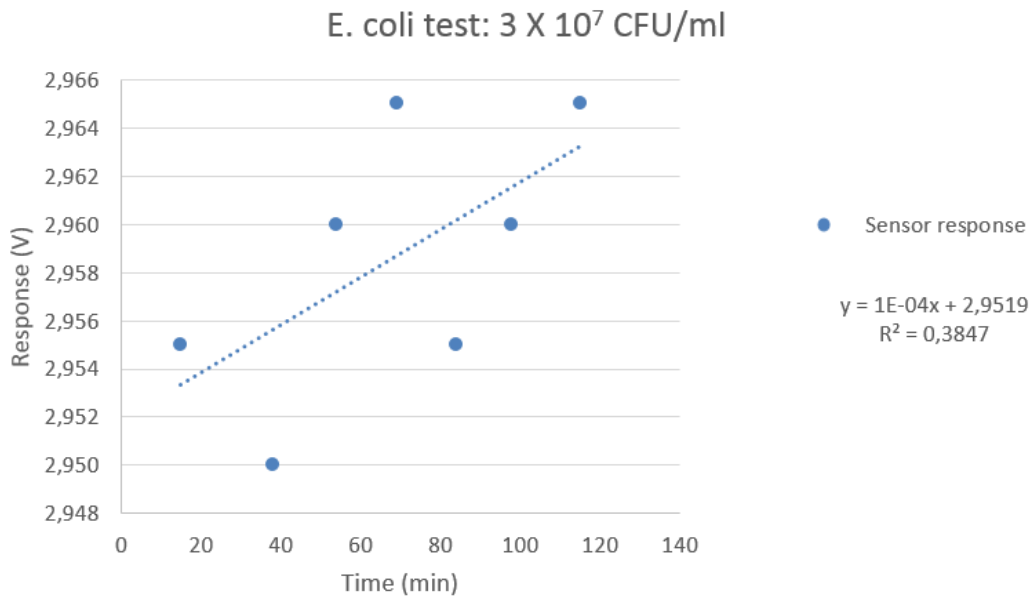


Figure 5.21: E. coli test (3×10^7 CFU/ml, test 1). After two hours a clear increase in the signal can be seen. This may be due to the change in refractive index occurring due to bacterial adhesion onto the fiber surface.

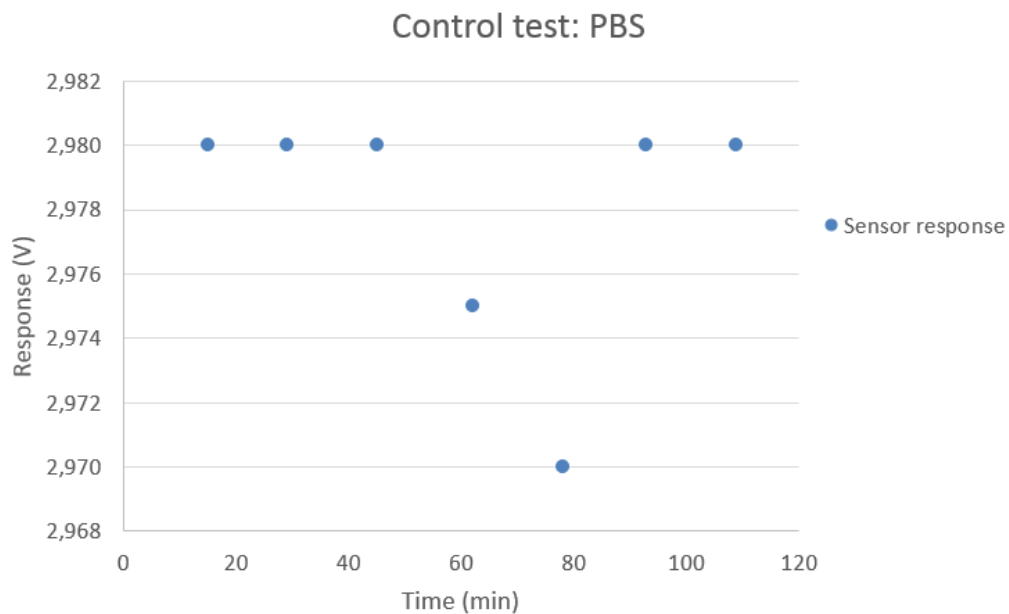


Figure 5.22: PBS control test

Figure 5.22 shows a control test for the sensor and Figure 5.22 shows the E. coli (3×10^7 CFU/ml) test response curve and linear regression line. As can be seen the control test is quite stable over time. There is a clear linear increase in response when bacteria is tested. These tests were conducted on

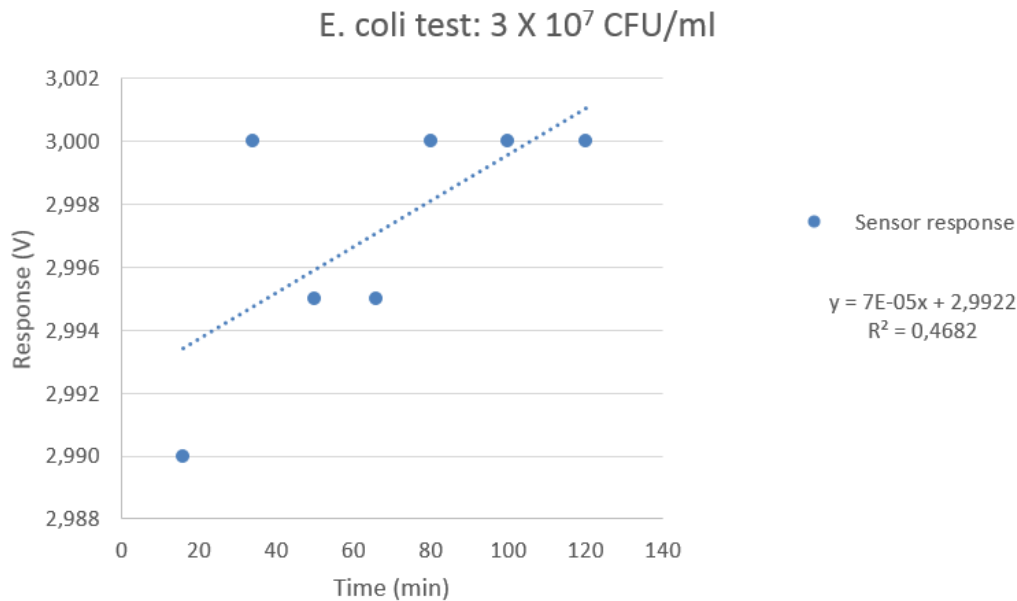


Figure 5.23: *E. coli* test (3×10^7 CFU/ml, test 2). After two hours a clear increase in the signal can be seen. This may be due to the change in refractive index occurring due to bacterial adhesion onto the fiber surface.

the same fiber.

Figure 5.24 shows the response curve for a higher concentration of bacteria (5.77×10^8). As can be seen there is still a linear increase in voltage as time goes on. The gradient of the linear fit is slightly higher than the average of the first two tests (3×10^7 CFU/ml). This may be indicative of a way to quantify the concentration of the sample.

These initial tests reveal that there is an indication that different concentrations of bacteria have higher responses. These tests must be repeated to ensure reproducibility of this effect. The immobilisation method, LED and PD types must be varied to compare the best results. It can be seen that there is a variation in the results around an approximate linear fit. This variation may be due to various factors. There may be interference with the light entering/exiting the fiber due to rough surfaces (due to the fiber being cut and not polished). The GPS on the surface has various non-uniformities that may cause light to be scattered or reflected in/out of the fiber.

The binding of bacteria to the surface of the fiber has shown that there is an increase in the response. This is due to a change in the net refractive index of the fiber. As more bacteria bind, they act as a cladding. This increases the TIR of the fiber. The effect that various wavelengths of light on the fiber (relating to absorbance occurring) must be investigated in future de-

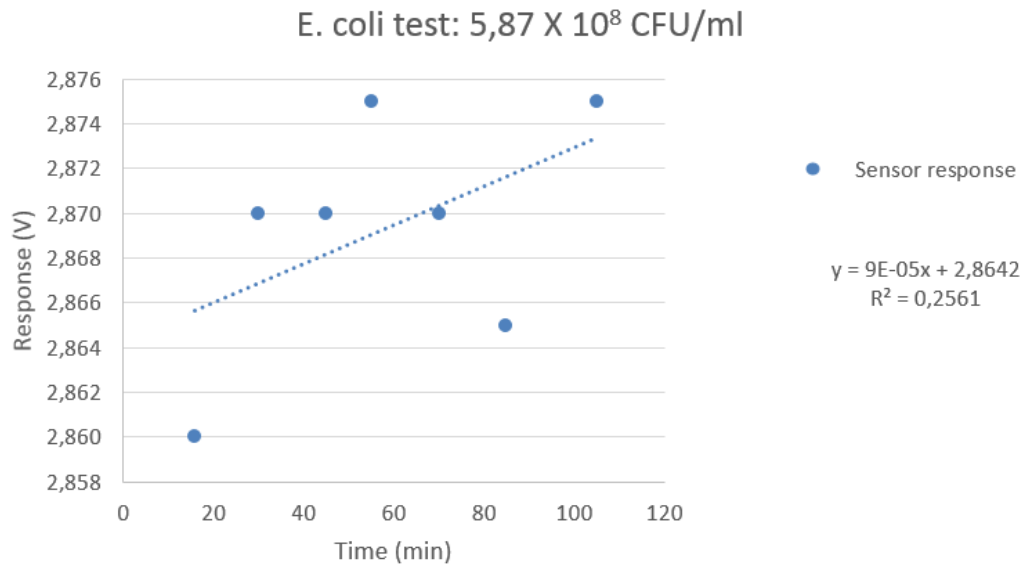


Figure 5.24: E. coli test on optical fiber ($5,77 \times 10^8$ CFU/ml). After two hours a clear increase in the signal can be seen. The linear regression fit gradient is slightly higher for the higher concentration of bacteria.

velopment. A fiber-optic biosensor, that shows a clear response when bacterial samples with a concentration as low as 3×10^7 CFU/ml is measured, with a response time of under 120 minutes was successfully manufactured.

5.7 Conclusion

These initial tests of the optical fiber biosensor have revealed some achievements and limitations of the sensor and testing method. The achievements are that the initial tests do indicate that the sensor can detect E. coli in the samples, compared to PBS. Another achievement is that this proves that the immobilisation procedure was successful. It proves that a low-cost sensor was developed, as well as a low-cost testing procedure. This allows for rapid development of prototypes due to the low-cost of the fibers and test setup. There was also some indication of concentration difference in the samples that could be noted. The design of the sensor was also done in such a way that it can easily be integrated into a portable device.

There are some limitations to the sensor and the test setup. Many more tests are required to accurately determine a few important characteristics of the biosensor, such as the LOD, specificity, minimum and maximum response and reproducibility (response related to concentration). The LOD can be determined by repeating the tests for different dilutions of bacteria, up to where an observable response can be seen. The specificity can be determined by

adding other bacteria (e.g. Salmonella) to the sample and seeing if it responds in a similar manner. Other strains of *E. coli* must also be tested, to ensure that a wide range of strains can be detected with this sensor.

The manufacturing process for this sensor has been defined. An indication of the attachment kinetics of the bacteria to the optical fiber surface has been seen. Rapid development of this sensor has been enabled by lowering costs, simplifying the test setup and allowing for interchangeable analytes to be detected. This is due to the crosslinker binding to the amine group of the IgG PAb. This amine group is present in all IgG antibodies, and thus allows a plug-and-play approach to be used in biosensor development. Future research can improve upon the fiber-optic biosensor which has been produced and tested.

Chapter 6

Recommendations for Future Development

6.1 Evaluation of sensors

An electrochemical impedance and fiber-optic biosensor were tested. Both sensors were successful in detecting *E. coli* bacteria. The sensors were developed to be manufactured at a low-cost, and can be easily integrated into a portable device. For use in a prototype, however, there are certain improvements that could be made.

Both sensors could be scaled up for mass-production, resulting in a very low cost difference between the two (depending on the choice of electronics). The response time of the electrochemical sensor was much faster than that of the fiber-optic sensor. This was due to antibody-antigen binding time on the fiber surface. The fiber-optic sensor, however, employs a biorecognition element which would outperform in selectivity of *E. coli* bacteria. The fiber-optic biosensor is also much more sensitive than the electrochemical sensor. Both sensors are relatively easy to integrate into portable systems. The ease-of-manufacture of the electrochemical sensor is much simpler than that of the fiber-optic sensor, which requires many more processing steps, including antibody immobilisation procedures. This could be simplified with further research and development.

The EIS sensor used a voltage source and computer for analysing the signal. These components must be replaced with smaller electronics, specifically designed for a portable device. The electrodes could also be improved by manufacturing chips specifically aimed at bacterial detection (novel electrode structures). The sensitivity of the sensor could be improved by filtering the input voltages, and by filtering certain unwanted harmonics. The specificity of the sensor needs to be determined by testing with other bacterial strains. The possibility of using the sensor to test drinking water can be achieved by filtering certain ions either by the use of novel membranes, or electronically by subtracting ionic harmonics. The use of biorecognition elements, such as antibodies, must be explored to improve on selectivity of bacterial detection.

The fiber-optic biosensor used a very sensitive multimeter for detection. This

has to be simplified by designing a signal analysis circuit specifically for a portable device. The sensitivity and specificity of the sensor must be re-evaluated, testing various fiber geometries, different immobilisation procedures and different light sources. The use of different photodiodes, specifically to understand the effects of certain wavelengths, could improve the sensitivity of the sensor.

Both sensors have proven that they could be used in low-cost, portable biosensor prototypes. The application of the sensor will determine which type of sensor is more suited, as well as the specifications for such a device.

6.2 Recommended specifications and applications

The application of biosensors should govern the specifications they have to be designed for. To develop a fully integrated prototype the cost, size, sensitivity and specificity, amongst others, should all be critically evaluated to determine the most appropriate design. Following the tests, the following design requirements were derived. The biosensor prototype must be:

- robust
- easy-to-use
- of a low-cost to produce
- fully portable
- highly sensitive
- highly selective
- able to detect a wide variety of *E. coli* strains
- mass producible
- quick to respond to the presence of *E. coli* bacteria
- quantifiable
- reproducible
- validated
- energy efficient (i.e. it must have a low energy consumption)
- able to handle liquid samples automatically with little user input

- no larger than a cellular telephone
- re-usable with minimum user input

The specifications for the prototype were derived from the requirements. The suggested specifications are seen in Table 6.1. These specifications act as a

Table 6.1: Design specifications for a biosensor prototype

Requirement	Specification	Value
Robust device	Operating temperature	-5 to 40 deg C
	Resists dust	Dust resistant
	PH - operability	6 - 8
	Water clarity operability	0 - 5 NTU
Easy-to-use device	Low user input	<5 user input steps
	Clear operation instructions	Indicated on device
Low cost	Device cost	< R200
	Consumable sensor cost	< R20
Fully portable	Operation time without recharge	12 hours
	Weight	< 150 g
Sensitive sensor	Limit of detection	10^6 CFU/ml
	Linearity error	+ 10 %
	Sensitivity error	+ 10%
	Repeatability error	+ 10%
Selective sensor	Low ionic interference operation	Conductivity at 25 deg C of < 200 mS/m
	Only detects E.coli in presence of other microbes	E.coli bacteria only detected
Sensor must be able to detect a wide variety of E.coli microbes	E.coli strains detectable	95 % (including O, H and K)
Mass-producible	Simple manufacturing process	< 20 processing steps
	Few components	< 40 components
	Scale-up possibility	All manufacturing methods
Quick response time	Response time	<60 min
Reproducible device	Prototype reproduceability	3 Prototypes produced
Low-energy consumption	Operating voltage	24 V
	Battery operating time	12 hours
Automatic liquid handling	Minimum user input	< 5 user input steps
	Controlled volume	10 μ l \pm 10%
	Operating voltage	< 24 V
	Reuseability	3 tests with same device
Small, handheld device	Dimensions	120 x 60 x 20 mm

guideline from which prototype development can start. The specifications will vary depending on the application of the biosensor.

Water testing is a promising field for biosensor development, but may be limited. Water sources are typically very large, and biosensors may not prove to be more cost effective than established testing methods. Other applications, in areas such as research and development (laboratories) and biomedical sensors, are much more appropriate. The large market share, potential of applications and growing trends in biosensor research are all aimed at biomedical applications. This project could form the basis of such a biosensor.

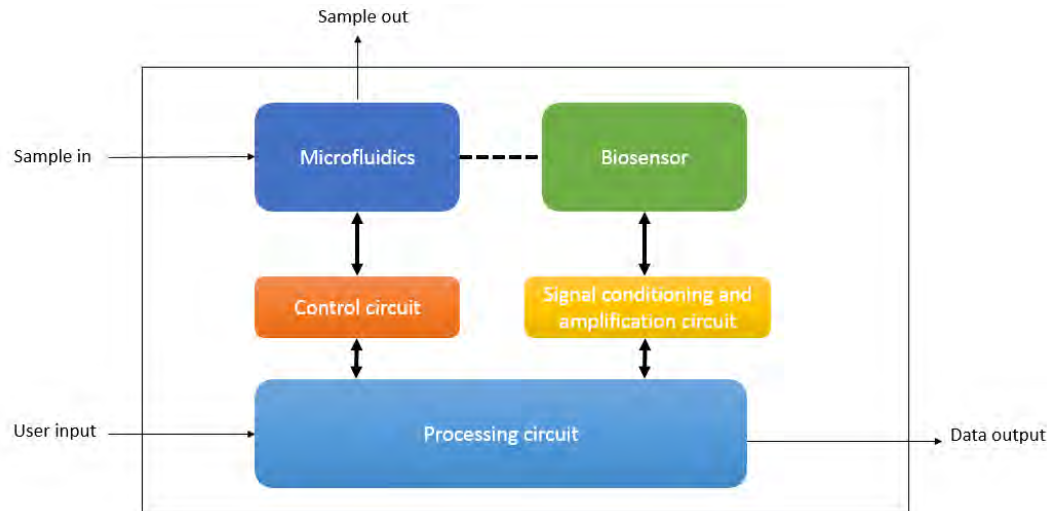


Figure 6.1: System model

6.3 System model

A system model for a biosensor is shown in Figure 6.1. This system model can be used for various biosensor prototypes. The main subsystems include:

- Microfluidic platform
- Biosensor
- Fluidic control circuit
- Signal conditioning and amplification circuit
- Processing circuit
- Casing

The main inputs to the system are a water droplet (the sample) and user input. The main output from the system is a read-out of the bacteria concentration present in the sample in CFU/ml and the liquid sample. When a sample is inserted into the device, it can be passively transported to the microfluidic platform through an inlet. The droplet can be moved automatically by use of microfluidics. A study on microfluidics is included in Appendix A. The droplet will typically interact with a sensing region (a dedicated electrode or fiber-optic sensor). Time is allowed for antigen-antibody binding to occur (if biorecognition elements such as antibodies are used). The detection signal is then generated by interaction between the sensor and the sample. This signal is transmitted to the signal conditioning circuit. The analog signal is converted into a digital signal (A/D conversion) and processed. A digital readout of the concentration of the sample is given to the user. This process can be summarised as follows:

- Insert droplet
- Move droplet to sensor
- Detect analyte
- Move droplet out
- Convert signal (A/D)
- Digital readout of concentration
- Washing and reset steps

This model can be used as the basis from which to design the prototype. Each subsystem must be designed with the application and specifications in mind, as well as considering all interactions between systems.

6.4 Future development

The following topics need to be investigated for future development of a fully integrated biosensor prototype:

- The electrochemical biosensor's signal analysis circuitry should be simplified and designed for portability. The input voltage must be filtered to decrease the threshold voltage for distilled water, thus increasing the sensitivity of the sensor.
- The sensitivity and specificity of both sensors must be thoroughly studied. Testing in various media (tap water, river water etc.) and with different target analytes (various *E. coli* strains, *Salmonella* etc.) will determine the operation limits of the sensors.
- The effect of light on the bacteria in the fiber-optic sensor must be evaluated. This can be done by interchanging various optoelectronics, or using a spectrophotometer to determine the effect that various wavelengths of light have on the bacteria.
- The immobilisation method of antibodies onto optical fibers must be improved. This can be done by using various crosslinking agents, different antibodies, and varying the deposition times to improve immobilisation efficiency.
- A fully integrated sensor can be designed and manufactured including a fluid handling system, signal analysis circuitry and processing circuits. The application of the device must be carefully considered before the design of such a prototype.

These recommendations are based on the information gathered in this project, and must be expanded upon. The continuation of the project can lead to promising developments in the fields of electrochemical impedance and fiber-optic biosensors.

Chapter 7

Conclusion

A study on low-cost, portable biosensors for the detection of *E. coli* in water has been conducted. A review of all relevant literature regarding biosensors and *E. coli* detection methods has been performed. An electrochemical impedance biosensor and a fiber-optic based biosensor were evaluated. The relevant theory was described in detail. Both sensors were tested and evaluated. The testing methods, namely non-linear impedance spectroscopy and simplified optical analysis, were performed and showed that the sensors were successful in detecting *E. coli*.

The following are the main contributions made by this project:

- A review was supplied concentrating on low-cost portable biosensors, their operations principles and the recent developments in detecting *E. coli* using these types of sensors.
- Various *E. coli* testing methods were evaluated, which indicated that most methods are laborious and resource intensive. Many methods to detect *E. coli* are suitable for laboratory use, but there is a need for portable, low-cost sensors that can detect bacteria.
- A non-linear impedance biosensor was tested and evaluated. The method of determining bacteria using this sensor was developed, and bacteria was successfully detected (concentrations as low as 1.1×10^{10} CFU/ml were detected in less than 4 minutes). This sensor could be used in future testing and development of biosensor prototypes.
- A method to immobilise antibodies to optical fibers has been established.
- A fiber-optic sensor was manufactured that could detect *E. coli* during initial tests (3×10^7 CFU/ml was detected in less than 120 minutes).
- A low-cost testing method using optoelectronics and 3D printed parts was developed. This could be used for future biosensor testing and improvement.
- A non-linear EIS and fiber-optic biosensor were compared for use in a biosensing system. This could be used in further development and guide research efforts in the field.

- A simple PCB based microfluidic platform was designed. This could be used as a design for use in future portable sensing systems.
- The specifications and possible applications for a biosensor prototype, including a system model, has been provided. These could be used as the basis from which future biosensor development could start.

The objectives for the project have all been achieved. There are, however, some limitations to the work done.

The electrochemical impedance biosensor was only tested for one strain of bacteria. Other strains of bacteria have to be tested to determine the specificity of the sensor. The sensor showed good sensitivity for ionic solutions, but could pose a problem when testing in drinking water samples. These samples contain certain contaminants and ions that may effect the measurement. A method to determine bacteria amongst these ions must be established. The sensitivity of the sensor can be greatly improved. This can be done by using filters at the input to lower the threshold voltage for distilled water, using novel ionic membranes or by developing digital filters to exclude certain harmonic frequency responses.

The fiber-optic biosensor was successfully immobilised with antibodies, and bacterial adhesion was seen. The method of immobilisation has not been optimised, with non-uniform deposition being present. This can be improved by lowering immobilisation times or by exploring the use of different crosslinking agents. Only a few initial sensor tests were performed indicating successful detection of *E. coli*. These tests must be repeated, and various bacterial strains must be tested to ensure that the sensor is specific to *E. coli*. Only one set of optoelectronics was tested. The effect of various wavelengths of light, fiber geometries and optoelectronics must be evaluated in future research efforts.

These limitations lead to interesting subjects for future project work. The following topics are suggested for future research on the topic:

- Determination of the specificity of non-linear harmonic biosensors
- Optimisation of sensitivity of non-linear harmonic biosensors
- Optimisation of immobilisation process for fiber-optic based biosensors
- Optimisation of the test setup of a simplified evanescent wave biosensor
- Evaluation of light wavelength effects of low-cost optoelectronics in a fiber-optical biosensor setup

Water testing is a promising field for biosensor development, but may be limited. Water sources are typically very large, such as rivers or lakes, and biosensors may not prove to be more cost effective or sensitive than established testing methods like colony counting methods.

Other possible applications for these sensors are in areas such as research and development (laboratories) and biomedical sensors. The large market share, potential of applications and growing trends in biosensor research are all aimed at biomedical applications. These projects could form the basis of such a biosensor prototype, which could be developed to target a specific analyte relevant to a biomedical analysis.

Two biosensors have been evaluated. A novel method (non-linear electrochemical impedance spectroscopy) was used to detect *E. coli* bacterial concentrations as low as 1.1×10^{10} CFU/ml in less than 4 minutes. A fiber-optic based biosensor, using simplified optoelectronics and hand-made fibers, was manufactured. The fiber was successfully immobilised with primary anti-*E. coli* antibodies as biorecognition element. The method of immobilisation was evaluated, and bacteria had successfully adhered to the surface of the fibers through this method. Initial bacterial tests indicated that bacterial concentrations as low as 3×10^7 CFU/ml could be determined in less than 120 minutes. Both these sensors have the potential to be integrated onto a fully automated, low-cost, portable biosensing system in the future.

Appendices

Appendix A

Microfluidics

A.1 Introduction

The following is a short study conducted on microfluidics. Microfluidics is defined as the science of manipulating micro-sized droplets of liquid by various methods. Microfluidics can be seen as an enabling technology allowing the sensing of decreasing sample volumes [96] in biosensor applications. The scaling down of dimensions allow for reduced reagent consumption, higher throughput, enhanced analytical performance, less waste, lower unit cost, and reduced energy consumption, all of which make it an appropriate technology for portable sensing devices [97]. This section will explore the relevant literature concerning microfluidic technologies, as well as a focus on electrowetting-on-dielectric (EWOD) microfluidics. The basic design for such a microfluidic platform is explored, including an evaluation of the feasibility of such a platform for use in a biosensor

A.2 Literature review

Microfluidics concerns the manipulation of fluids on a micro scale. The basic fluidic operations include droplet moving, mixing, valving and dispensing [98]. There are two main categories of microfluidics: droplet based and continuous flow microfluidics. Droplet based microfluidics can be divided into electrowetting, acoustic pumping and two phase liquid flow microfluidics [98]. Continuous flow microfluidics deals with the mechanisms regarding flow of fluids in micro-sized channels. Continuous flow microfluidics is less suitable for applications requiring a high degree of flexibility and complicated fluid manipulations [96]. Microfluidic analysis can offer a low-cost solution for sample manipulation due to the benefits of portability, minimal energy consumption and cost saving due to mass producibility [99]. The investigation into low-cost platforms such as printed circuit board (PCB) substrates for use as microfluidic platforms is essential to low-cost sensor development.

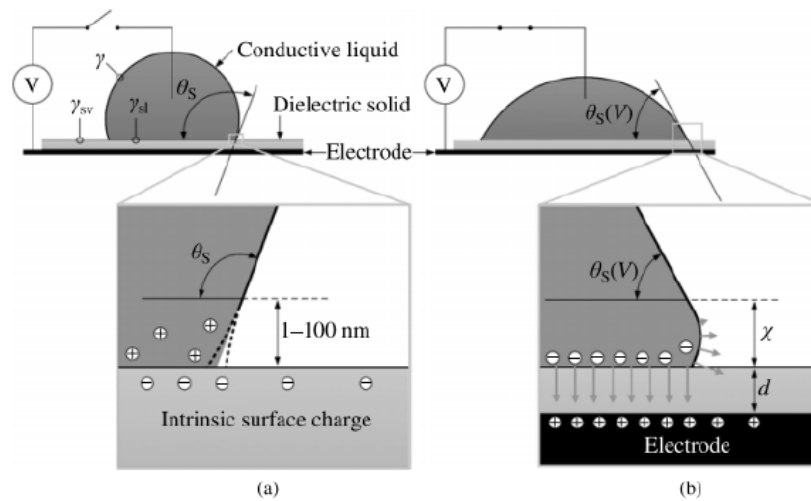


Figure A.1: Surface charging and contact angle change during EWOD [100]

A.2.1 Electrowetting-on-dielectric (EWOD) microfluidics

The principle of electrowetting-on-dielectric (EWOD) is defined as the change of free energy on the surface of a dielectric material due to electric charge accumulation when a voltage is applied [101]. This surface energy changes the wettability of the surface and thus the droplet contact angle [101]. The basic setup for EWOD is shown in Figure A.1. When a voltage is applied the droplet "sticks" to the surface. This is known as hydrophilic behaviour, meaning an "affinity for water". Charge accumulates at the solid-liquid interface leading to a change in contact angle from hydrophobic to hydrophilic [102]. When there is no applied electrical field the droplet contact angle changes and the surface acts hydrophobically, meaning the "fear of water". This causes movement of droplets by applying a field on an electrode adjacent to the one the droplet sits on. Surfaces acquire a net charge during actuation, but droplets remain electro-neutral [100]. This can be achieved by using a sandwich device consisting of an electrode, dielectric layer and hydrophobic coating. The hydrophobic layer allows less resistance to liquid movement [100], and increases the hydrophobicity of the droplet. The actuation voltage plays a major role in portable devices, because it determines the feasibility of small power sources (batteries).

One major manipulation is the splitting of droplets from a reservoir, illustrated in Figure A.2. To split a droplet, the gap between plates should be smaller than the critical value determined by the material and device parameters [104]. It must be noted that surface tension is an inherently dominant force on the micro-scale [102].

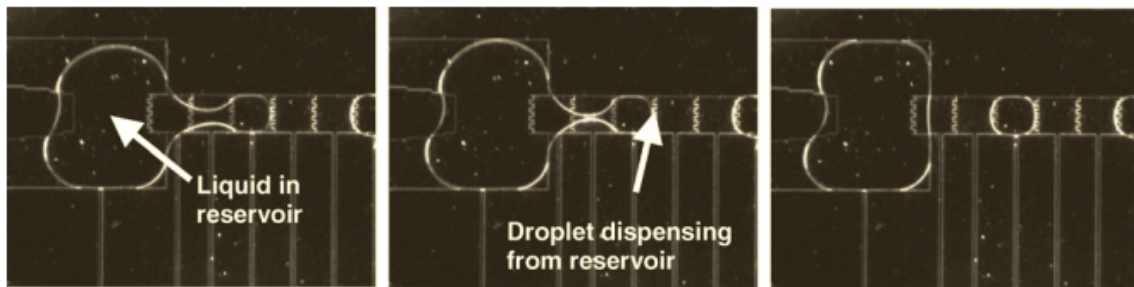


Figure A.2: Droplet splitting from a reservoir on an EWOD microfluidic platform [103]

A.2.2 EWOD theory

The dielectric constant of a material relates to the permittivity of that material and is described by the Greek letter ϵ [105]. Permittivity expresses the ability of insulating material to polarise in response to an applied electric field [105]. If greater polarisation in a given field is achieved, it results in a higher ϵ value for the material [105]. The actuation voltage of droplets on an EWOD device can be described by

$$\cos \theta_V = \cos \theta_0 + \frac{1}{2\gamma_{lv}} \frac{\epsilon_d \epsilon_0}{d} V^2 \quad (\text{A.2.1})$$

where $\cos \theta_V$ is the contact angle between the horizontal surface and the droplet when a voltage is applied, $\cos \theta_0$ is the droplet contact angle when no voltage is applied, γ_{lv} is the liquid-vapour interfacial energy, ϵ_d is the dielectric constant of the dielectric layer, ϵ_0 the permittivity of free space, d is the dielectric layer thickness and V the actuation voltage required for droplet movement. This force competes with the dielectric breakdown strength of a material. Dielectric breakdown occurs when the dielectric strength of a material is surpassed, thus showing the maximum allowed electrical field that can be applied to a material [105], and can be described by

$$V_{DB} = E_{DB}d \quad (\text{A.2.2})$$

where V_{DB} is the dielectric breakdown voltage, E_{DB} the dielectric strength and d the thickness of the dielectric layer.

A.2.3 Recent developments in low-voltage EWOD

Zeng and Korsmeyer [106] provides a comparison between EWOD and dielectrophoresis (DEP) used in microfluidics. The use of thinner dielectric films with higher dielectric constants and higher dielectric breakdown strengths can lead to much lower actuation voltages for droplet manipulation [102]. Actuation voltages of 6 V have been achieved [102]. An EWOD device that uses Ta_2O_5 as the dielectric layer was fabricated that can actuate droplets at less

than 15 V [107]. A low voltage EWOD device was fabricated by Gao et al. [108] using Si_3N_4 as the dielectric layer, achieving actuation voltages of less than 15 V. Juncker et al. [109] reported on an autonomous microfluidic capillary system which may be used for autonomous inlets and outlets on a portable device.

Producing an EWOD device offers simple device configuration and fabrication, enables the generation of large forces on the micro scale and consumes very little energy, making it an appropriate platform for portable microfluidics [110]. The dielectric thin-film used greatly influences the device configuration and actuation voltages that can be achieved.

A.2.4 Dielectric thin-films

A thin-film is a layer of material with dimensions less than a millimeter. A dielectric insulator is defined as a material that can transmit electric force without conduction, thus making it an insulator. A range of dielectric materials and deposition processes have been developed for use in EWOD microfluidics. Materials used include silicon oxide (SiO_2), silicon nitrides (SiO_xN_y), aluminium oxide (Al_2O_3), yttrium oxide (Y_2O_3), zirconium oxide (ZrO_2), tantalum oxide (Ta_2O_5) and various liquid polymers.

Aluminium oxide, or alumina, is a well studied dielectric material. It has a dielectric constant (ϵ_d) of 9.1 and a dielectric strength of $425 \text{ V}/\mu\text{m}$. Lomer [111] investigated aluminium oxide thin-films and noted that the dielectric strength of the material rises as the film thickness decreases. It is also dependent on the temperature of the film [111]. Al_2O_3 is a wide bandgap dielectric material and methods of depositing Al_2O_3 thin-films include atomic layer deposition (ALD), plasma enhanced chemical vapour deposition (PECVD), sol-gel methods, sputtering, plasma layer deposition (PLD) and physical vapour deposition (PVD) [112]. The thickness and stoichiometry of Al_2O_3 thin-films depend on the underlying surface chemistry during film growth [113]. The thickness of layers can be determined by using ex situ stylus profilometry and ellipsometry [113], or atomic force microscopy (AFM) step-edge methods.

RF sputter coating of Al_2O_3 results in low deposition rates, while DC reactive sputtering can result in stoichiometric Al_2O_3 at high deposition rates [114]. A key parameter to notice is the temperature of deposition which can greatly influence the stoichiometry of the thin-film as well as limit the type of substrate on which can be deposited on [114]. Pei and Wu [115] developed a light actuating digital microfluidics (LADM) device that uses Al_2O_3 as the dielectric layer achieving low voltage actuation (16 V_{P-P}). Advances in ALD have led to the deposition of high quality, conformal, pin-hole free layers of dielectric films and of a superior quality to PECVD techniques [116].

Polymers are suitable materials for use as dielectrics due to simpler manufacturing processes, flexibility of the material, and better resistance to chemical attack [105, 117]. Polymers that have relatively high dielectric constants, good chemical properties and acceptable insulative properties have recently been developed [117]. Materials such as polyimide, methylsilsesquioxane, polyarelene ether, polyethylene, polystyrene and Teflon have been widely used as dielectric materials in the manufacturing of electronics [117]. The disadvantages of polymers, however, are that they are not temperature resistant, have large coefficients of thermal expansion and are susceptible to atmospheric and hydrolytic degradation [105]. SU-8 (a type of photoresist) and Teflon have been investigated as dielectric and hydrophobic coating layers in EWOD microfluidic devices [118]. Other polymers can also be investigated as dielectric layers in EWOD devices. There is thus a possibility to fabricate thin-film dielectric layers with good material properties at a low-cost and high throughput.

A.2.5 Printed circuit board microfluidics

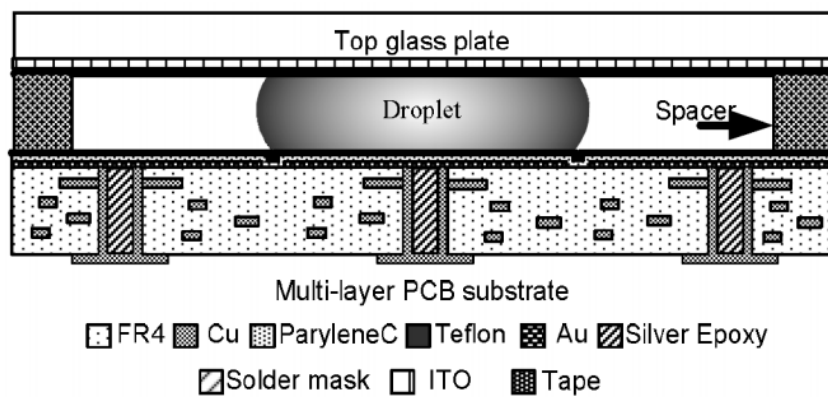


Figure A.3: Cross-section of PCB substrate microfluidics device developed by Gong and Kim [119]

Gong and Kim [119] demonstrated control of droplet volumes on multilayer printed circuit boards (PCBs) with through-substrate electrical contacts to eliminate side connecting lines. Gong and Kim [110] developed a microfluidic system on a PCB as can be seen in Figure A.3. This novel method offers a simple and mature manufacturing technique used in electronics to be used as the base for electrowetting-on-dielectric (EWOD) microfluidic chips. Droplets were manipulated on a two-dimensional surface [110]. Two key parameters for microfluidics is volume accuracy and the repeatability of droplet creation [110], both of which could be achieved with a PCB microfluidic device. It is also much more cost effective to mass produce PCBs for use in microfluidics

compared to photolithographic techniques typically used to develop electrode arrays.

A.3 Suggested design

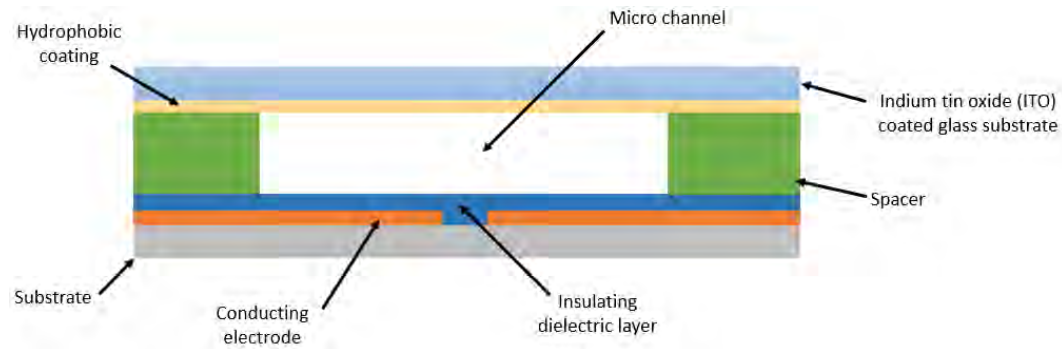


Figure A.4: Cross section of EWOD microfluidic platform

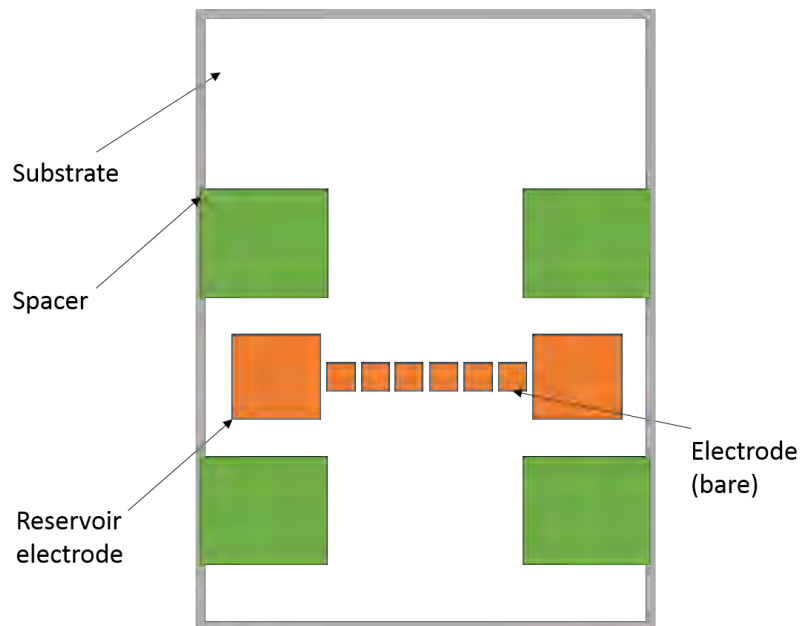


Figure A.5: Top view of bare electrode array on EWOD platform

Illustrations of the microfluidic platform is shown in Figure A.4 and Figure A.5. As a droplet is inserted onto the reservoir (the large electrode) a voltage is applied to the neighbouring electrode. This causes a change in the droplet contact angle (due to EWOD), inducing movement of the droplet towards the active electrode. A droplet is thus split from the reservoir. As voltages are

applied to electrodes adjacent to the one on which the droplet sits, the droplet is translated in the microchannel formed between the two plates. The droplet is translated to the active electrode, which interfaces with the biosensor. The droplets are digitally controlled by a control circuit.

The theoretical actuation voltage (derived from the electrowetting equation) is defined as

$$V_{act} = \frac{2\gamma_{lv}d(\cos(\sigma_v) - \cos(\sigma_0))}{\epsilon_d\epsilon_0} \quad (\text{A.3.1})$$

where γ_{lv} is the surface tension between water and air, d is the thickness of the dielectric thin-film, σ_v is the droplet contact angle when a voltage is applied, σ_0 is the no-voltage droplet contact angle, ϵ_d is the dielectric constant of thin-film dielectric and ϵ_0 is the permittivity of free space. This actuation voltage must be compared with the dielectric breakdown voltage of the thin-film dielectric to find the optimum point of operation (lowest actuation voltage whilst not causing dielectric breakdown). The dielectric breakdown voltage can be described by

$$V_{bd} = E_{bd}d \quad (\text{A.3.2})$$

where E_{bd} is the dielectric strength of the insulator and d is the thickness of the dielectric thin-film. The actuation voltage must always comply with

$$V_{bd} > V_{act} \quad (\text{A.3.3})$$

to ensure that electrolysis does not occur. The ratio that enables droplet splitting is defined as

$$AR = \frac{h}{0.5R} \quad (\text{A.3.4})$$

where h is the height of the spacer in the micro channel and R is the electrode width (for square electrodes). The ratio must comply with

$$AR < 0.22 \quad (\text{A.3.5})$$

to enable droplets to be split from a reservoir. The approximate volume of a droplet can be estimated as

$$\text{Vol} \approx hR^2 \quad (\text{A.3.6})$$

where h is the spacer height and R is the width of a single electrode.

The preferred specification for actuation voltage, for a portable biosensor, is lower than 24 V. Figure A.6 compares the theoretical actuation voltage (from Equation A.3.1) and the dielectric breakdown voltage (from Equation A.3.2) of Al_2O_3 . It can be seen that for an Al_2O_3 thin-film of under 500 nm the actuation voltage will be below the 24 V threshold. An electrode width and length of 2×2 mm was chosen. Using Equation A.3.4 and Equation A.3.5 it was calculated that the spacer height (and thus the micro channel height) must

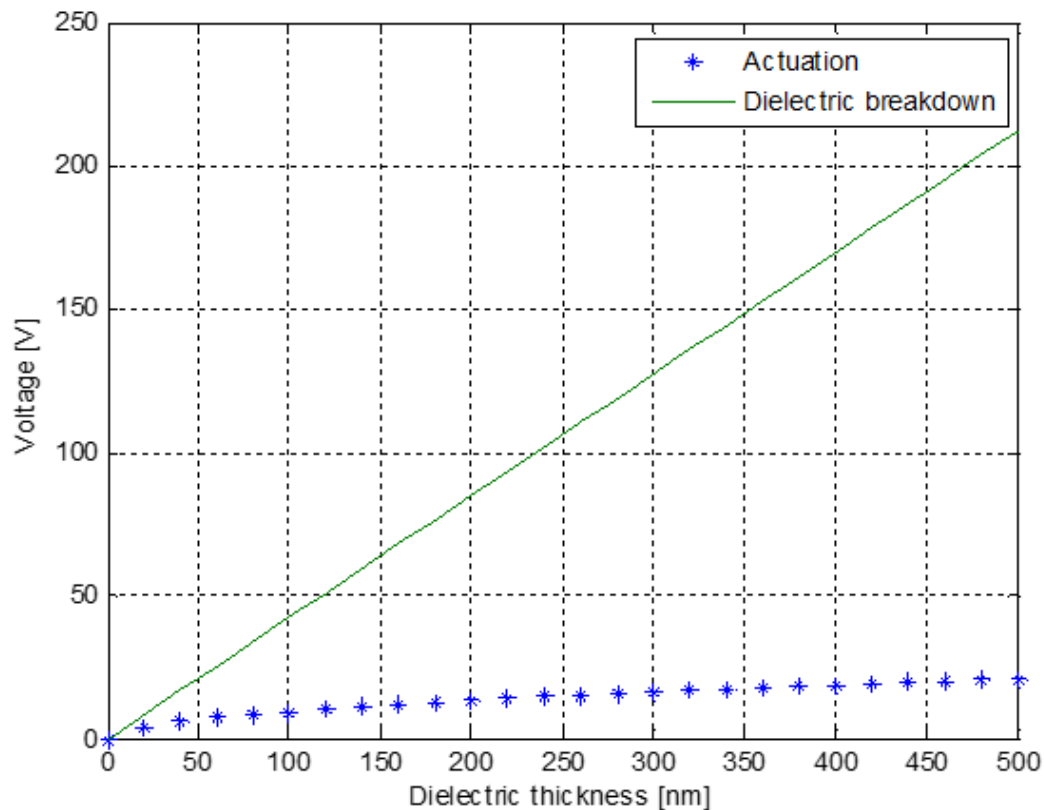


Figure A.6: Actuation vs breakdown voltage for Al_2O_3 thin-film. As the thickness of the layer increases, the dielectric breakdown voltage increases. The crossing point between the dielectric breakdown and the required actuation voltage is the theoretical limit for successful droplet movement.

be less than $220 \mu\text{m}$. The maximum droplet volume was then calculated to be approximately $0.8 \mu\text{l}$.

The control circuit for controlling droplet position is can be relatively simple, using transistor switching circuits. The fluid control circuit is shown in Figure A.7. It shows each analog input from a processor (A_n) and each impedance (Z_{Ln}). The impedance represents the electrode, dielectric layer and sample. Each electrode can be addressed individually by digitally controlling the output via transistor switching. The input voltage (V_{cc}) is the actuation voltage calculated from (A.3.1).

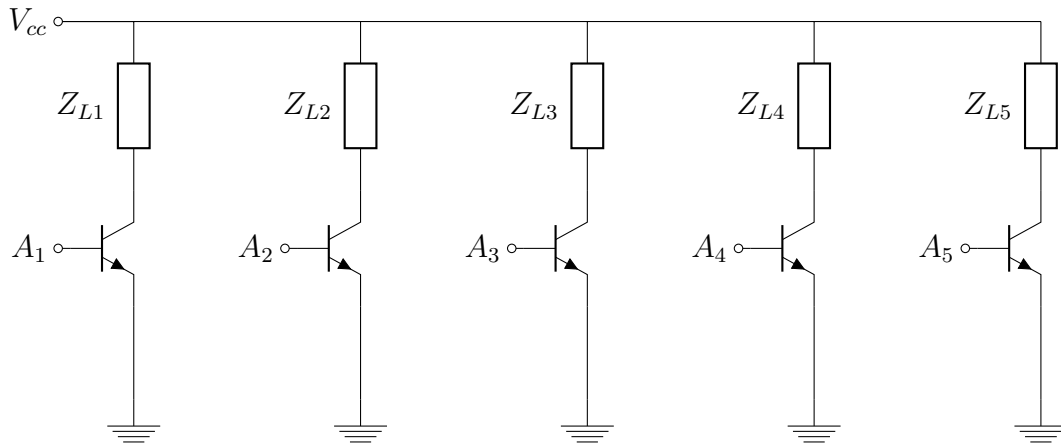


Figure A.7: Microfluidic control circuit

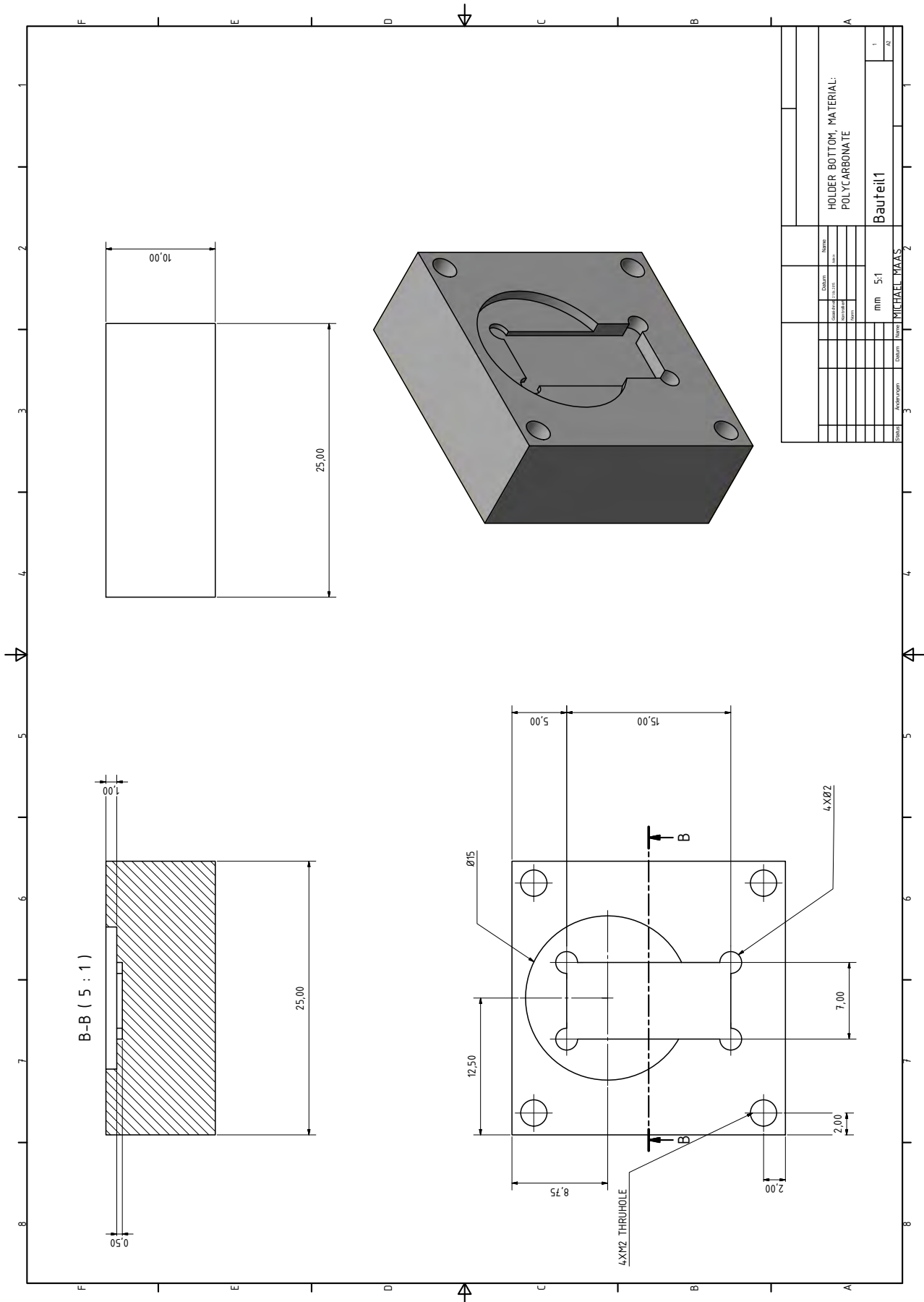
A.4 Conclusion

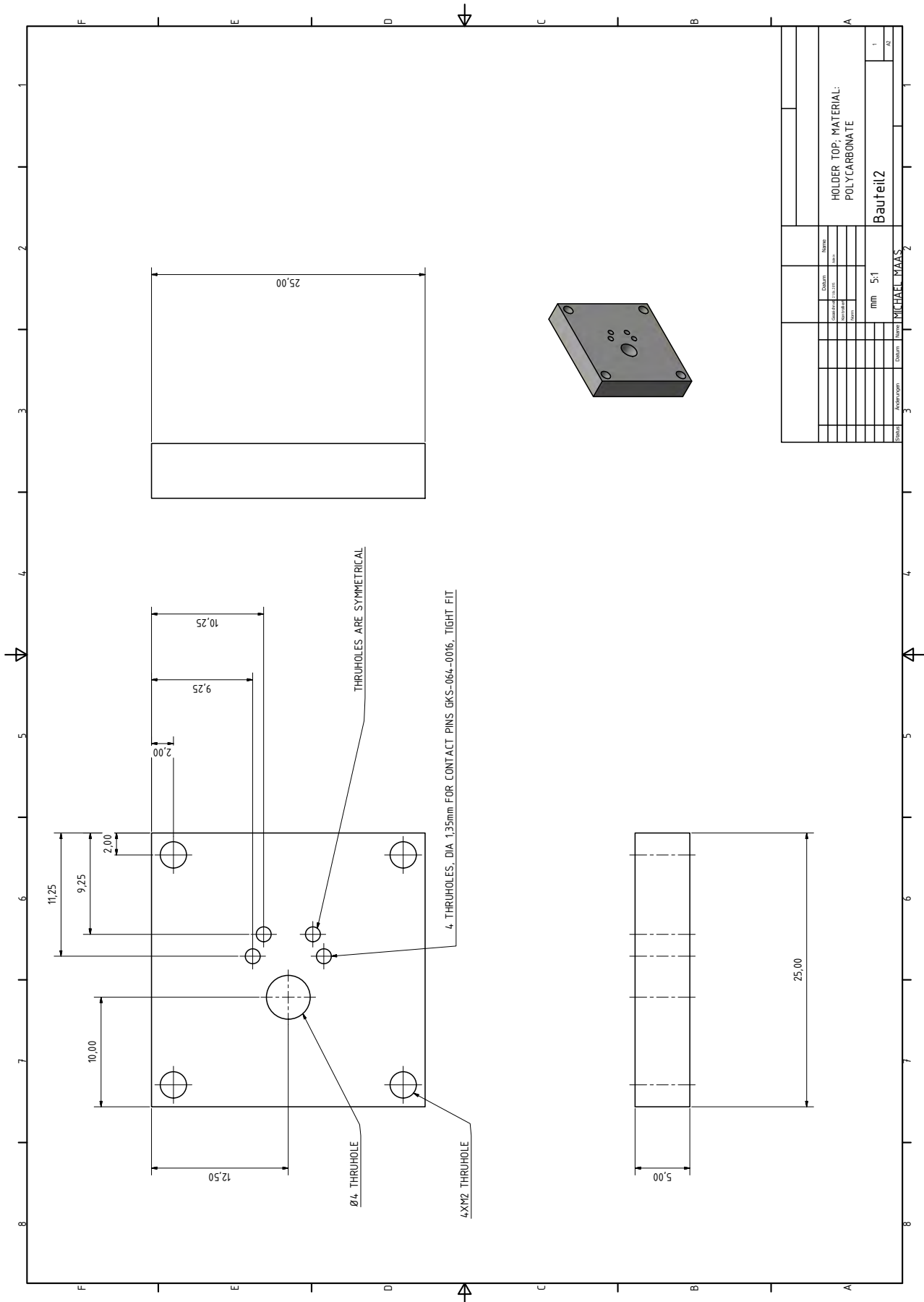
Microfluidics is a promising technology for developing simple, cost effective fluid manipulation platforms for biosensors. The use of mature technologies, such as PCBs, decreases overall costs due to economies of scale. Thinner dielectric insulators and novel materials such as Al_2O_3 and polymers could lower actuation voltages and simplify manufacturing. The proposed design could be integrated with a biosensor, such as those evaluated in this project, to create a fully automated, low-cost, portable biosensing system.

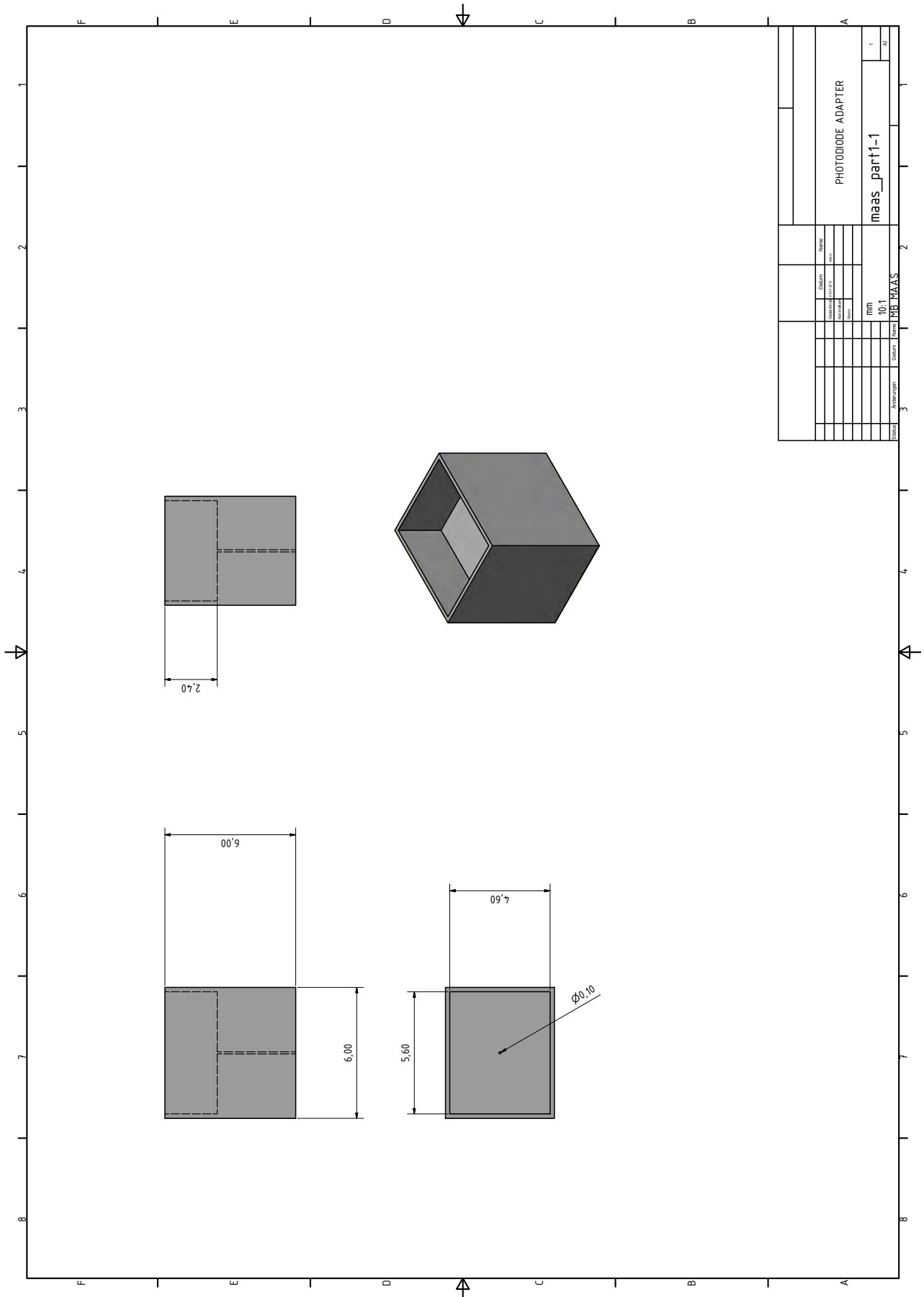
Appendix B

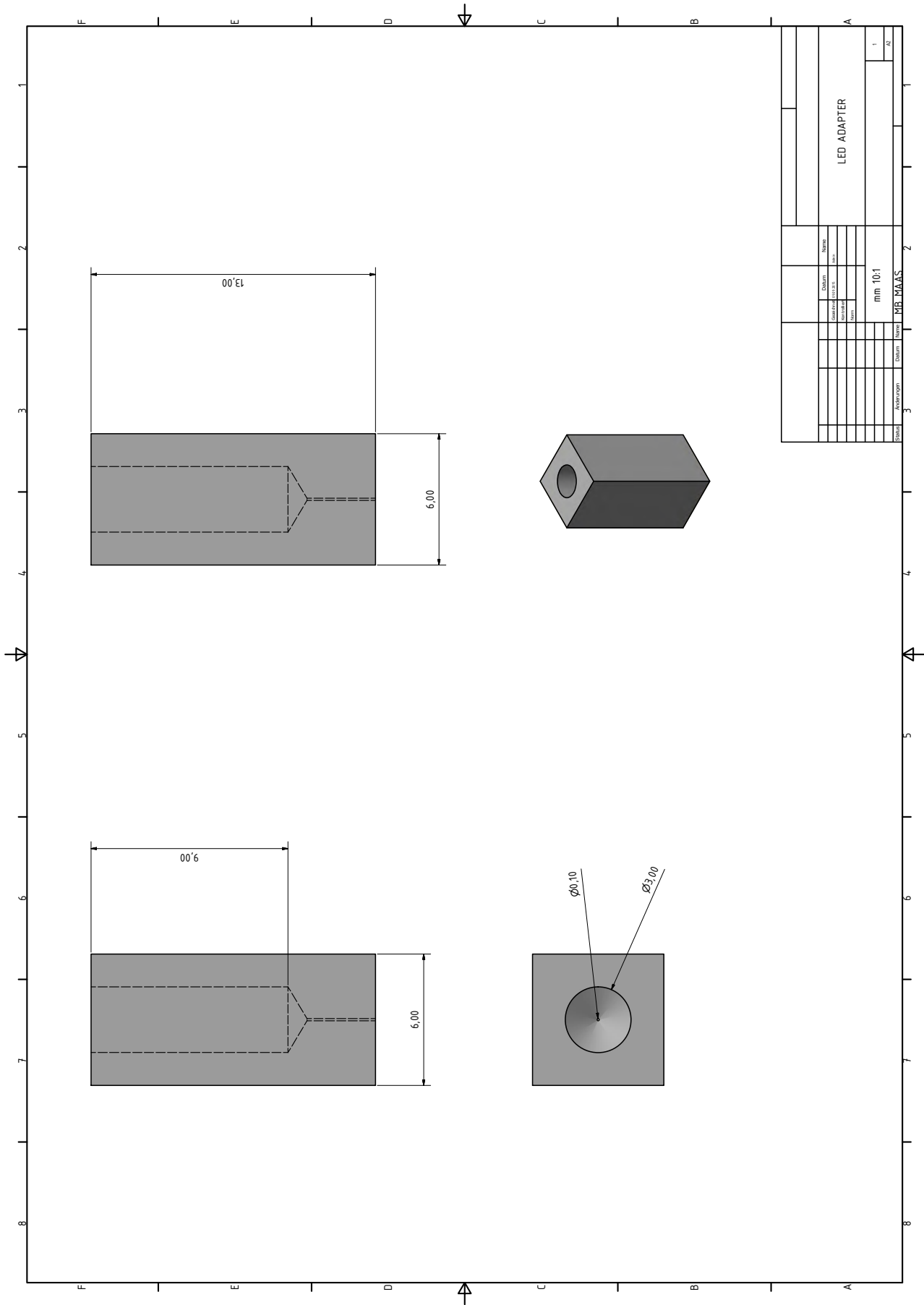
Technical Drawings

- Chip holder - bottom
- Chip holder- top
- 3D printed adapter - Photodiode
- 3D printed adapter - LED









Appendix C

Calculations

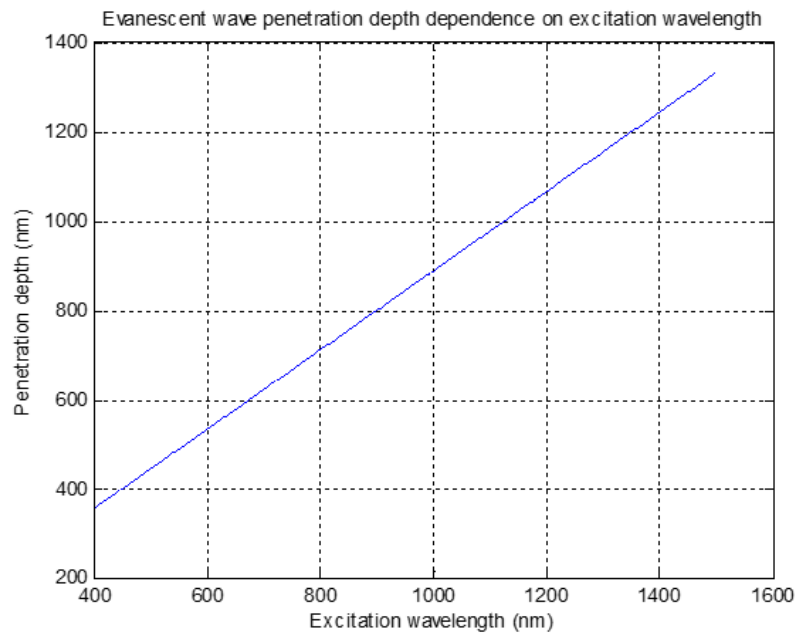


Figure C.1: Evanescent wave vs excitation wavelength

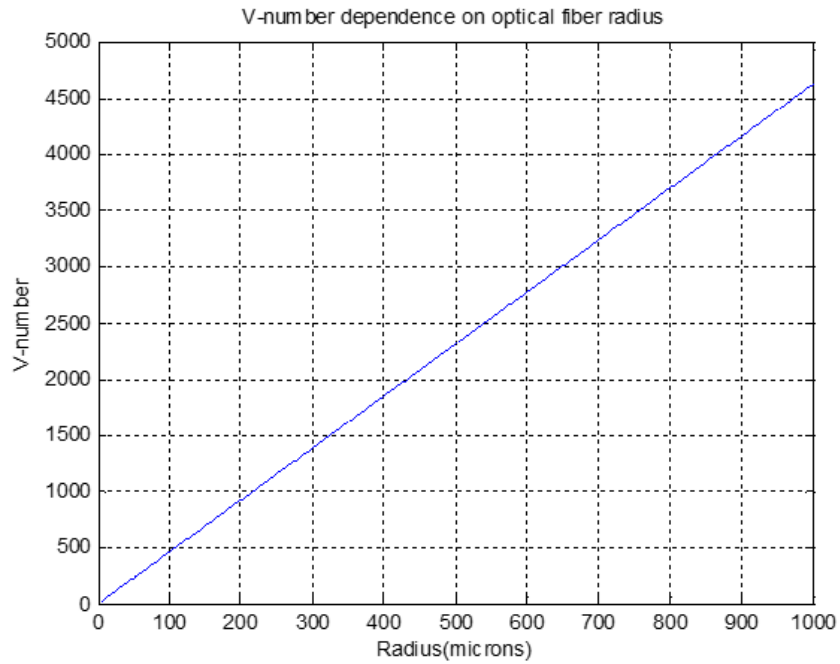


Figure C.2: V-number vs core radius

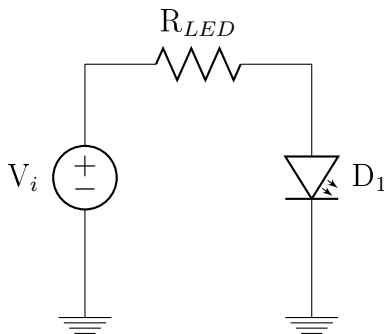


Figure C.3: LED circuit diagram

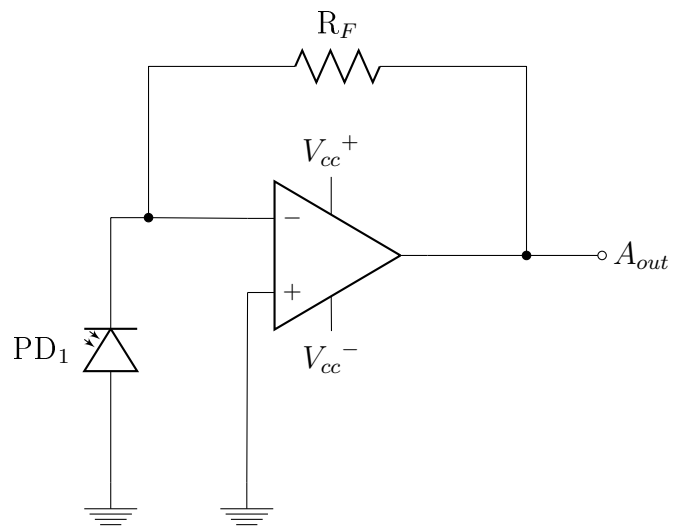


Figure C.4: Photodiode circuit diagram

Appendix D

Additional Figures

D.1 Electrochemical impedance biosensor

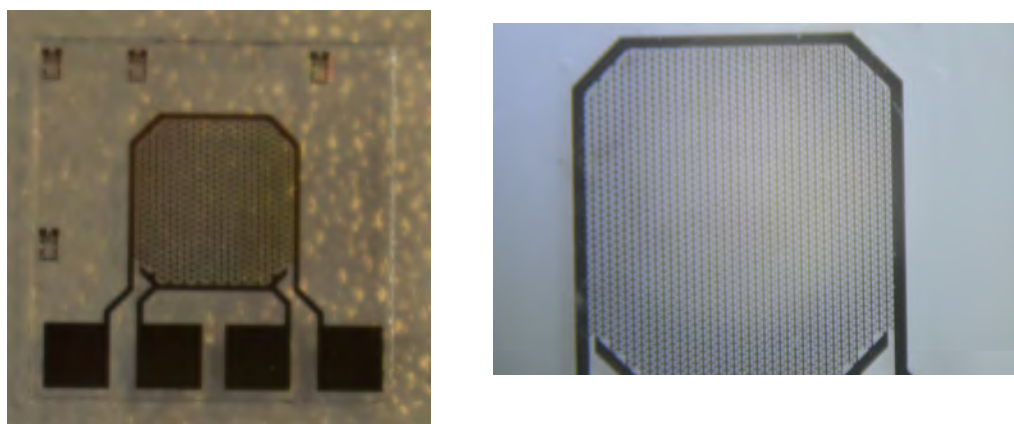


Figure D.1: Interdigitated microelectrode (IME) chip provided by TUM (Pt, 10 mm×10 mm)

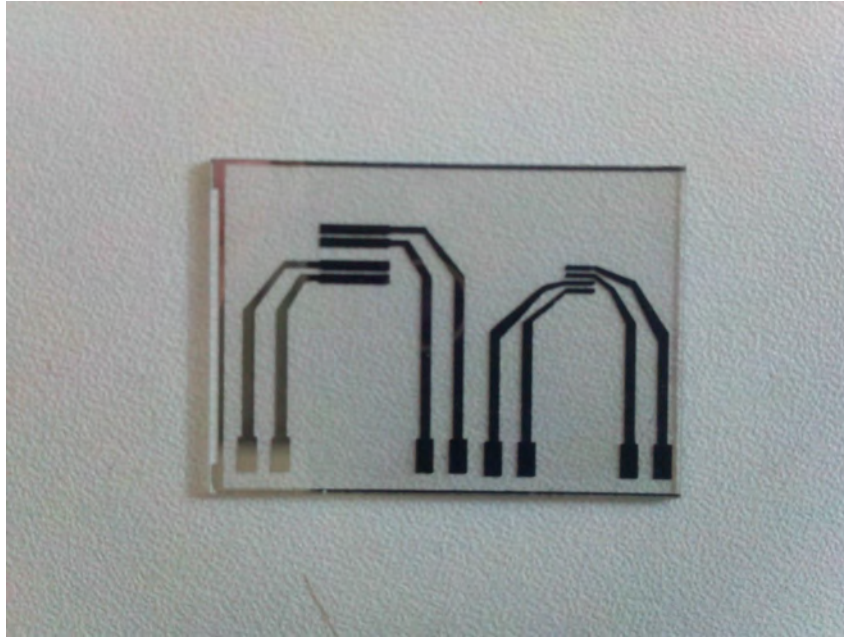


Figure D.2: Symmetrical electrode chip provided by TUM (Pt, 24 mm×36 mm)

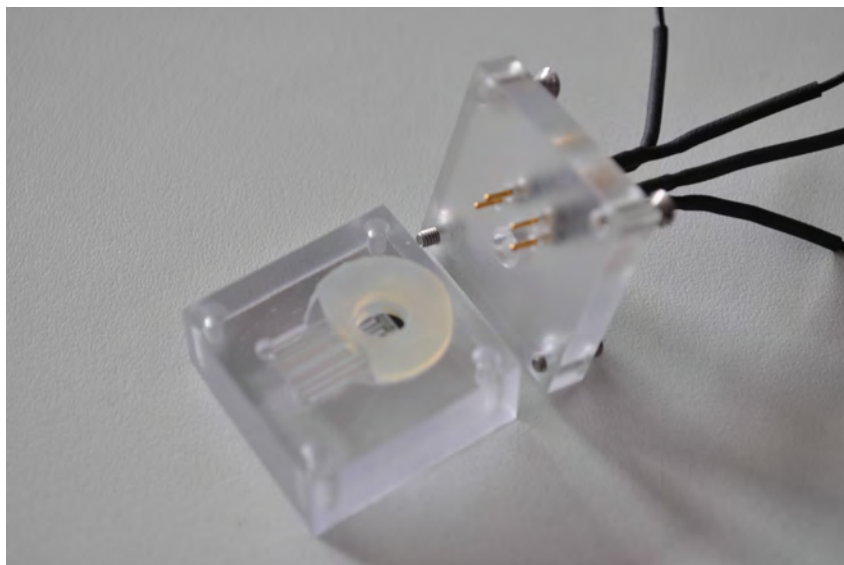


Figure D.3: Chip holder (polycarbonate, 25 mm×25 mm×15 mm)

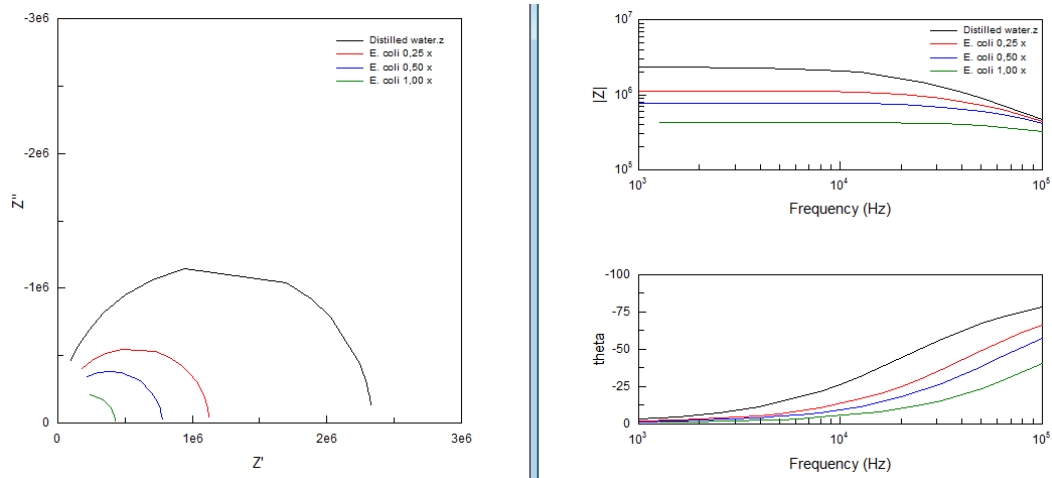


Figure D.4: Impedance spectrum at varying bacterial concentrations (Ti electrodes)

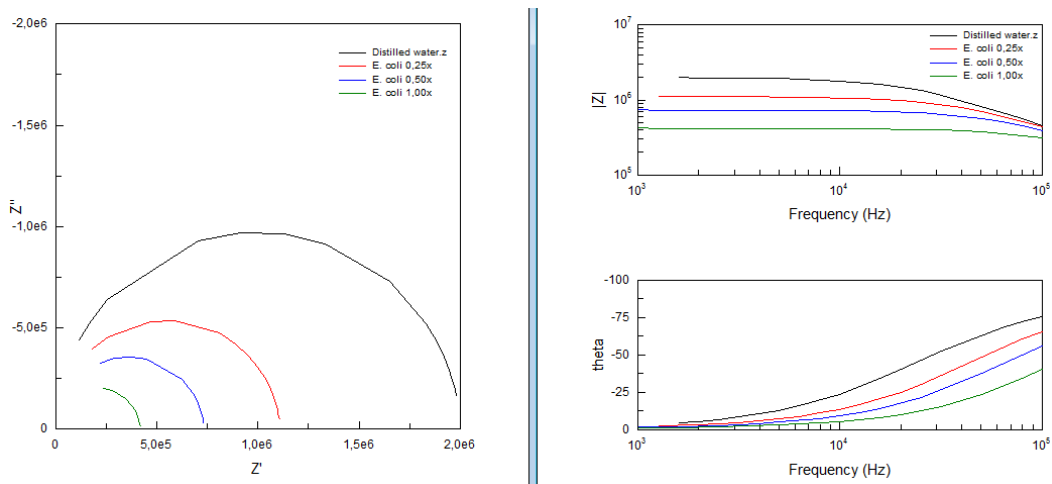


Figure D.5: Impedance spectrum at varying bacterial concentrations (Symmetrical electrodes)

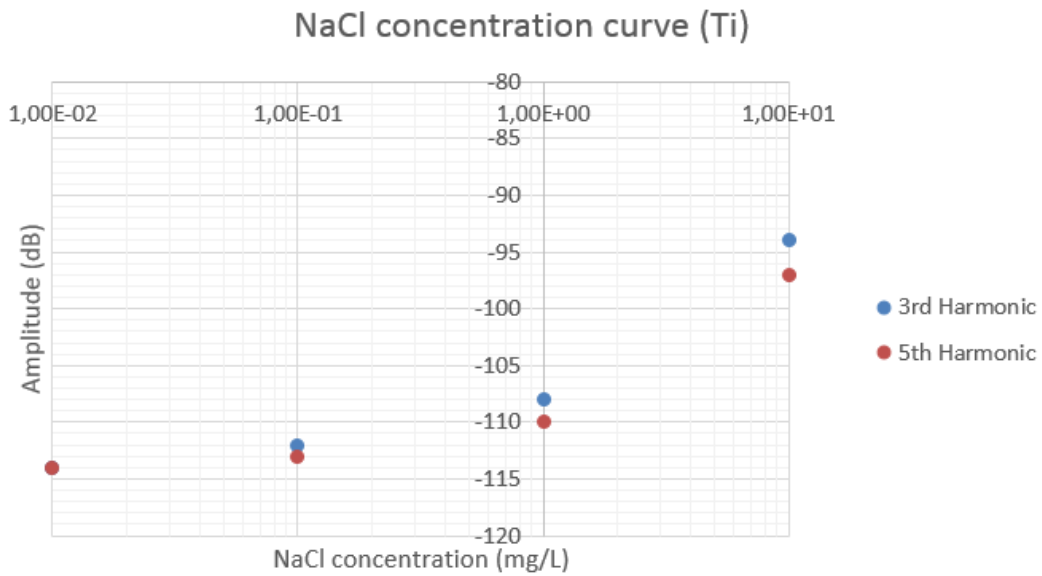


Figure D.6: Concentration curve of NaCl on Ti electrodes ($V_{p-p} = 2.987$ V, $f = 1$ kHz, Gain = 0.6)

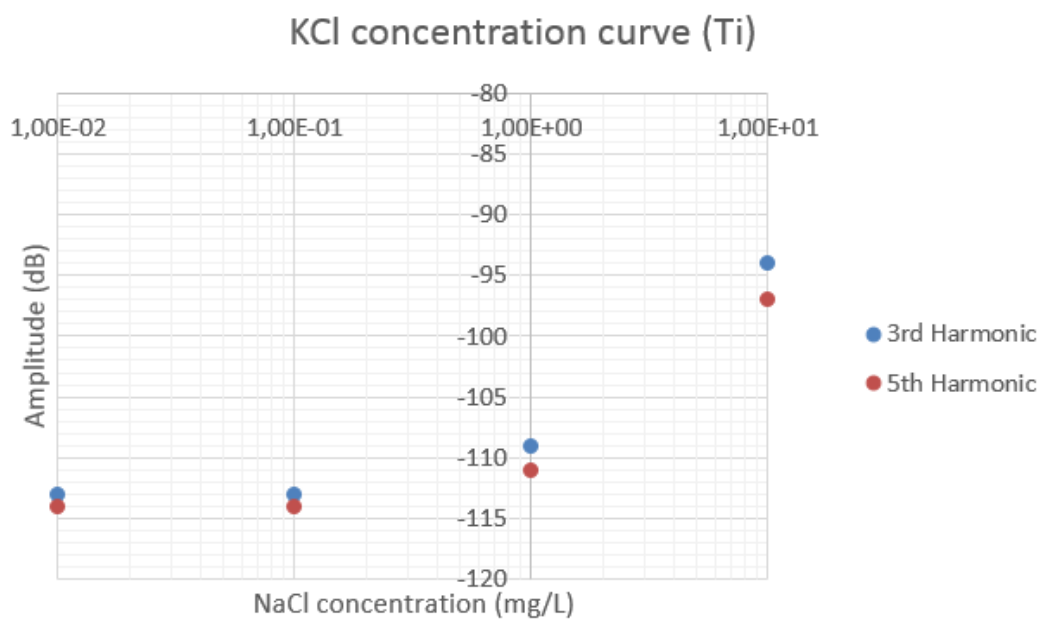


Figure D.7: Concentration curve of KCl on Ti electrodes ($V_{p-p} = 2.987$ V, $f = 1$ kHz, Gain = 0.6)

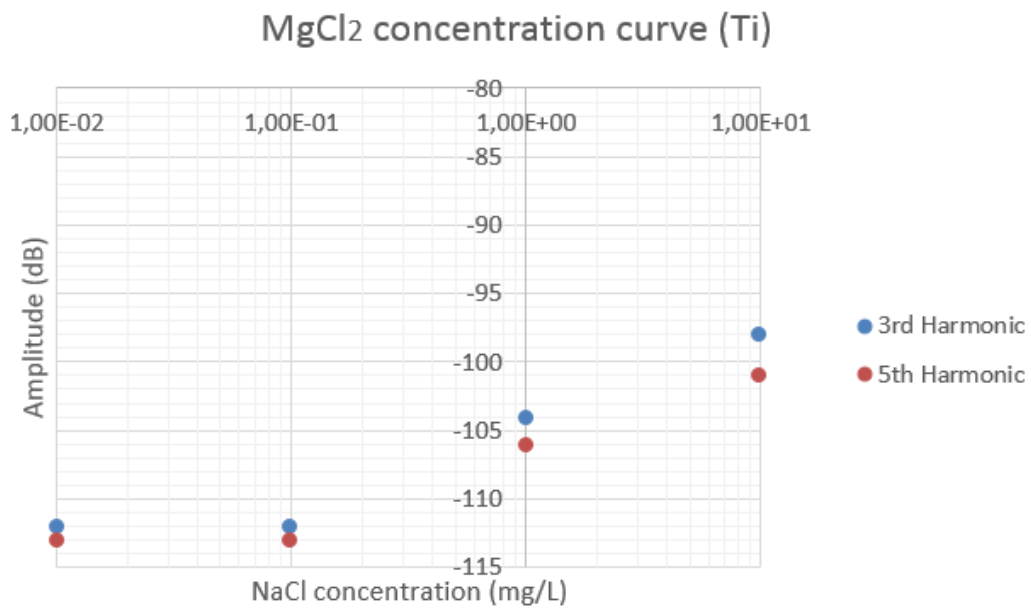


Figure D.8: Concentration curve of MgCl₂ on Ti electrodes ($V_{p-p} = 2.987$ V, $f = 1$ kHz, Gain = 0.6)

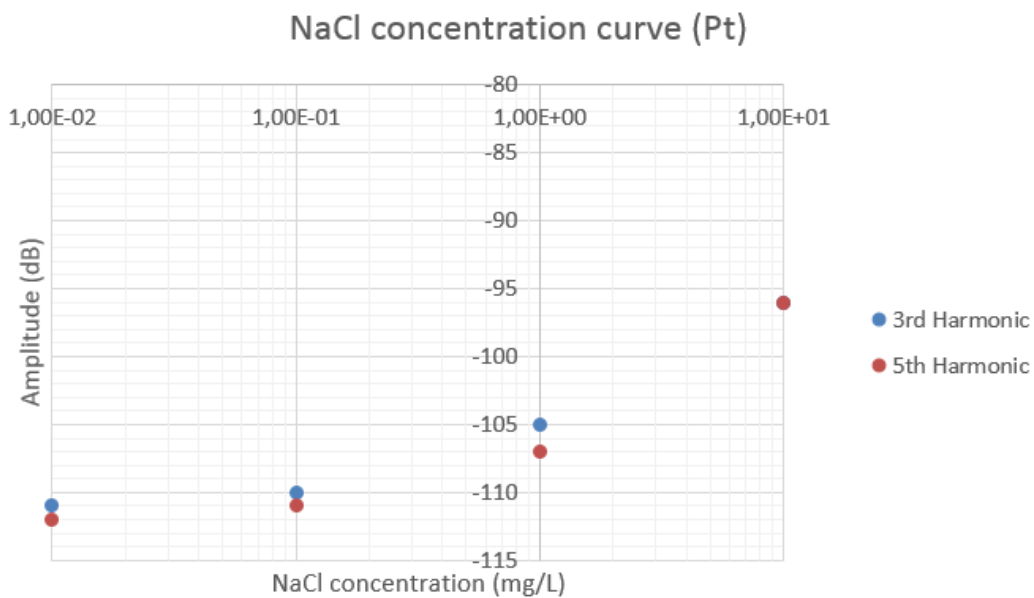


Figure D.9: Concentration curve of NaCl on Pt electrodes ($V_{p-p} = 2.987$ V, $f = 1$ kHz, Gain = 0.6)

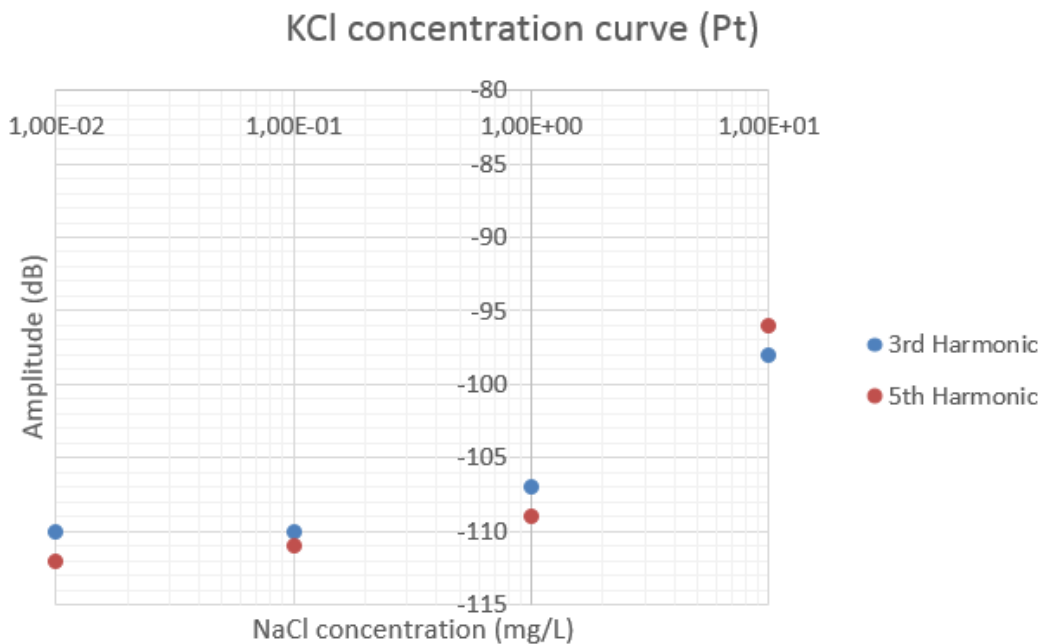


Figure D.10: Concentration curve of KCl on Pt electrodes ($V_{p-p} = 2.987$ V, $f = 1$ kHz, Gain = 0.6)

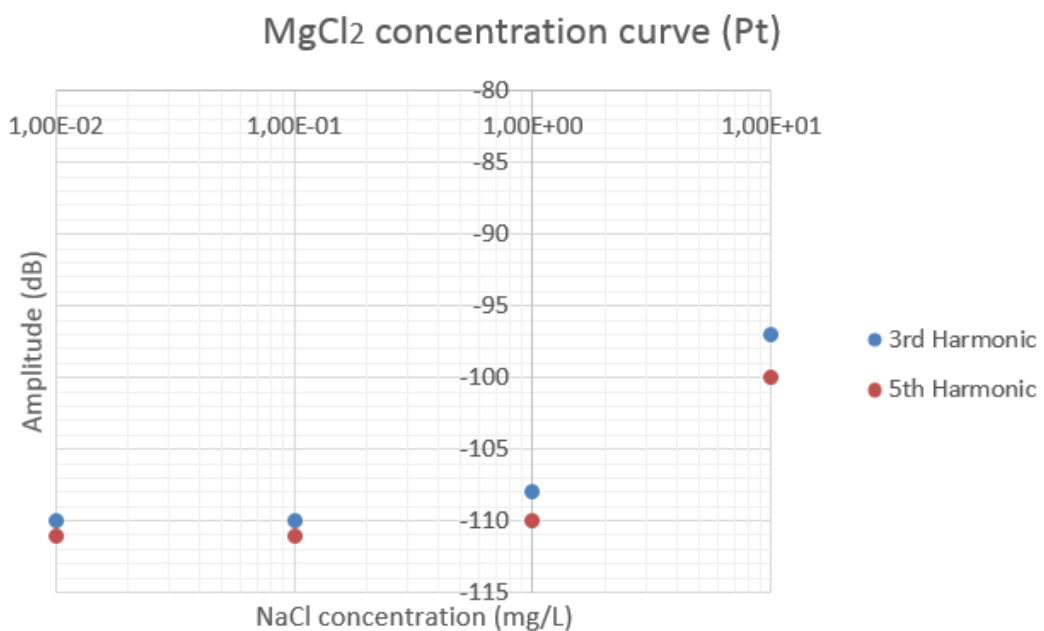


Figure D.11: Concentration curve of MgCl₂ on Pt electrodes ($V_{p-p} = 2.987$ V, $f = 1$ kHz, Gain = 0.6)

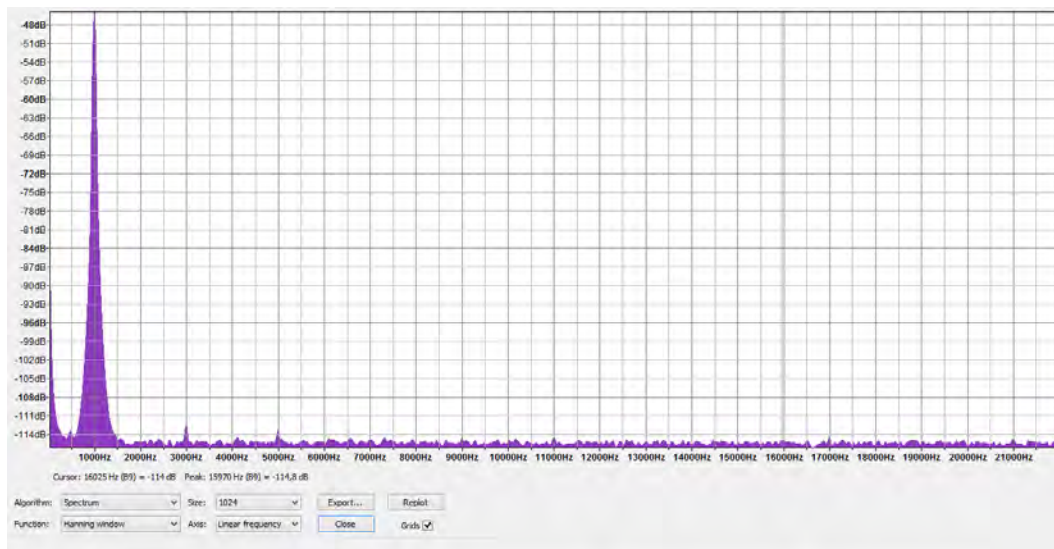


Figure D.12: Harmonic spectrum of *E. coli* on Ti electrodes (1.1×10^{10} CFU/ml)

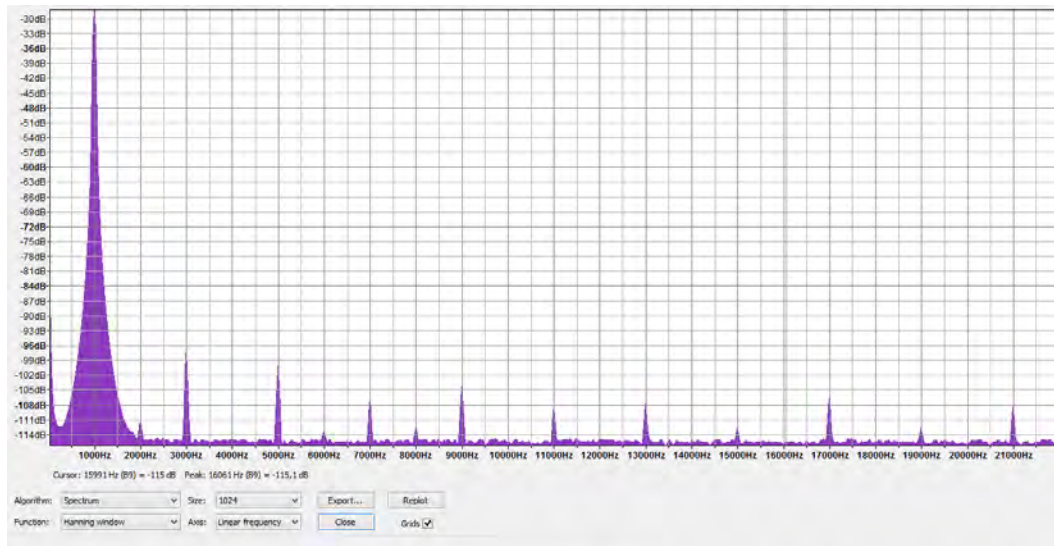


Figure D.13: Harmonic spectrum of *E. coli* on Ti electrodes (1.1×10^{12} CFU/ml)

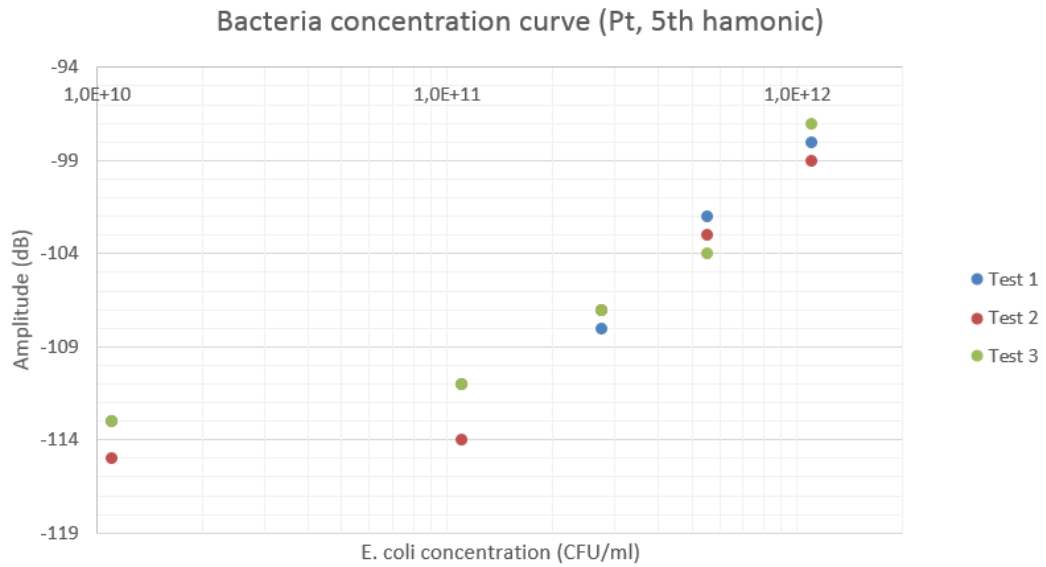


Figure D.14: Concentration curve for Pt electrodes (5th harmonic)

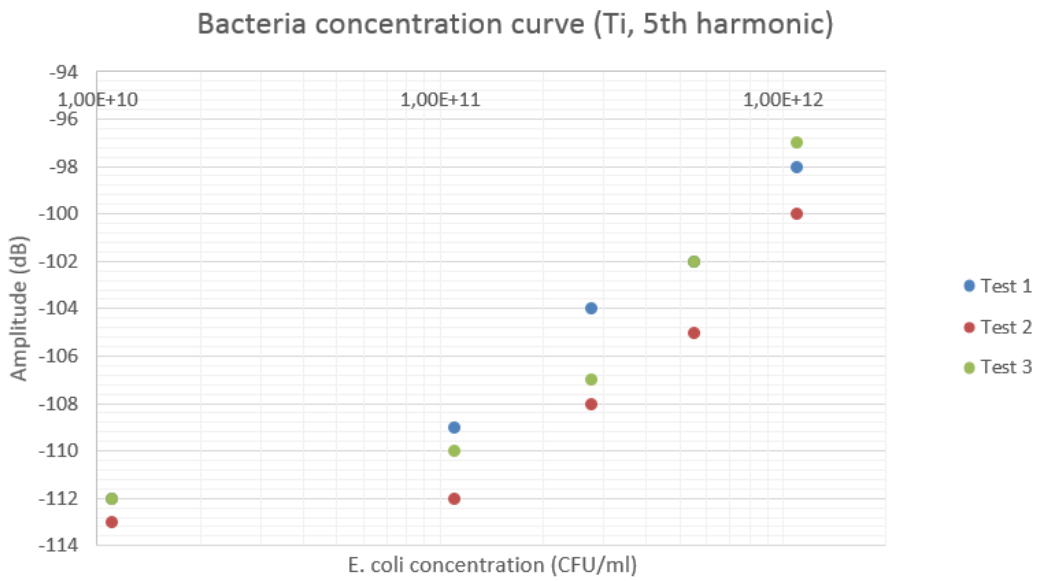


Figure D.15: Concentration curve for Ti electrodes (5th harmonic)

D.2 Fiber-optic biosensor

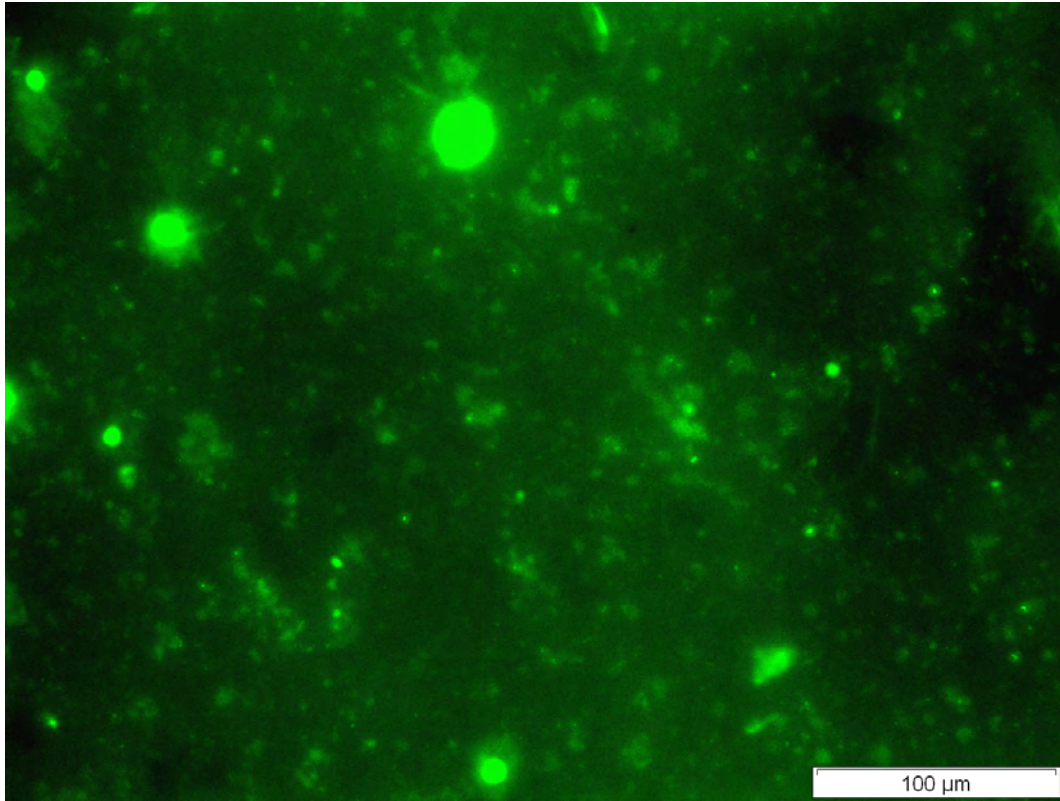
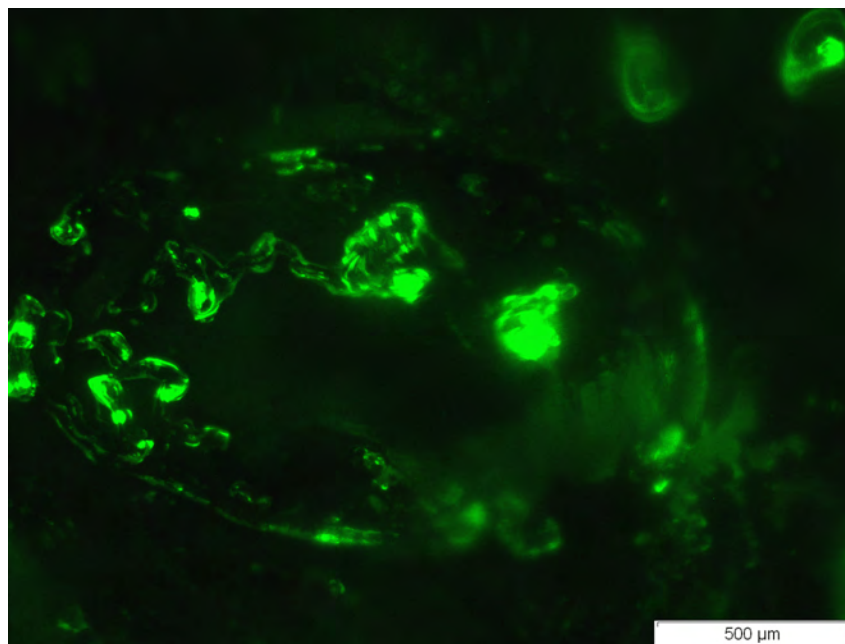
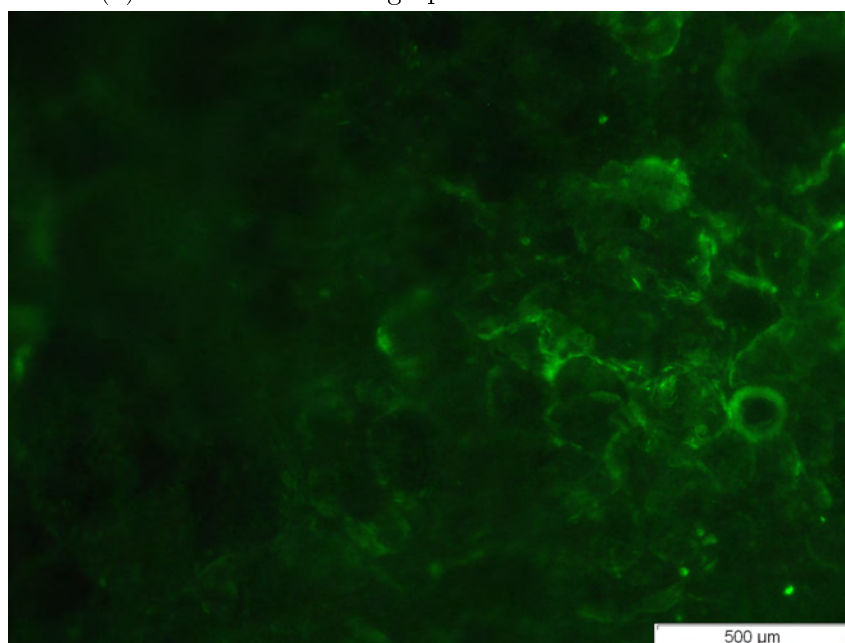


Figure D.16: Fluorescence micrograph of Glass-PAb-SAb slide (20× magnification)



(a) Fluorescence micrograph of Glass-PAb-SAb slide



(b) Fluorescence micrograph of Glass-PAb-SAb slide

Figure D.17: Fluorescence micrographs of Glass-PAb-SAb slides (4× magnification)

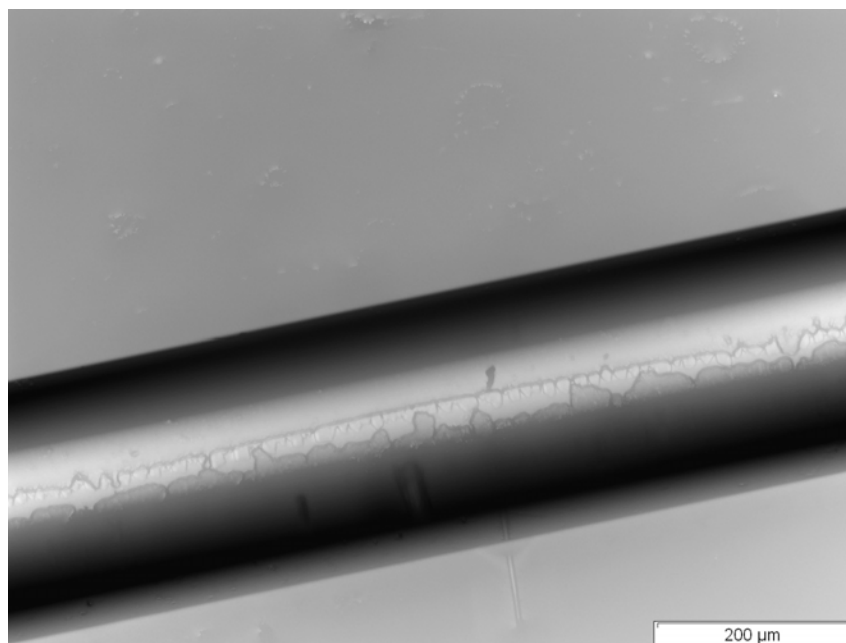


Figure D.18: Transmitted light image of a fiber (Glass, 10× magnification)



Figure D.19: Transmitted light image of a fiber (Glass + GPS, 10× magnification)



Figure D.20: Transmitted light image of optical fiber with crosslinker and PAb (4× magnification)

Appendix E

Datasheets

- Abcam: Anti-E. coli antibody ab25823
- Abcam: Donkey Anti-Goat IgG H&L (Alexa Fluor 488)
- Kingbright: L-144HDT Bright red LED
- TAOS: TSL12S light-to-voltage converter

Product Datasheet

Anti-E. coli antibody ab25823



★★★★☆ 3 Abreviews | 5 References

Overview

Product name	Anti-E. coli antibody
Description	Goat polyclonal to E. coli
Specificity	ab25823 recognises all E. coli species tested. The following species of E. coli were used in the antigen prep: Heat killed sonicate of E. coli from K12, TOP 10F, XS127/P3, JM109, HB101, and DH5a and BL21. We have also extensively tested K-12 Since there is 95% homology between the strains, all species of E.coli should react with this antibody.
Tested applications	ICC/IF, Electron Microscopy, WB, ELISA, Dot Blot
Species reactivity	Reacts with: Escherichia coli
Immunogen	Tissue/ cell preparation (Escherichia coli): Heat killed sonicate of E. coli (cocktail blend of strains of E. coli including the most commonly used DH5a and BL21).

Properties

Form	Liquid
Storage instructions	Shipped at 4°C. Store at +4°C short term (1-2 weeks). Upon delivery aliquot. Store at -20°C or -80°C. Avoid freeze / thaw cycle.
Storage buffer	Preservative: None Constituents: 150mM Sodium chloride, ~25mM HEPES, pH 7.0 to 7.4 The buffer contains trace amounts of citric acid and sodium phosphate. There are no preservatives or any other amine containing compounds and as such this material can be directly conjugated to enzymes, biotin etc. by most chemistries without the need to diafilter.
Purity	Protein G purified
Clonality	Polyclonal
Isotype	IgG

Applications

Our [Abpromise guarantee](#) covers the use of **ab25823** in the following tested applications.

The application notes include recommended starting dilutions; optimal dilutions/concentrations should be determined by the end user.

Application	Abreviews	Notes
ICC/IF	★★★★☆	Use at an assay dependent concentration. PubMed: 22427638
Electron Microscopy		Use at an assay dependent concentration. PubMed: 24253282
WB		Use a concentration of 0.5 - 2 µg/ml. Note: Reacts with more than 50 proteins by Western Blot.
ELISA	★★★★☆	Use at an assay dependent concentration.
Dot Blot		Use at an assay dependent concentration.

Target

Relevance	Escherichia coli is a gram negative bacillus that belongs to a larger group of Enterobacteriae - bacteria that inhabit the gastrointestinal tract. Although usually a harmless resident of the gut, some strains have the potential to cause serious problems, especially where there is an immature immune system or immunosuppression, or where the subtype of organism has acquired the ability to produce pathogenic toxins.
------------------	--

Please note: All products are "FOR RESEARCH USE ONLY AND ARE NOT INTENDED FOR DIAGNOSTIC OR THERAPEUTIC USE"

Our Abpromise to you: Quality guaranteed and expert technical support

Product Datasheet

- Replacement or refund for products not performing as stated on the datasheet
- Valid for 12 months from date of delivery
- Response to your inquiry within 24 hours

- We provide support in Chinese, English, French, German, Japanese and Spanish
- Extensive multi-media technical resources to help you
- We investigate all quality concerns to ensure our products perform to the highest standards

If the product does not perform as described on this datasheet, we will offer a refund or replacement. For full details of the Abpromise, please visit <http://www.abcam.com/abpromise> or contact our technical team.

Terms and conditions

- Guarantee only valid for products bought direct from Abcam or one of our authorized distributors

Visit us at: www.abcam.com

Product Datasheet

Donkey Anti-Goat IgG H&L (Alexa Fluor® 488)

ab150129



★★★★★ 1 Abreviews | 4 References | 4 Images

Overview

Product name	Donkey Anti-Goat IgG H&L (Alexa Fluor® 488)
Description	Donkey polyclonal Secondary Antibody to Goat IgG - H&L (Alexa Fluor® 488)
Target species	Goat
Tested applications	IHC-Fr, ICC/IF, Flow Cyt, IHC-P, ELISA
Conjugation	Alexa Fluor® 488. Ex: 495nm, Em: 519nm

Properties

Form	Liquid
Storage instructions	Store at +4°C short term (1-2 weeks). Upon delivery aliquot. Store at -20°C. Avoid freeze / thaw cycle.
Storage buffer	Preservative: 0.02% Sodium azide Constituents: PBS, 30% Glycerol, 1% BSA
Purity	Immunogen affinity purified
Purification notes	This antibody was isolated by affinity chromatography using antigen coupled to agarose beads.
Clonality	Polyclonal
Isotype	IgG

General notes

The Alexa Fluor® dye included in this product is provided under an intellectual property license from Life Technologies Corporation. As this product contains the Alexa Fluor® dye, the purchase of this product conveys to the buyer the non-transferable right to use the purchased product and components of the product only in research conducted by the buyer (whether the buyer is an academic or for-profit entity). As this product contains the Alexa Fluor® dye the sale of this product is expressly conditioned on the buyer not using the product or its components, or any materials made using the product or its components, in any activity to generate revenue, which may include, but is not limited to use of the product or its components: (i) in manufacturing; (ii) to provide a service, information, or data in return for payment (iii) for therapeutic, diagnostic or prophylactic purposes; or (iv) for resale, regardless of whether they are sold for use in research. For information on purchasing a license to use products containing Alexa Fluor® dyes for purposes other than research, contact Life Technologies Corporation, 5791 Van Allen Way, Carlsbad, CA 92008 USA or outlicensing@lifetech.com.

Applications

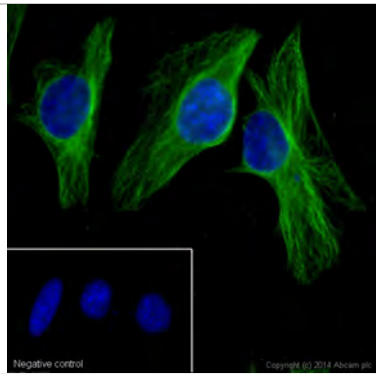
Our [Abpromise guarantee](#) covers the use of **ab150129** in the following tested applications.

The application notes include recommended starting dilutions; optimal dilutions/concentrations should be determined by the end user.

Application	Abreviews	Notes
IHC-Fr		Use at an assay dependent concentration.
ICC/IF	★★★★★	1/200 - 1/1000.
Flow Cyt		1/2000.
IHC-P		Use at an assay dependent concentration.
ELISA		Use at an assay dependent concentration.

Donkey Anti-Goat IgG H&L (Alexa Fluor® 488) images

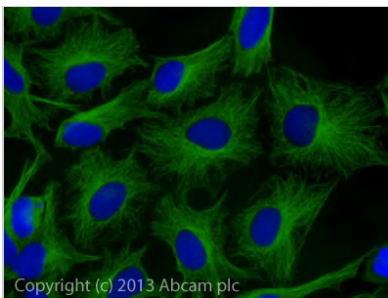
Product Datasheet



Immunocytochemistry/ Immunofluorescence -
Donkey Anti-Goat IgG H&L (Alexa Fluor® 488)
(ab150129)

ICC/IF image of [ab7291](#) stained HeLa cells. The cells were 100% methanol fixed (5 min) and then incubated in 1%BSA/ 0.3Mglycine in 0.1% PBS-Tween for 1h to permeabilise the cells and block non-specific protein-protein interactions. The cells were then incubated with the antibody ([ab7291](#), 1µg/ml) overnight at +4°C. Ab98800, goat anti-mouse IgG, was then added as a secondary bridging antibody, at 1/250 dilution for 1h. Ab150129 Alexa Fluor® 488 donkey anti-goat IgG (H+L) (shown in green) was then used at 1µg/ml for 1h as a tertiary antibody. DAPI was used to stain the cell nuclei (blue) at a concentration of 1.43µM.

The negative control (inset) is a secondary-only assay to demonstrate low non-specific binding of the secondary antibody.



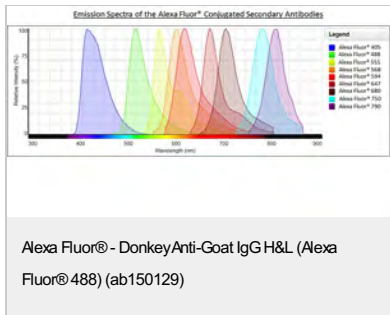
Immunocytochemistry/ Immunofluorescence -
Donkey polyclonal Secondary Antibody to IgG- H&L
(Alexa Fluor® 488), pre-adsorbed (ab150129)

ICC/IF image of [ab7291](#) stained HeLa cells. The cells were 100% methanol fixed (5 min) and then incubated in 1%BSA/ 0.3Mglycine in 0.1% PBS-Tween for 1h to permeabilise the cells and block non-specific protein-protein interactions. The cells were then incubated with the antibody ([ab7291](#), 1µg/ml) overnight at +4°C. Ab98800, goat anti-mouse IgG, was then added as a secondary bridging antibody, at 1/250 dilution for 1h. Ab150129 Alexa Fluor® 488 donkey anti-goat IgG (H+L) (green) was then used at 2µg/ml for 1h as a tertiary antibody. DAPI was used to stain the cell nuclei (blue) at a concentration of 1.43µM.

Immunocytochemistry/ Immunofluorescence -
Donkey Anti-Goat IgG H&L (Alexa Fluor® 488)
(ab150129)

HeLa cells showing negative staining by ICC/IF using only tertiary antibody. The cells were 100% methanol fixed (5 min) and then incubated in 1%BSA/ 0.3Mglycine in 0.1% PBS-Tween for 1h to permeabilise the cells and block non-specific protein-protein interactions. [ab150129](#) Alexa Fluor® 488 donkey anti-goat IgG (H+L) (green) was then used at 2µg/ml for 1h as a tertiary antibody. DAPI was used to stain the cell nuclei (blue) at a concentration of 1.43µM.

Product Datasheet



Please note: All products are "FOR RESEARCH USE ONLY AND ARE NOT INTENDED FOR DIAGNOSTIC OR THERAPEUTIC USE"

Our Abpromise to you: Quality guaranteed and expert technical support

- Replacement or refund for products not performing as stated on the datasheet
- Valid for 12 months from date of delivery**
- Response to your inquiry within 24 hours
- We provide support in Chinese, English, French, German, Japanese and Spanish
- Extensive multi-media technical resources to help you
- We investigate all quality concerns to ensure our products perform to the highest standards

If the product does not perform as described on this datasheet, we will offer a refund or replacement. For full details of the Abpromise, please visit <http://www.abcam.com/abpromise> or contact our technical team.

Terms and conditions

- Guarantee only valid for products bought direct from Abcam or one of our authorized distributors
- **Regional variations to our Abpromise may apply to the following countries: China, Korea, Singapore, Malaysia, Taiwan and Thailand, which operate a 120 day guarantee. Please contact your regional office for further details

Visit us at: www.abcam.com



1.9x3.9mm RECTANGULAR SOLID LAMPS

- | | |
|------------------------------|-----------------|
| L-144HDT BRIGHT RED | L-144GDT GREEN |
| L-144IDT HIGH EFFICIENCY RED | L-144EDT ORANGE |
| L-144SRDT SUPER BRIGHT RED | L-144YDT YELLOW |

Features

- LOW POWER CONSUMPTION.
- ULTRA BRIGHTNESS IS AVAILABLE .
- RELIABLE AND RUGGED.
- EXCELLENT UNIFORMITY OF LIGHT OUTPUT.
- SUITABLE FOR LEVEL INDICATOR.
- LONG LIFE - SOLID STATE RELIABILITY.

Description

The Bright Red source color devices are made with Gallium Phosphide Red Light Emitting Diode.

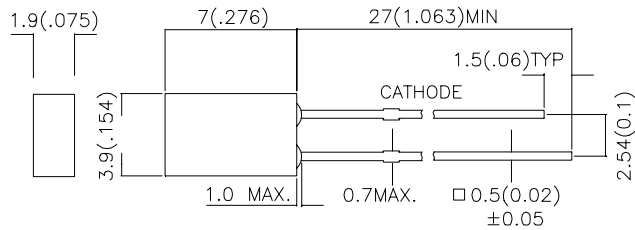
The High Efficiency Red and Orange source color devices are made with Gallium Arsenide Phosphide on Gallium Phosphide Orange Light Emitting Diode.

The Green source color devices are made with Gallium Phosphide Green Light Emitting Diode.

The Yellow source color devices are made with Gallium Arsenide Phosphide on Gallium Phosphide Yellow Light Emitting Diode.

The Super Bright Red source color devices are made with Gallium Aluminum Arsenide Red Light Emitting Diode.

Package Dimensions



- Notes:
1. All dimensions are in millimeters (inches).
 2. Tolerance is $\pm 0.25(0.01)$ unless otherwise noted.
 3. Lead spacing is measured where the lead emerge package.
 4. Specifications are subject to change without notice.

SPEC NO: KDA0281
APPROVED: J.LU

REV NO: V.1
CHECKED:

DATE: SEP/14/2001
DRAWN: J.X.FU

PAGE: 1 OF 6

Kingbright

Selection Guide					
Part No.	Dice	Lens Type	Iv (mcd) @ 10 mA *20mA		Viewing Angle
			Min.	Typ.	
L-144HDT	BRIGHT RED (GaP)	RED DIFFUSED	0.5	1	110°
L-144IDT	HIGH EFFICIENCY RED (GaAsP/GaP)	RED DIFFUSED	3	6	110°
L-144EDT	ORANGE (GaAsP/GaP)	ORANGE DIFFUSED	3	6	110°
L-144GDT	GREEN (GaP)	GREEN DIFFUSED	1	4	110°
L-144YDT	YELLOW (GaAsP/GaP)	YELLOW DIFFUSED	1	3	110°
L-144SRDT	SUPER BRIGHT RED (GaAlAs)	RED DIFFUSED	*40	*70	110°

Notes:
 1. $\theta_{1/2}$ is the angle from optical centerline where the luminous intensity is 1/2 the optical centerline value.
 2. * Luminous intensity with asterisk is measured at 20mA.

Electrical / Optical Characteristics at $T_A=25^\circ\text{C}$

Symbol	Parameter	Device	Typ.	Max.	Units	Test Conditions
λ_{peak}	Peak Wavelength	Bright Red High Efficiency Red Orange Green Yellow Super Bright Red	700 627 627 565 590 660		nm	IF=20mA
λ_D	Dominate Wavelength	Bright Red High Efficiency Red Orange Green Yellow Super Bright Red	660 625 625 568 588 640		nm	IF=20mA
$\Delta\lambda_{1/2}$	Spectral Line Halfwidth	Bright Red High Efficiency Red Orange Green Yellow Super Bright Red	45 45 45 30 35 20		nm	IF=20mA
C	Capacitance	Bright Red High Efficiency Red Orange Green Yellow Super Bright Red	40 15 15 15 20 45		pF	VF=0V;f=1MHz
V_F	Forward Voltage	Bright Red High Efficiency Red Orange Green Yellow Super Bright Red	2.25 2.0 2.0 2.2 2.1 1.85	2.5 2.5 2.5 2.5 2.5 2.5	V	IF=20mA
I_R	Reverse Current	All		10	μA	VR = 5V

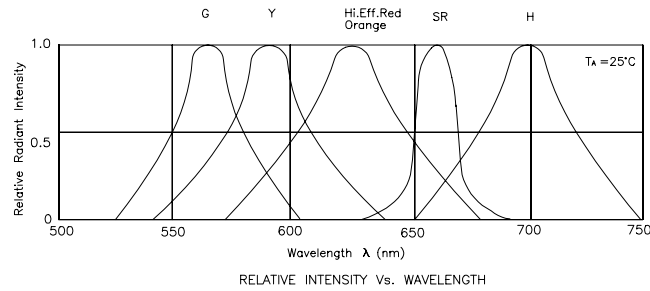
Kingbright

Absolute Maximum Ratings at T_A=25°C

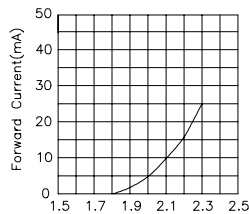
Parameter	Bright Red	High Efficiency Red	Orange	Green	Yellow	Super Bright Red	Units
Power dissipation	120	105	105	105	105	100	mW
DC Forward Current	25	30	30	25	30	30	mA
Peak Forward Current [1]	120	160	160	140	140	155	mA
Reverse Voltage	5	5	5	5	5	5	V
Operating/Storage Temperature	-40°C To +85°C						
Lead Solder Temperature [2]	260°C For 5 Seconds						

Notes:

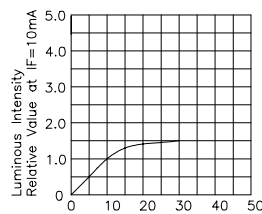
- 1/10 Duty Cycle, 0.1ms Pulse Width.
- 4mm below package base.



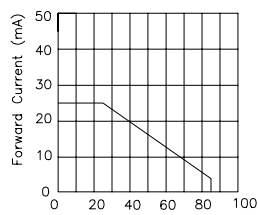
Bright Red L-144HDT



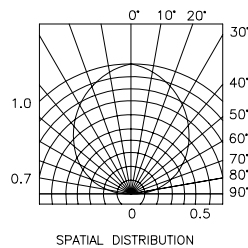
Forward Voltage(V)
FORWARD CURRENT Vs.
FORWARD VOLTAGE



I_f-Forward Current (mA)
LUMINOUS INTENSITY Vs.
FORWARD CURRENT



Ambient Temperature T_A(°C)
FORWARD CURRENT
DERATING CURVE



SPEC NO: KDA0281
APPROVED: J.LU

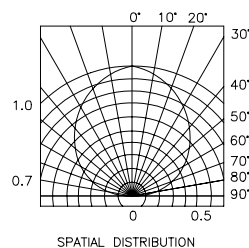
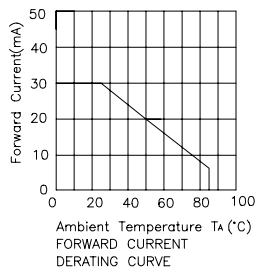
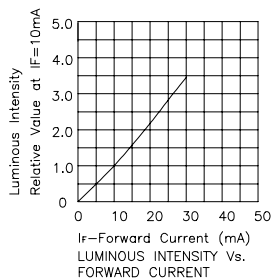
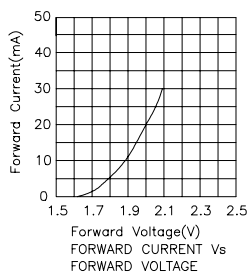
REV NO: V.1
CHECKED:

DATE: SEP/14/2001
DRAWN: J.X.FU

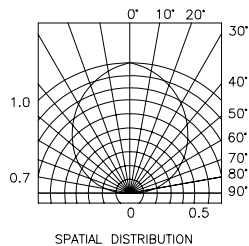
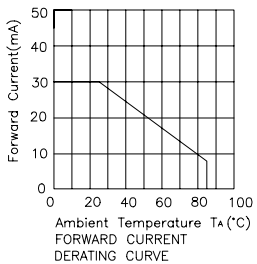
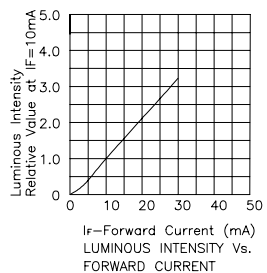
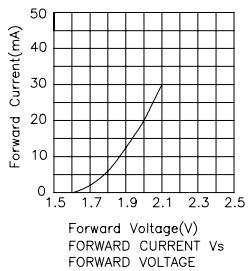
PAGE: 3 OF 6

Kingbright

High Efficiency Red L-144IDT



Orange L-144EDT



SPEC NO: KDA0281
APPROVED: J.LU

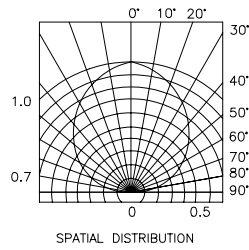
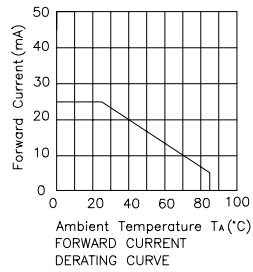
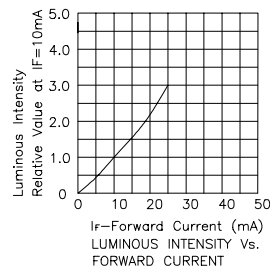
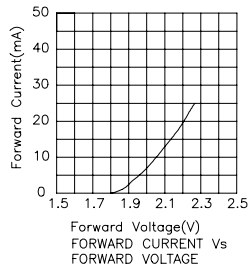
REV NO: V.1
CHECKED:

DATE: SEP/14/2001
DRAWN: J.X.FU

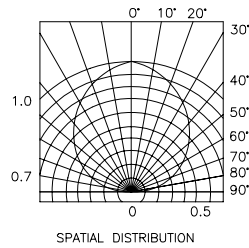
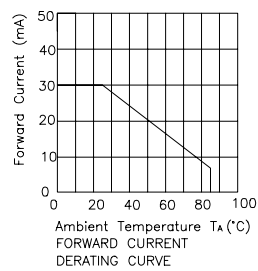
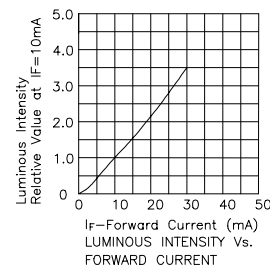
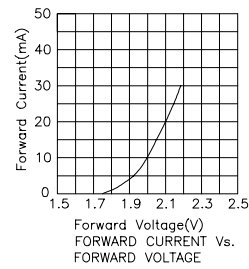
PAGE: 4 OF 6

Kingbright

Green L-144GDT

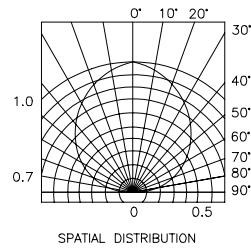
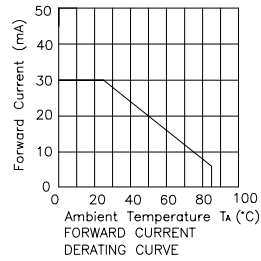
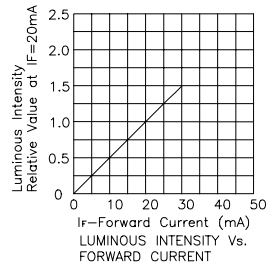
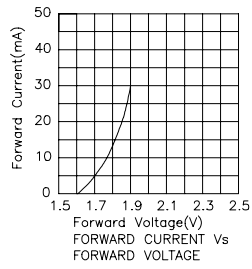


Yellow L-144YDT



Kingbright

Super Bright Red L-144SRDT





TAOS Inc.

is now

ams AG

The technical content of this TAOS datasheet is still valid.

Contact information:

Headquarters:

ams AG
Tobelbaderstrasse 30
8141 Unterpremstaetten, Austria
Tel: +43 (0) 3136 500 0
e-Mail: ams_sales@ams.com

Please visit our website at www.ams.com

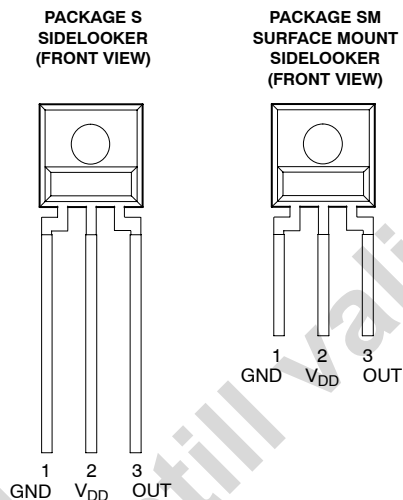




**TSL12S, TSL13S, TSL14S
LIGHT-TO-VOLTAGE CONVERTERS**

TAOS051E - SEPTEMBER 2007

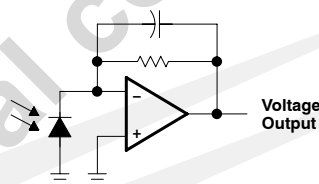
- Converts Light Intensity to Output Voltage
- Monolithic Silicon IC Containing Photodiode, Transconductance Amplifier, and Feedback Components
- Single-Supply Operation . . . 2.7 V to 5.5 V
- High Irradiance Responsivity . . . Typical 246 mV/(μ W/cm²) at $\lambda_p = 640$ nm (TSL12S)
- Low Supply Current . . . 1.1 mA Typical
- Sidelooker 3-Lead Package
- RoHS Compliant (-LF Package Only)



Description

The TSL12S, TSL13S, and TSL14S are cost-optimized, highly integrated light-to-voltage optical sensors, each combining a photodiode and a transimpedance amplifier (feedback resistor = 80 M Ω , 20 M Ω , and 5 M Ω , respectively) on a single monolithic integrated circuit. The photodiode active area is 0.5 mm x 0.5 mm and the sensors respond to light in the range of 320 nm to 1050 nm. Output voltage is linear with light intensity (irradiance) incident on the sensor over a wide dynamic range. These devices are supplied in a 3-lead clear plastic sidelooker package (S). When supplied in the lead (Pb) free package, the device is RoHS compliant.

Functional Block Diagram



**TSL12S, TSL13S, TSL14S
LIGHT-TO-VOLTAGE CONVERTERS**

TAOS051E – SEPTEMBER 2007

Available Options

DEVICE	T _A	PACKAGE – LEADS	PACKAGE DESIGNATOR	ORDERING NUMBER
TSL12S	0°C to 70°C	3-lead Sidelooker	S	TSL12S
TSL12S	0°C to 70°C	3-lead Sidelooker — Lead (Pb) Free	S	TSL12S-LF
TSL12S	0°C to 70°C	3-lead Surface-Mount Sidelooker — Lead (Pb) Free	SM	TSL12SM-LF
TSL13S	0°C to 70°C	3-lead Sidelooker	S	TSL13S
TSL13S	0°C to 70°C	3-lead Sidelooker — Lead (Pb) Free	S	TSL13S-LF
TSL13S	0°C to 70°C	3-lead Surface-Mount Sidelooker — Lead (Pb) Free	SM	TSL13SM-LF
TSL14S	0°C to 70°C	3-lead Sidelooker	S	TSL14S
TSL14S	0°C to 70°C	3-lead Sidelooker — Lead (Pb) Free	S	TSL14S-LF
TSL14S	0°C to 70°C	3-lead Surface-Mount Sidelooker — Lead (Pb) Free	SM	TSL14SM-LF

Terminal Functions

TERMINAL NAME	NO.	TYPE	DESCRIPTION
GND	1		Power supply ground (substrate). All voltages are referenced to GND.
OUT	3	O	Output voltage.
V _{DD}	2		Supply voltage.

Absolute Maximum Ratings over operating free-air temperature range (unless otherwise noted)†

Supply voltage, V _{DD} (see Note 1)	6 V
Output current, I _O	±10 mA
Duration of short-circuit current at (or below) 25°C (see Note 2)	5 s
Operating free-air temperature range, T _A	-25°C to 85°C
Storage temperature range, T _{stg}	-25°C to 85°C
Lead temperature 1,6 mm (1/16 inch) from case for 10 seconds (S Package)	260°C
Reflow solder, in accordance with J-STD-020C or J-STD-020D (SM Package)	260°C

† Stresses beyond those listed under "absolute maximum ratings" may cause permanent damage to the device. These are stress ratings only, and functional operation of the device at these or any other conditions beyond those indicated under "recommended operating conditions" is not implied. Exposure to absolute-maximum-rated conditions for extended periods may affect device reliability.

NOTES: 1. All voltages are with respect to GND.

2. Output may be shorted to supply.

Recommended Operating Conditions

	MIN	NOM	MAX	UNIT
Supply voltage, V _{DD}	2.7		5.5	V
Operating free-air temperature, T _A	0		70	°C



TSL12S, TSL13S, TSL14S LIGHT-TO-VOLTAGE CONVERTERS

TAOS051E - SEPTEMBER 2007

Electrical Characteristics at $V_{DD} = 5\text{ V}$, $T_A = 25^\circ\text{C}$, $\lambda_p = 640\text{ nm}$, $R_L = 10\text{ k}\Omega$ (unless otherwise noted)
(see Notes 3, 4, 5)

PARAMETER	TEST CONDITIONS	TSL12S			TSL13S			TSL14S			UNIT	
		MIN	TYP	MAX	MIN	TYP	MAX	MIN	TYP	MAX		
V_{OM}	Maximum output voltage	4.6	4.9		4.6	4.9		4.6	4.9		V	
V_O	Output voltage	$E_e = 8\ \mu\text{W}/\text{cm}^2$	1.5	2	2.5							V
		$E_e = 31\ \mu\text{W}/\text{cm}^2$				1.5	2	2.5				
		$E_e = 120\ \mu\text{W}/\text{cm}^2$							1.5	2	2.5	
		$E_e = 16\ \mu\text{W}/\text{cm}^2$		4								
		$E_e = 62\ \mu\text{W}/\text{cm}^2$				4						
$E_e = 240\ \mu\text{W}/\text{cm}^2$								4				
R_e	Irradiance responsivity	Note 6	248		64			16			mV/ ($\mu\text{W}/\text{cm}^2$)	
V_{OS}	Extrapolated offset voltage	Note 6	-0.02	0.03	0.08	-0.02	0.03	0.08	-0.02	0.03	0.08	V
V_d	Dark voltage	$E_e = 0$	0	0.08		0	0.08		0	0.08		V
I_D	Supply current	$E_e = 8\ \mu\text{W}/\text{cm}^2$		1.1	1.7							mA
		$E_e = 31\ \mu\text{W}/\text{cm}^2$				1.1	1.7					
		$E_e = 120\ \mu\text{W}/\text{cm}^2$							1.1	1.7		

- NOTES:
- Measurements are made with $R_L = 10\text{ k}\Omega$ between output and ground.
 - Optical measurements are made using small-angle incident radiation from an LED optical source.
 - The 640 nm input irradiance E_e is supplied by an AlInGaP LED with peak wavelength $\lambda_p = 640\text{ nm}$.
 - Irradiance responsivity is characterized over the range $V_O = 0.2$ to 4 V. The best-fit straight line of Output Voltage V_O versus irradiance E_e over this range may have a positive or negative extrapolated V_O value for $E_e = 0$. For low irradiance values, the output voltage V_O versus irradiance E_e characteristic is non linear with a deviation toward $V_O = 0$, $E_e = 0$ origin from the best-fit straight line referenced above.

Dynamic Characteristics at $V_{DD} = 5\text{ V}$, $T_A = 25^\circ\text{C}$, $\lambda_p = 640\text{ nm}$, $R_L = 10\text{ k}\Omega$ (unless otherwise noted)
(see Figure 1)

PARAMETER	TEST CONDITIONS	TSL12S			TSL13S			TSL14S			UNIT
		MIN	TYP	MAX	MIN	TYP	MAX	MIN	TYP	MAX	
t_{dr}	Output pulse delay time for rising edge (0% to 10%)	Min $V_O = 0\text{ V}$; Peak $V_O = 2\text{ V}$		13		1.7		0.9			μs
		Min $V_O = 0.5\text{ V}$; Peak $V_O = 2\text{ V}$		2.3		1.2		0.6			
t_r	Output pulse rise time (10% to 90%)	Min $V_O = 0\text{ V}$; Peak $V_O = 2\text{ V}$		20		7.2		2.6			μs
		Min $V_O = 0.5\text{ V}$; Peak $V_O = 2\text{ V}$		10		6.5		2.9			
t_{df}	Output pulse delay time for falling edge (100% to 90%)	Min $V_O = 0\text{ V}$; Peak $V_O = 2\text{ V}$		2.3		1.2		0.8			μs
		Min $V_O = 0.5\text{ V}$; Peak $V_O = 2\text{ V}$		2.2		1.1		0.7			
t_f	Output pulse fall time (90% to 10%)	Min $V_O = 0\text{ V}$; Peak $V_O = 2\text{ V}$		10		6.8		2.9			μs
		Min $V_O = 0.5\text{ V}$; Peak $V_O = 2\text{ V}$		9		6.4		2.8			



**TSL12S, TSL13S, TSL14S
LIGHT-TO-VOLTAGE CONVERTERS**

TAOS051E – SEPTEMBER 2007

PARAMETER MEASUREMENT INFORMATION

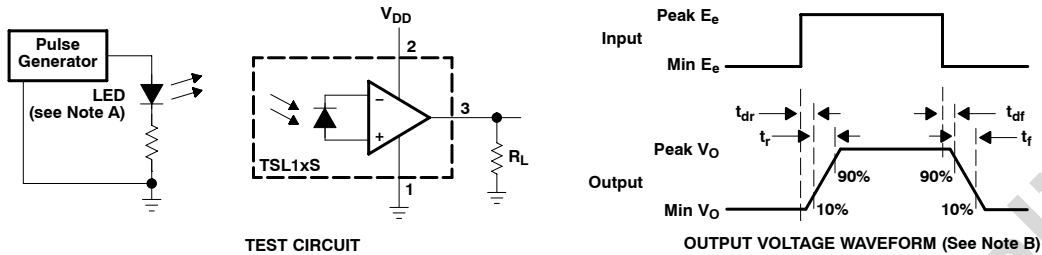


Figure 1. Switching Times

TYPICAL CHARACTERISTICS

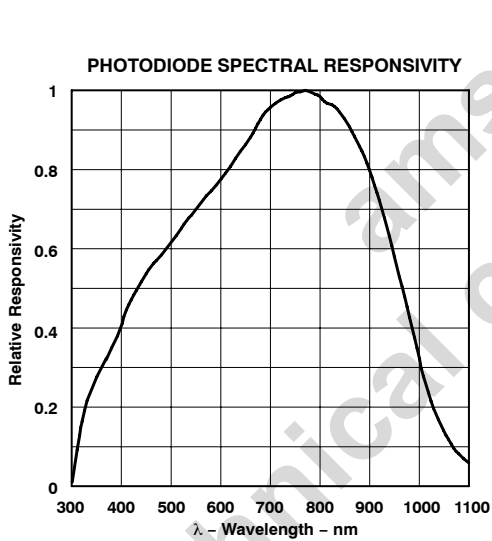


Figure 2

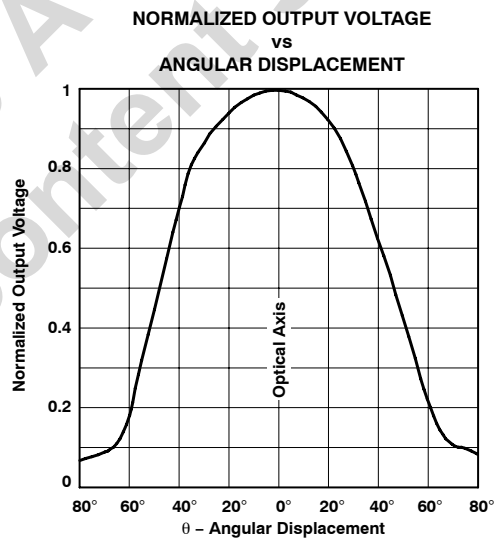


Figure 3

**TSL12S, TSL13S, TSL14S
LIGHT-TO-VOLTAGE CONVERTERS**

TAOS051E - SEPTEMBER 2007

TYPICAL CHARACTERISTICS

TSL12S

**RISING EDGE DYNAMIC CHARACTERISTICS
vs.
PEAK OUTPUT VOLTAGE**

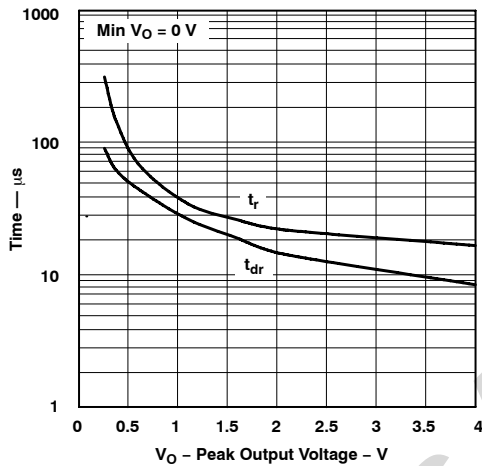


Figure 4

**RISING EDGE DYNAMIC CHARACTERISTICS
vs.
PEAK OUTPUT VOLTAGE**

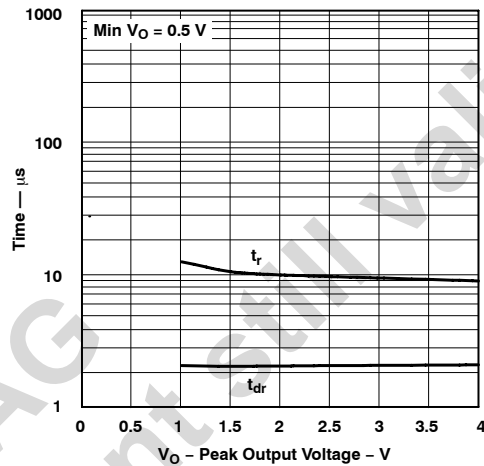


Figure 5

**FALLING EDGE DYNAMIC CHARACTERISTICS
vs.
PEAK OUTPUT VOLTAGE**

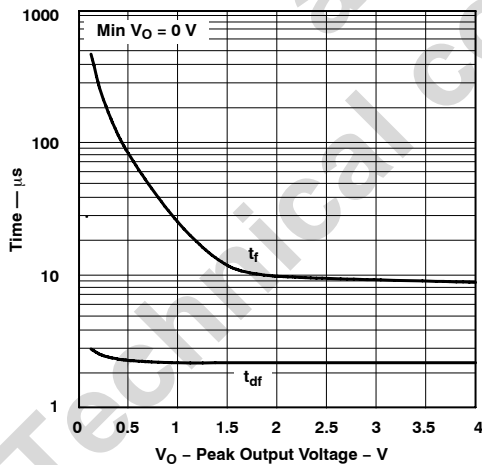


Figure 6

**FALLING EDGE DYNAMIC CHARACTERISTICS
vs.
PEAK OUTPUT VOLTAGE**

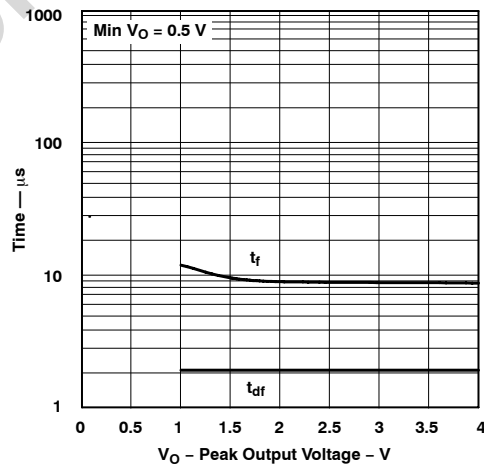


Figure 7

**TSL12S, TSL13S, TSL14S
LIGHT-TO-VOLTAGE CONVERTERS**

TAOS051E – SEPTEMBER 2007

TYPICAL CHARACTERISTICS

TSL13S

**RISING EDGE DYNAMIC CHARACTERISTICS
vs.
PEAK OUTPUT VOLTAGE**

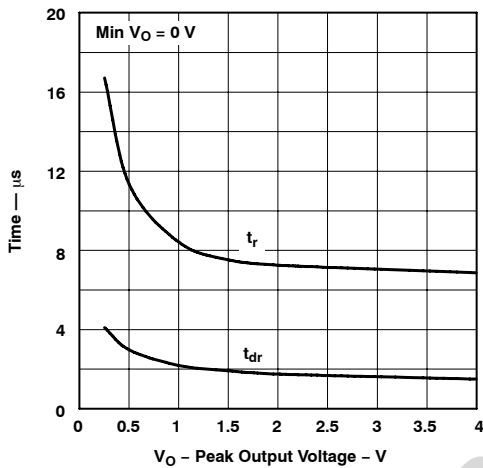


Figure 8

**RISING EDGE DYNAMIC CHARACTERISTICS
vs.
PEAK OUTPUT VOLTAGE**

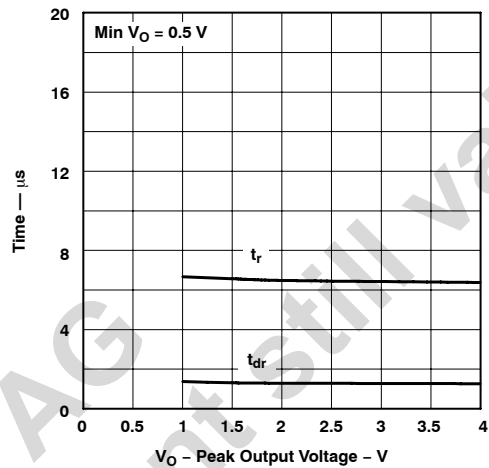


Figure 9

**FALLING EDGE DYNAMIC CHARACTERISTICS
vs.
PEAK OUTPUT VOLTAGE**

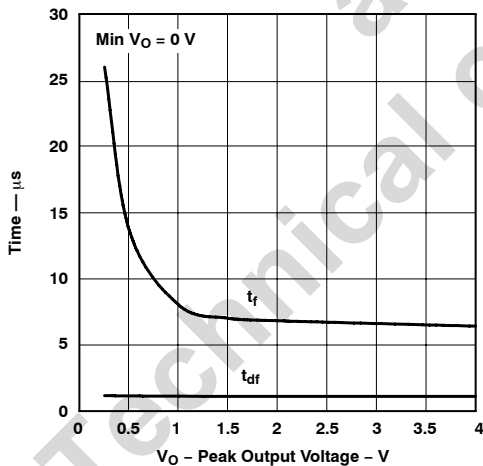


Figure 10

**FALLING EDGE DYNAMIC CHARACTERISTICS
vs.
PEAK OUTPUT VOLTAGE**

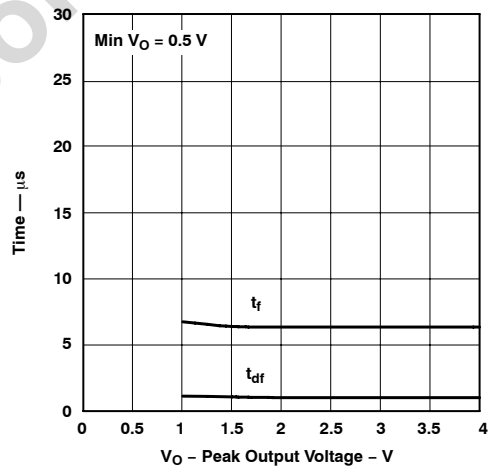


Figure 11

**TSL12S, TSL13S, TSL14S
LIGHT-TO-VOLTAGE CONVERTERS**

TAOS051E - SEPTEMBER 2007

TYPICAL CHARACTERISTICS

TSL14S

**RISING EDGE DYNAMIC CHARACTERISTICS
vs.
PEAK OUTPUT VOLTAGE**

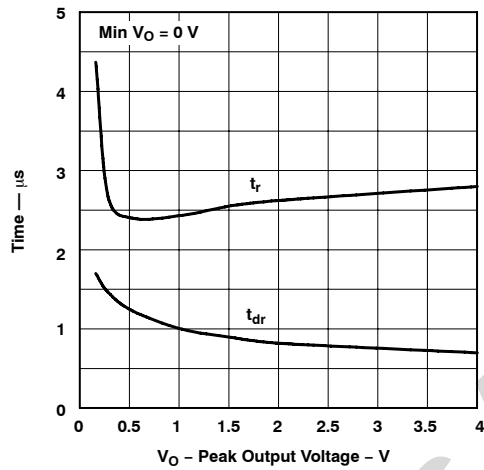


Figure 12

**RISING EDGE DYNAMIC CHARACTERISTICS
vs.
PEAK OUTPUT VOLTAGE**

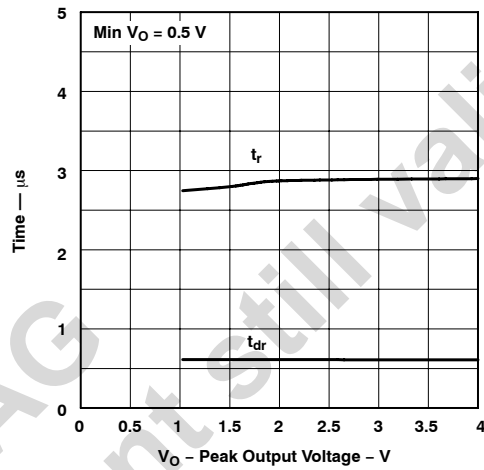


Figure 13

**FALLING EDGE DYNAMIC CHARACTERISTICS
vs.
PEAK OUTPUT VOLTAGE**

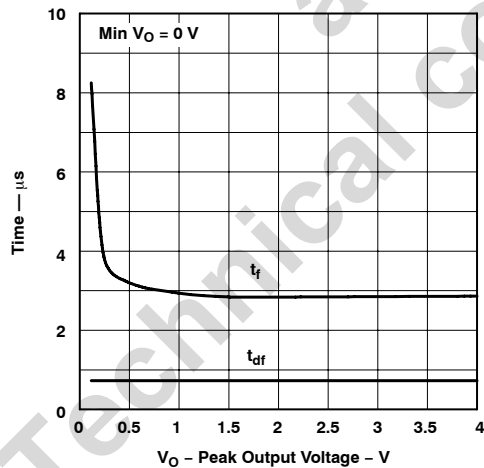


Figure 14

**FALLING EDGE DYNAMIC CHARACTERISTICS
vs.
PEAK OUTPUT VOLTAGE**

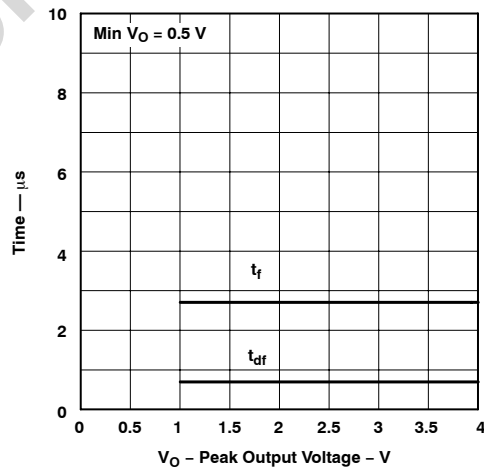


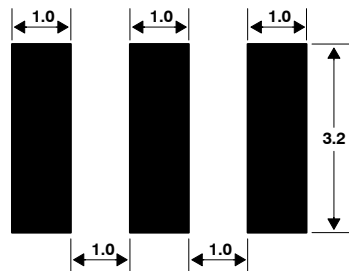
Figure 15

**TSL12S, TSL13S, TSL14S
LIGHT-TO-VOLTAGE CONVERTERS**

TAOS051E – SEPTEMBER 2007

APPLICATION INFORMATION**PCB Pad Layout**

Suggested PCB pad layout guidelines for the SM surface mount package are shown in Figure 16.



- NOTES: A. All linear dimensions are in millimeters.
B. This drawing is subject to change without notice.

Figure 16. Suggested SM Package PCB Layout

**TSL12S, TSL13S, TSL14S
LIGHT-TO-VOLTAGE CONVERTERS**

TAOS051E – SEPTEMBER 2007

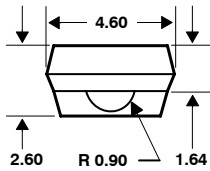
MECHANICAL DATA

The TSL12S, TSL13S, and TSL14S are supplied in a clear 3-lead through-hole package with a molded lens.

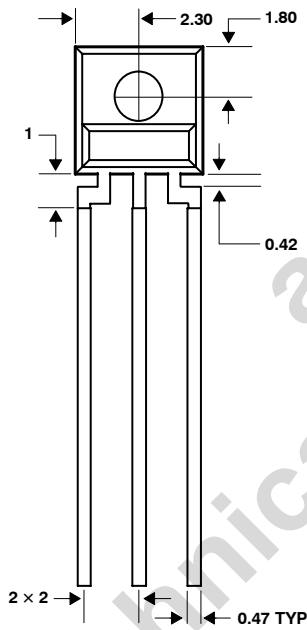
PACKAGE S

PLASTIC SINGLE-IN-LINE SIDE-LOOKER PACKAGE

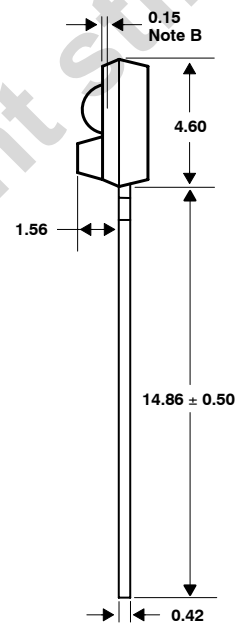
TOP VIEW



FRONT VIEW



SIDE VIEW



Lead Free Available

- NOTES: A. All linear dimensions are in millimeters; tolerance is ± 0.25 mm unless otherwise stated.
 B. Dimension is to center of lens arc, which is located below the package face.
 C. The 0.50 mm \times 0.50 mm integrated photodiode active area is typically located in the center of the lens and 0.97 mm below the top of the lens surface.
 D. Index of refraction of clear plastic is 1.55.
 E. Lead finish for TSL1xS: solder dipped, 63% Sn/37% Pb. Lead finish for TSL1xS-LF: solder dipped, 100% Sn.
 F. This drawing is subject to change without notice.

Figure 17. Package S — Single-In-Line Side-Looker Package Configuration



**TSL12S, TSL13S, TSL14S
LIGHT-TO-VOLTAGE CONVERTERS**

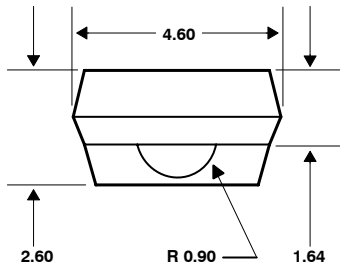
TAOS051E – SEPTEMBER 2007

MECHANICAL DATA

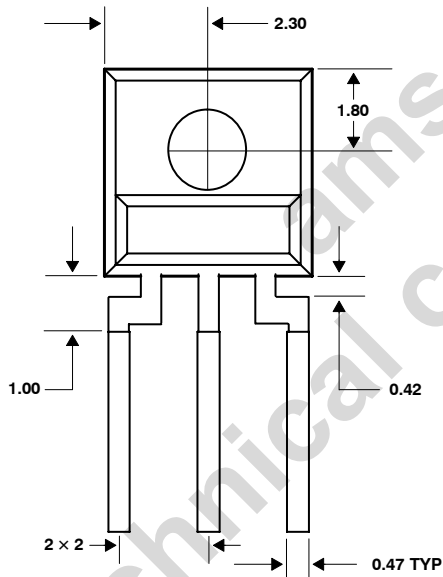
PACKAGE SM

PLASTIC SURFACE MOUNT SIDE-LOOKER PACKAGE

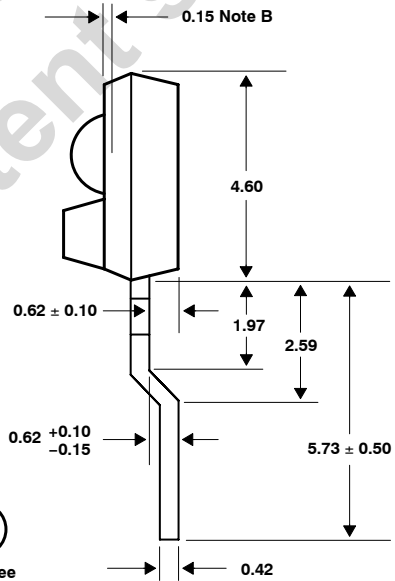
TOP VIEW



FRONT VIEW



SIDE VIEW



- NOTES: A. All linear dimensions are in millimeters; tolerance is ± 0.25 mm unless otherwise stated.
 B. Dimension is to center of lens arc, which is located below the package face.
 C. The integrated photodiode active area is typically located in the center of the lens and 0.97 mm below the top of the lens surface.
 D. Index of refraction of clear plastic is 1.55.
 E. Lead finish for TSL1xSM-LF: solder dipped, 100% Sn.
 F. This drawing is subject to change without notice.

Figure 18. Package SM — Surface Mount Side-Looker Package Configuration

**TSL12S, TSL13S, TSL14S
LIGHT-TO-VOLTAGE CONVERTERS**

TAOS051E - SEPTEMBER 2007

PRODUCTION DATA — information in this document is current at publication date. Products conform to specifications in accordance with the terms of Texas Advanced Optoelectronic Solutions, Inc. standard warranty. Production processing does not necessarily include testing of all parameters.

LEAD-FREE (Pb-FREE) and GREEN STATEMENT

Pb-Free (RoHS) TAOS' terms *Lead-Free* or *Pb-Free* mean semiconductor products that are compatible with the current RoHS requirements for all 6 substances, including the requirement that lead not exceed 0.1% by weight in homogeneous materials. Where designed to be soldered at high temperatures, TAOS Pb-Free products are suitable for use in specified lead-free processes.

Green (RoHS & no Sb/Br) TAOS defines *Green* to mean Pb-Free (RoHS compatible), and free of Bromine (Br) and Antimony (Sb) based flame retardants (Br or Sb do not exceed 0.1% by weight in homogeneous material).

Important Information and Disclaimer The information provided in this statement represents TAOS' knowledge and belief as of the date that it is provided. TAOS bases its knowledge and belief on information provided by third parties, and makes no representation or warranty as to the accuracy of such information. Efforts are underway to better integrate information from third parties. TAOS has taken and continues to take reasonable steps to provide representative and accurate information but may not have conducted destructive testing or chemical analysis on incoming materials and chemicals. TAOS and TAOS suppliers consider certain information to be proprietary, and thus CAS numbers and other limited information may not be available for release.

NOTICE

Texas Advanced Optoelectronic Solutions, Inc. (TAOS) reserves the right to make changes to the products contained in this document to improve performance or for any other purpose, or to discontinue them without notice. Customers are advised to contact TAOS to obtain the latest product information before placing orders or designing TAOS products into systems.

TAOS assumes no responsibility for the use of any products or circuits described in this document or customer product design, conveys no license, either expressed or implied, under any patent or other right, and makes no representation that the circuits are free of patent infringement. TAOS further makes no claim as to the suitability of its products for any particular purpose, nor does TAOS assume any liability arising out of the use of any product or circuit, and specifically disclaims any and all liability, including without limitation consequential or incidental damages.

TEXAS ADVANCED OPTOELECTRONIC SOLUTIONS, INC. PRODUCTS ARE NOT DESIGNED OR INTENDED FOR USE IN CRITICAL APPLICATIONS IN WHICH THE FAILURE OR MALFUNCTION OF THE TAOS PRODUCT MAY RESULT IN PERSONAL INJURY OR DEATH. USE OF TAOS PRODUCTS IN LIFE SUPPORT SYSTEMS IS EXPRESSLY UNAUTHORIZED AND ANY SUCH USE BY A CUSTOMER IS COMPLETELY AT THE CUSTOMER'S RISK.

LUMENOLOGY, TAOS, the TAOS logo, and Texas Advanced Optoelectronic Solutions are registered trademarks of Texas Advanced Optoelectronic Solutions Incorporated.



**TSL12S, TSL13S, TSL14S
LIGHT-TO-VOLTAGE CONVERTERS**

TAOS051E - SEPTEMBER 2007

ams AG
Technical content still valid

List of References

- [1] D. R. Thévenot, K. Toth, R. A. Durst, and G. S. Wilson, "Electrochemical biosensors: recommended definition and classification," International Union of Pure and Applied Chemistry, Tech. Rep., 1999.
- [2] World Health Organization and United Nations Children's Fund Joint Monitoring Programme for Water Supply and Sanitation (JMP), *Progress on Drinking Water and Sanitation: Special Focus on Sanitation*, World Health Organisation and UNICEF, Ed. World Health Organisation and UNICEF, 2008.
- [3] D. K. Plate, B. I. Strassmann, and M. L. Wilson, "Water sources are associated with childhood diarrhoea prevalence in rural east-central mali," *Tropical Medicine and International Health*, 2004.
- [4] J. Tokas, R. Begum, S. Jain, and H. Yadav, "Biosensor: General principles and applications - presentation," Online.
- [5] S. Rodriguez-Mozaz., M. J. L. de Alda, and D. Barceló, "Biosensors as useful tools for environmental analysis and monitoring," *Anal. Bioanal Chem*, 2006.
- [6] Water Supply and Sanitation Technology Platform, "Strategic research agenda: Water research - a necessary investment in our common future," *WSSTP*, 2006.
- [7] World Health Organisation, *The World health report - 2003 : Shaping the future*, WHO, Ed. World Health Organisation, 2003.
- [8] World Health Organisation and UNICEF, *Meeting the MDG drinking water and sanitation target : the urban and rural challenge of the decade*, World Health Organisation and UNICEF, Ed. World Health Organisation and UNICEF, 2006.
- [9] World Health Organisation and the United Nations Children's fund, *Global water supply and sanitation assessment 2000 report*, WHO, Ed. World Health Organisation and the United Nations Children's fund, 2000.
- [10] MOHSW and WHO, "Lesotho - health indicators - june 5, 2002," Online: www.who.int/disasters/repo/7773.doc, 2002.
- [11] P. Gwinbi, "The microbial quality of drinking water in manonyane community: Maseru district (lesotho)," *African Health Sciences*, 2011.

- [12] T. Könnölä, "Future outlook on water quality monitoring technologies," 2006.
- [13] A. Rossouw, "Modified track-etched membranes using photocatalytic semiconductors for advanced oxidation water treatment processes," Master's thesis, University of Stellenbosch, 2013.
- [14] A. Rossouw, "Research proposal for the degree of doctor of philosophy in engineering at the university of Stellenbosch: The development of composite photocatalytic thin films on track etched membranes for use in water treatment," 2014.
- [15] Department of Water Affairs: Republic of South Africa, "2012/2013 annual report."
- [16] UNEP, *Challenges to International Waters - Regional Assessments in a Global Perspective*, UNEP, Ed. United Nations Environment Programme, Nairobi, Kenya, 2006.
- [17] A. Koyun, E. Ahlatcıoğlu, and Y. K. İpek, *Biosensors and Their Principles, A Roadmap of Biomedical Engineers and Milestones*, Prof. Sadic Kara, Ed. InTech, 2012.
- [18] A. Sassolas, L. J. Blum, and B. D. Leca-Bouvier, "Immobilization strategies to develop enzymatic biosensors," *Biotechnology Advances*, 2012.
- [19] T. Vo-Dinh and B. Cullum, "Biosensors and biochips: advances in biological and medical diagnostics," *Fresenius J Anal Chem.*, 2000.
- [20] M. Trojanowicz, "Miniaturized biochemical sensing devices based on planar bilayer lipid membranes," *Fresenius J Anal Chem.*, 2001.
- [21] World Health Organisation, *Water Quality: Guidelines, Standards and Health*, L. Fetrell and J. Bartram, Eds. IWA Publishing, 2001.
- [22] X. Luo and J. J. Davis, "Electrical biosensors and the label free detection of protein disease biomarkers," *Chemical Society Reviews*, 2013.
- [23] J. Mairhofer, K. Roppert, and P. Ertl, "Microfluidic systems for pathogen sensing: A review," *Sensors*, 2009.
- [24] World Health Organisation, *Guidelines for Drinking-Water Quality - Second Edition - Volume 2 - Health Criteria and Other Supporting Information*. World Health Organisation, 1996.
- [25] SABS, *South African National Standard 241-1:2011 Drinking water Part 1: Microbiological, physical, aesthetic and chemical determinands*, SABS Std.

- [26] World Health Organisation, *Guidelines for drinking-water quality - second edition Volume 3 - Surveillance and control of community supplies*, WHO, Ed. World Health Organisation, 1997.
- [27] O. Lazcka, F. J. D. Campo, and F. X. Muñoz, "Pathogen detection: A perspective of traditional methods and biosensors," *Biosensors and Bioelectronics*, 2007.
- [28] J.-Y. Yoon and B. Kim, "Lab-on-a-chip pathogen sensors for food safety," *Sensors*, 2012.
- [29] K. Rijal, A. Leung, P. Shankar, and R. Mutharasan, "Detection of pathogen escherichia coli o157:h7 at 70 cells/ml using antibody-immobilized biconical tapered fiber sensors," *Biosensors and Bioelectronics*, 2005.
- [30] B. Kuswandi, Nuriman, J. Huskens, and W. Verboom, "Optical sensing systems for microfluidic devices: A review," *Analytica Chimica Acta*, 2007.
- [31] D. DeMarco and D. Lim, "Detection of escherichia coli o157:h7 in 10- and 25-gram ground beef samples with an evanescent-wave biosensor with silica and polystyrene waveguides," *Journal of Food Protection*, 2002.
- [32] M. Taniguchi, E. Akai, T. Koshida, K. Hibi, H. Kudo, K. Otsuka, H. Saito, K. Yano, H. Endo, and K. Mitsubayashi, "A fiber optic immunosensor for rapid bacteria determination," *IFMBE Proceedings*, 2007.
- [33] K. Miyajima, T. Koshida, T. Arakawa, H. Kudo, H. Saito, K. Yano, and K. Mitsubayashi, "Fiber-optic fluoroimmunoassay system with a flow-through cell for rapid on-site determination of escherichia coli o157:h7 by monitoring fluorescence dynamics," *Biosensors*, 2013.
- [34] S. M. Radke and E. C. Alocilja, "A high density microelectrode array biosensor for detection of e. coli o157:h7," *Biosensors and Bioelectronics*, 2005.
- [35] J. Huzior, I. Struzycka, P. Los, M. Brischwein, J. Perek, M. Tyc, K. Ziemiecka, and M. Just, "A new non-linear electrochemical impedance spectroscopy method of second dental caries detection based on microbiological markers," *Polish Journal of Environmental Studies*, 2013.
- [36] K. Ziemiecka, I. Struzycka, P. Los, J. Perek, M. Just, M. Tyc, J. Huzior, and M. Brischwein, "Scientific description of an in vitro model of second caries test new bio-impedance detection method based on microbiological marker," *Polish Journal of Environmental Studies*, 2013.

- [37] D. Ivnitski, I. Abdel-Hamid, P. Atanasov, and E. Wilkins, "Biosensors for detection of pathogenic bacteria," *Biosensors and Bioelectronics*, 1999.
- [38] A. Sadana, *Binding and Dissociation Kinetics for Different Biosensor Applications Using Fractals*. Elsevier Science, 2006.
- [39] G. Liu and Y. Lin, "Electrochemical sensor for organophosphate pesticides and nerve agents using zirconia nanoparticles as selective sorbents," *Analytical Chemistry*, 2005.
- [40] S. Rodriguez-Mozaz, M.-P. Marco, M. J. L. de Alda, and D. Barceló, "Biosensors for environmental applications: Future development trends," *Pure and Applied Chemistry*, 2004.
- [41] P. Leonard, S. Hearty, J. Brennan, L. Dunne, J. Quinn, T. Chakraborty, and R. O'Kennedy, "Advances in biosensors for detection of pathogens in food and water," *Enzyme and Microbial Technology*, 2003.
- [42] H. K. Hunt and A. M. Armani, "Label-free biological and chemical sensors," *Nanoscale*, 2010.
- [43] P. Kim, N. Kohli, B. Hassler, N. Dotson, A. Mason, R. M. Worden, and R. Ofoli, "An electrochemical interface for integrated biosensors," *Sensors*, 2003.
- [44] J. P. Chambers, B. P. Arulanandam, L. L. Matta, and A. W. J. J. Valdes, "Biosensor recognition elements," *Current Issues in Molecular Biology*, 2008.
- [45] Y. Xiao and C. M. Li, "Nanocomposites: From fabrications to electrochemical bioapplications," *Electroanalysis*, 2008.
- [46] Y.-H. Yun, E. Eteshola, A. Bhattacharya, Z. Dong, J.-S. Shim, L. Conforti, D. Kim, M. J. Schulz, C. H. Ahn, and N. Watts, "Tiny medicine: Nanomaterial-based biosensors," *Sensors*, 2009.
- [47] J. D. Corcuera and R. Cavalieri, "Biosensors," *Encyclopedia of Agricultural, Food, and Biological Engineering*, 2003.
- [48] J. Zang, C. M. Li, X. Cui, J. W. X. Sun, H. Dong, and C. Q. Sun, "Tailoring zinc oxide nanowires for high performance amperometric glucose sensor," *Electroanalysis*, 2007.
- [49] W. Feng and P. Ji, "Enzymes immobilized on carbon nanotubes," *Biotechnology Advances*, 2011.
- [50] B. Kuswandi, R. Andresa, and R. Narayanaswamy, "Optical fibre biosensors based on immobilised enzymes," *Analyst*, 2001.

- [51] N. Jaffrezic-Renault and S. Dzyadevych, "Conductometric microbiosensors for environmental monitoring," *Sensors*, 2008.
- [52] R. University. (2015) Antibody illustration. Creative commons. <http://cnx.org/contents>.
- [53] Abcam, "Polyclonal and monoclonal: A comparison online: www.abcam.com."
- [54] T. Mairal, V. C. Özalp, P. L. S. M. Mir, I. Katakis, and C. K. O'Sullivan, "Aptamers: molecular tools for analytical applications," *Anal. Bioanal Chem*, 2008.
- [55] Life technologies, "Biotinylation," Online: www.lifetechnologies.com, 2015. [Online]. Available: <https://www.lifetechnologies.com/de/de/home/life-science/protein-biology/protein-biology-learning-center/protein-biology-resource-library/pierce-protein-methods/biotinylation.html>
- [56] U. Spichiger-Keller, *Chemical and Biochemical Sensors (Chapter 2)*, In: *Chemical Sensors and Biosensors for Medical and Biological Applications*, Weinheim, Ed. WCH-Wiley, 1998.
- [57] W. Heineman and P. Kissinger, *Large amplitude controlled potential techniques in laboratory techniques in electroanalytical chemistry*, P. Kissinger and W. Heineman, Eds. Marcel Dekker, Inc, New York, 1996.
- [58] C. Berggren, P. Stålhandske, J. Brundell, and G. Johansson, "A feasibility study of a capacitive biosensor for direct detection of dna hybridization," *Electroanalysis*, 1999.
- [59] A. Millner, J. V. Rushworth, N. Hirst, and P. Millner, "Biosensors for whole-cell bacterial detection," *Clinical Microbiology Reviews*, 2014.
- [60] M. Bosch, A. Sánchez, F. Rojas, and C. Ojeda, "Recent development in optical fiber biosensors," *Sensors*, 2007.
- [61] D. J. Monk and D. Walt, "Optical fiber-based biosensors," *Anal Bioanal Chem*, 2004.
- [62] R. B. Queiros, J. Noronha, P. Marques, and M. G. F. Sales, *Emerging (Bio)Sensing Technology for Assessing and Monitoring Freshwater Contamination - Methods and Applications, Ecological Water Quality - Water Treatment and Reuse*, D. Voudouris, Ed. InTech, 2012.

- [63] R. Bharadwaj, V. Sai, K. T. A. Dhawangale, T. Kundu, S. Titus, P. K. Verma, and S. Mukherji, "Evanescent wave absorbance based fiber optic biosensor for label-free detection of e. coli at 280 nm wavelength," *Biosensors and Bioelectronics*, 2011.
- [64] M. O'Toole and D. Diamond, "Absorbance based light emitting diode optical sensors and sensing devices," *Sensors*, 2008.
- [65] Q. Ramadan and M. A. M. Gijs, "Microfluidic applications of functionalized magnetic particles for environmental analysis: focus on waterborne pathogen detection," *Microfluid Nanofluid*, 2012.
- [66] K. Hodgson, "SANS 241-1:2011 part 1: Microbiological, physical, aesthetic and chemical determinands - presentation."
- [67] T. Apps, *Apps Laboratories: What do your water test results mean?*, Apps Laboratories, 115 Collie Rd Gembrook 3783, Australia, www.appslabs.com.au.
- [68] SABS, *South African National Standard 241-2:2011 Drinking water Part 2: Application of SANS 241-1*, SABS Std.
- [69] —, *South African National Standard 5221:2011 Microbiological analysis of water - General test methods*, SABS Std.
- [70] S. T. Odonkor and J. K. Ampofo, "Escherichia coli as an indicator of bacteriological quality of water: an overview," *Microbiology Research*, 2013.
- [71] Centers for Disease Control and Prevention. (2014, May) General information - escherichia coli. Online: <http://www.cdc.gov/ecoli/general>. CDC.
- [72] D. Small, "Evaluation of an amperometric biosensor for the detection of echerichia coli o157:h7," Master's thesis, Louisiana State University, 2006.
- [73] X. Guan, H. jing Zhang, Y. nan Bi, L. Zhang, and D. ling Hao, "Rapid detection of pathogens using antibody-coated microbeads with bioluminescence in microfluidic chips," *Biomed Microdevices*, 2010.
- [74] Wagtech WTD, "Portable water quality test: datasheet."
- [75] Wilhelmshen Ships Service, "Marine chemical: Nalfleet potable water test solution."
- [76] H. Bridle, B. Miller, and M. P. Desmulliez, "Application of microfluidics in waterborne pathogen monitoring: A review," *Water Research*, 2014.

- [77] O. Tokarskyy and D. L. Marshall, "Immunosensors for rapid detection of escherichia coli o157:h7 - perspectives for use in the meat processing industry," *Food Microbiology*, 2008.
- [78] M. Costa, B. Veigas, J. Jacob, D. Santos, J. Gomes, P. Baptista, R. Martins, J. Inácio, and E. Fortunato, "A low cost, safe, disposable, rapid and self-sustainable paper-based platform for diagnostic testing: lab-on-paper," *Nanotechnology*, 2014.
- [79] S. K. Vashist, O. Mudanyali, E. M. Schneider, R. Zengerle, and A. Ozcan, "Cellphone-based devices for bioanalytical sciences," *Anal. Bioanal Chem*, 2014.
- [80] C. Sicard and J. Brennan, "Bioactive paper: Biomolecule immobilization methods and applications in environmental monitoring," *Materials Research Society Bulletin*, 2013.
- [81] C. García-Aljaro, L. N. Cella, D. J. Shirale, M. Park, F. J. Muñoz, M. V. Yates, and A. Mulchandani, "Carbon nanotubes-based chemiresistive biosensors for detection of microorganisms," *Biosensors and Bioelectronics*, 2010.
- [82] Y. Teng, X. Zhang, Y. Fu, H. Liu, Z. Wangb, L. Jin, and W. Zhang, "Optimized ferrocene-functionalized zno nanorods for signal amplification in electrochemical immunoassay of escherichia coli," *Biosensors and Bioelectronics*, 2011.
- [83] C. Ercole, M. Pantalone, S. Santucci, L. Mosiello, C. Laconi, and A. Lepidi, "A biosensor for escherichia coli based on a potentiometric alternating biosensing (pab) transducer," *Sensors and Actuators, B: Chemical*, 2002.
- [84] D. J. You, K. J. Geshell, and J.-Y. Yoon, "Direct and sensitive detection of foodborne pathogens within fresh produce samples using a field-deployable handheld device," *Biosensors and Bioelectronics*, 2011.
- [85] S.-H. Ohk and A. K. Bhunia, "Multiplex fiber optic biosensor for detection of listeria monocytogenes, escherichia coli o157:h7 and salmonella enterica from ready-to-eat meat samples," *Food Microbiology*, 2013.
- [86] S. Mura, G. Greppi, M. L. Marongiu, P. P. Roggero, S. P. Ravindranath, L. J. Mauer, N. Schibeci, F. Perria, M. Piccinini, P. Innocenzi, and J. Iru-dayaraj, "Ftir nanobiosensors for escherichia coli detection," *Beilstein Journal of Nanotechnology*, 2012.
- [87] H. Zhu, U. Sikora, and A. Ozcan, "Quantum dot enabled detection of escherichia coli using a cell-phone," *Analyst*, 2012.

- [88] S. M. Z. Hossain, C. Ozimok, C. Sicard, S. D. Aguirre, M. M. Ali, Y. Li, and J. D. Brennan, "Multiplexed paper test strip for quantitative bacterial detection," *Anal. Bioanal Chem*, 2012.
- [89] L. Yang and R. Bashir, "Electrical/electrochemical impedance for rapid detection of foodborne pathogenic bacteria," *Biotechnology Advances*, 2008.
- [90] L. Yang, Y. Li, C. L. Griffis, and M. G. Johnson, "Interdigitated micro-electrode (ime) impedance sensor for the detection of viable salmonella typhimurium," *Biosensors and Bioelectronics*, 2004.
- [91] B. Tribollet and M. E. Orazem, *Electrochemical Impedance Spectroscopy*. Wiley-Interscience, 2008.
- [92] R. Ahmed and K. Reifsnider, "Study of influence of electrode geometry on impedance spectroscopy," *International Journal of Electrochemical Science*, 2011.
- [93] A. Leung, P. M. Shankar, and R. Mutharasan, "A review of fiber-optic biosensors," *Sensors and Actuators B*, 2007.
- [94] J. Ma and W. J. Bock, "Dramatic performance enhancement of evanescent-wave multimode fiber fluorometer using non-lambertian light diffuser," *Optics Express*, 2007.
- [95] C. Corso, A. Dickherber, and W. Hunt, "An investigations of antibody immobilization methods employing organosilanes on planar zno surfaces for biosensor applications," *Biosensors and Bioelectronics*, 2008.
- [96] K.-K. Liu, R.-G. Wu, Y.-J. Chuang, H. S. Khoo, S.-H. Huang, and F.-G. Tseng, "Microfluidic systems for biosensing," *Sensors*, 2010.
- [97] T. M. Squires, "Microfluidics: Fluid physics at the nanoliter scale," *Reviews of Modern Physics*, 2005.
- [98] R. Zengerle and J. Duerée, "The future of microfluidics: Low-cost technologies and microfluidic platforms," *IMTEK - University of Freiburg*, 2004.
- [99] European Comission, "Research directorate-general - growth programme: Microfluidic analysis offers low-cost solution for water quality monitoring research."
- [100] W. C. Nelson and C.-J. Kim, "Droplet actuation by electrowetting-on-dielectric (ewod): A review," *Journal of Adhesion Science and Technology*, 2012.

- [101] M. G. Pollack, R. B. Fair, and A. D. Shenderov, "Electrowetting-based actuation of liquid droplets for microfluidic applications," *Applied Physics Letters*, 2000.
- [102] F. Saeki, J. Baum, H. Moon, J.-Y. Yoon, C.-J. C. Kim, and R. L. Garrell, "Electrowetting on dielectrics (ewod): Reducing voltage requirements for microfluidics," *Unknown*, Unknown.
- [103] Y. Li, W. Parkes, L. Haworth, J. Stevenson, A. Ross, and A. Walton, "Room temperature fabrication of anodic tantalum pentoxide for low voltage electro-wetting on dielectric," *Journal of Microelectromechanical Systems*, 2008.
- [104] S. K. Cho, H. Moon, and C.-J. Kim, "Creating, transporting, cutting, and merging liquid droplets by electrowetting-based actuation for digital microfluidic circuits," *Journal of Microelectromechanical Systems*, 2003.
- [105] Z. Ahmad, *Polymer Dielectric Materials, Dielectric material*, M. A. Silaghi, Ed. In, 2012.
- [106] J. Zeng and T. Korsmeyer, "Principles of droplet electrohydrodynamics for lab-on-a-chip," *Lab Chip*, 2004.
- [107] J. K. Luo, Y. Fu, Y. Li, X. Du, A. Flewitt, A. Walton, and W. Milne, "Moving-part-free microfluidic systems for lab-on-a-chip," *J. Micromech. Microeng.*, 2009.
- [108] A.-R. Gao, X. Liu, X.-L. Gao, T. Li, H.-M. Gao, P. Zhou, and Y.-L. Wang, "A low voltage driven digital-droplet-transporting-chip by electrostatic force," *Chinese Physics Letter*, 2011.
- [109] D. Juncker, H. Schmid, U. Drechsler, H. Wolf, M. Wolf, B. Michel, N. de Rooij, and E. Delamarche, "Autonomous microfluidic capillary system," *Analytical Chemistry*, 2002.
- [110] J. Gon and C.-J. Kim, "All-electronic droplet generation on-chip with real-time feedback control for ewod digital microfluidics," *Lab Chip*, 2008.
- [111] P. Lomer, "The dielectric strength of aluminum oxide films," *Proceedings of the Physical Society. Section B.*, 1950.
- [112] W. Kessels, J. van Delft, G. Dingemans, and M. Mandoc, "Review on the prospects for the use of Al₂O₃ for high-efficiency solar cells."
- [113] J. W. Elam and S. M. George, "Growth of ZnO/Al₂O₃ alloy films using atomic layer deposition techniques," *Chem Mater.*, 2003.

- [114] Q. Li, Y.-H. Yu, C. S. Bhatia, L. Marks, S. Lee, and Y. Chung, “Low-temperature magnetron sputter-deposition, hardness, and electrical resistivity of amorphous and crystalline alumina thin films,” *Journal of Vacuum Science & Technology, A: Vacuum, Surfaces, and Films*, 2000.
- [115] S. N. Pei and M. C. Wu, “Light-actuated digital microfluidics for large-scale droplet manipulation,” Master’s thesis, University of California at Berkeley, 2011.
- [116] B. Raj, M. Dhindsa, N. R. Smith, R. Laughlin, and J. Heikenfeld, “Ion and liquid dependent dielectric failure in electrowetting systems,” *Langmuir*, 2009.
- [117] J. Webster, “Thin film polymer dielectrics for high-voltage applications under severe environments,” Master’s thesis, Virginia Polytechnic Institute and State University, 1998.
- [118] V. Kumar and N. N. Sharma, “Su-8 as hydrophobic and dielectric thin film in electrowetting-on-dielectric based microfluidics device,” *Journal of Nanotechnology*, 2012.
- [119] J. Gong and C.-J. Kim, “Two-dimensional digital microfluidic system by multi-layer printed circuit board (pcb),” *IEEE*, 2005.